Design of Lightweight Blended-Wing-Body MALE UAV with Solar-Extended Endurance Via Novel Lattice Structures

by

Ouadah Ilyes

A thesis submitted for the degree of

Master of Science in Aircraft Structures

Department of Mechanical Construction
Saad Dahleb, Blida 1

Supervisor: Prof. Aissa Boutte
Prof. Aimad Eddine Badereddine

May 2025

Declaration

I, Ouadah Ilyes, declare that this thesis titled, 'Design of Lightweight Blended-Wing-Body MALE UAV with Solar-Extended Endurance Via Novel Lattice Structures' and the work presented in it are my own. I confirm that:

- This work was done wholly or mainly while in candidature for a research degree at this University.
- Where any part of this thesis has previously been submitted for a degree or any other qualification at this University or any other institution, this has been clearly stated.
- Where I have consulted the published work of others, this is always clearly attributed.
- Where I have quoted from the work of others, the source is always given. With the exception of such quotations, this thesis is entirely my own work.
- I have acknowledged all main sources of help.
- Where the thesis is based on work done by myself jointly with others, I have made clear exactly what was done by others and what I have contributed myself.

Abstract

This thesis details the design and validation of a novel Blended-Wing-Body (BWB) Medium-Altitude, Long-Endurance (MALE) UAV, developed to meet the challenging performance requirements of the Algerian Space Agency (ASAL). The research addresses the need for a platform capable of extended endurance with a significant payload, a gap not filled by conventional designs.

A custom Multidisciplinary Design Optimization (MDO) framework was created to produce an aerodynamically efficient airframe, yielding a final design with a predicted endurance of 7.4 hours. The aircraft's performance and flight characteristics were then rigorously validated. This validation process integrated high-fidelity Computational Fluid Dynamics (CFD) with experimental data from wind tunnel testing of a physical prototype.

The results provide a definitive confirmation of the aircraft's inherent stability. A negative pitching moment slope was observed across all analyses, guaranteeing static stability, while subsequent simulations confirmed all critical flight modes are dynamically stable. This work successfully delivers a complete, validated design for a next-generation UAV and establishes a repeatable computational workflow, providing a foundational platform for future national scientific and technological development.

Keywords Blended-Wing-Body MALE UAV; solar-extended endurance; lattice structures; multidisciplinary design optimization; computational fluid dynamics; wind tunnel testing; flight stability; Algerian Space Agency.

Acknowledgments

This thesis is the culmination of years of hard work, and it would not have been possible without the guidance, support, and encouragement of many incredible people. I wish to express my deepest and most sincere gratitude to all those who have been part of this journey.

First and foremost, I offer my heartfelt thanks to my parents. Your unwavering love, immense support, and constant encouragement have been the bedrock of my academic and personal life. You have been my greatest champions, and for your endless sacrifices and belief in me, I am eternally grateful. This achievement is as much yours as it is mine.

I am profoundly indebted to the faculty at Saad Dahleb University. I extend my sincere appreciation to my professors, Mr. Rezzoug, Mr. Badreddine, and Mr. Sbaa, as well as Mrs. Mahi and Mrs. Sari. Your wisdom, expertise, and dedication to teaching have not only imparted invaluable knowledge but have also inspired me to strive for excellence. My gratitude also extends to the long list of other professors whose lectures and guidance have shaped my understanding and passion for this field.

I would like to express my special thanks to my university and the AIT department and its members. I am particularly grateful to the head of the department Mr. Boutte, Mr. Hedda, and Mr. Ismail. You welcomed me with open arms, guided me with patience and insight, and entrusted me with this incredible opportunity to pursue a project of this magnitude. Your mentorship was instrumental in navigating the complexities of this research, and your support gave me the confidence to aim for something great.

Finally, to my friends, thank you. Your camaraderie, late-night study sessions, and unwavering support have been an immense source of strength and motivation. Your help and friendship have made this challenging journey not only manageable but also memorable.

ASAL

History

The Algerian space program began in 1987, with the creation of the Centre national des techniques spatiales (CNTS). The Algerian Space Agency was created by presidential decree on January 16, 2002, as a special national public establishment, with the aim of designing and implementing Algerian space policy.

In September 2017, the Algerian space agency signed a partnership agreement with Algeria's Ministry of the Environment and Renewable Energies to provide its aerospace tools. From August 2019, the Algerian General Directorate of Forests has access to ASAL's services. In September 2020, ASAL signs a cooperation agreement with the Algerian Ministry of Culture and Arts to protect and preserve the country's cultural heritage and biodiversity (an archaeological map is drawn up in September 2020).

From 2002 to 2019, the agency has grown from 100 to 600 researchers and engineers. In June 2023, ASAL signed a space agreement with the Russian space agency Ros cosmos, providing for scientific and technical exchanges, as well as assistance from Ros cosmos in training Algerian personnel in the space industry. ASAL also cooperates with Italian, French, Chinese and South Korean space agencies.

Definition

The Agence Spatiale Algérienne (ASAL) is a special national public establishment, with legal personality and financial autonomy. It was created under the authority of the Head of Government by Presidential Decree no. 02-48 of January 16, 2002.

The Agency designs and implements national policy for the promotion and development of space activities at the technological, scientific and application levels, with a view to contribut-

ing to the country's economic, social and cultural development, and ensuring the security and well-being of the national community. It has a Board of Directors made up of representatives from 15 ministerial departments, and a Scientific Council made up of experts in space technologies.

The ASAL-funded satellite development center comprises a 31,849 m2 enclosed construction site, infrastructure, landscaping, perimeter road and execution plans. The Satellite Development Center comprises two parts; Part A includes administrative and technical units with a total enclosed construction area of 23,618 m2. It comprises an integration and testing building, an administration building and conference center, a geodetic unit, a geomatics unit, a remote sensing unit, a UDS unit, an entry control building, infrastructure and roadworks and landscaping. Part B comprises the total closed construction area of 8,231 m2, consisting of 4 buildings with 40 apartments, villas and sports facilities

Missions and responsibilities

- To propose to the government the elements of a national strategy in the field of space activity and to ensure its execution;
- Establish a space infrastructure designed to strengthen national capabilities;
- Implement annual and multi-year development programs for national space activities, in conjunction with the various sectors concerned, and ensure their monitoring and evaluation;
- Propose to the government the space systems best suited to national concerns, and design, build and operate them on behalf of the state;
- Propose to the government a bilateral and multilateral cooperation policy adapted to national needs;
- Monitor and evaluate commitments arising from the State's obligations under regional and international space agreements.
- ensuring the training, retraining and further training of staff in the structures attached to it.
- To propose to the government a policy of international cooperation adapted to national preoccupations in the fields of space techniques and their applications in liaison with the concerned institutions.

- To ensure the collection, conservation and dissemination of scientific and technical information and any other information relating to the field of space technology, in accordance with the regulations in force.

ASAL's operating entities

Space Technology Center (STC)

The Centre des Techniques Spatiales (CTS) is responsible for carrying out all scientific and technical studies and research in the following fields:

- space technology, in particular sensor technology, radiometers, space telecommunications, earth stations for reception and control, and earth and atmospheric observation devices and instruments.
- The physics of aerospace remote sensing, ground energy balance and atmospheric physics.
- Satellite image processing methodology and image databases;
- space geodesy and reference systems, satellite navigation techniques and systems, radio astronomy and space altimetry, gravity field and geoid determination, and geodynamic applications.
- geomatics, databases and geographic information systems, acquisition methods (topographic, photogrammetry, remote sensing and cartography), and geographic data processing and retrieval.

Center d'Applications Spatiale (CAS)

- The Centre des applications spatiales (CAS) is responsible for implementing satellite and system operations arising from space programs, in conjunction with the various user sectors.
- The center handles sectoral and cross-sectoral operational projects based on remote sensing and geographic information systems, particularly in the fields of the environment and natural hazards, agriculture and water resources, land use and urban planning, geology and earth sciences.

Centre Development de Satellite (CDS)

The CDS comprises modern facilities (workshops and laboratories) dedicated to satellite design and assembly, as well as environmental testing facilities. The Satellite Development Center (CDS) is responsible for the design, development and production of space systems as part of the national space program:

- The contribution of national industry in related fields of space technology, notably mechanics, electronics, optics, computing and telecommunications.
- The construction of satellites, the conduct of functional tests on satellites (interference and electromagnetic compatibility tests, thermal vacuum tests, vibration tests and acoustic tests); quality assurance of integration and testing activities on space systems; the emergence of an industrial fabric in related fields of space technologies, notably in the fields of electronics, computing, mechanics, optics and telecommunications.

Center d'exploitation des systèmes de télécommunications (CEST)

The Centre d'exploitation des systèmes de télécommunications (CEST) is responsible for the management, operation and marketing of telecommunications satellite products and services planned as part of the national space program, including :

- Technical management of terrestrial reception and control infrastructures.
- Management of satellite products and services in conjunction with the user sectors concerned
- Definition and implementation of a product and service marketing policy.

Contents

Abstract ii

Acknowledgments iii

ASAL iv

1 Introduction 1

1.1 Background and Motivation . . . 1
1.2 Problem Statement . . . 5
1.3 Thesis Objectives . . . 8
1.4 Scope of Research . . . 8
1.5 Contributions . . . 9

2 Literature Review 11

2.1 Context and Motivation . . . 11
2.2 The Proposed Technological Convergence . . . 11
2.3 Scope and Structure of the Review . . . 12
2.4 The Blended-Wing-Body Platform . . . 12
2.4.1 Aerodynamic Superiority and Historical Context . . . 13
2.4.2 The Stability and Control Conundrum . . . 15
2.4.3 Unique Structural and Integration Demands . . . 16
2.5 Solar Power Systems for Extended-Endurance Flight . . . 17
2.5.1 The Energy Balance Imperative for Perpetual Flight . . . 17
2.5.2 Integration of Energy Systems: Harvesting and Storage . . . 18
2.5.3 The Weight Penalty and Performance Trade-offs . . . 19
2.6 Lightweighting Through Additive Manufacturing and Novel Lattice Structures 20
2.6.1 A New Paradigm in Structural Design: Lattice Structures . . . 20
2.6.2 Enabling Technologies: Topology Optimization and Additive Manufacturing . . . 22

2.6.3 Application and Challenges in Aerospace Structures 23
2.7 Synthesis : Multidisciplinary Conflicts, Gaps, and Future Directions 25
2.7.1 Conflicting Viewpoints and Ongoing Debates 25
2.7.2 Gaps in the Current Literature 26
2.8 Conclusion 27
2.8.1 Summary of Findings 27
2.8.2 Reinforcement of Core Challenges 28
2.8.3 Justification for Thesis Work 28

3 Design Methodology 30
3.1 Introduction 30
3.2 Optimization Methodology and Framework Architecture 31
3.3 The Integrated Computational Framework 33
3.3.1 Parametric Vehicle and Mission Representation 33
3.3.2 Disciplinary Analysis Modules 33
3.3.3 Formulation of the Optimization Problem 36
3.4 Airfoil Selection 38
3.5 Optimization Results 40
3.5.1 Preliminary Design Configuration (Theoretical CLmax) 41
3.5.2 Final Design Configuration (Corrected CLmax) 41
3.6 Summary 43

4 Integrated Design, Analysis, and Validation 45
4.1 Introduction 45
4.2 Aerodynamic Design and Iterative Validation Loop 46
4.2.1 Initial Geometry and Analysis 46
4.2.2 High-Fidelity CFD Analysis 48
4.2.3 Experimental Validation 57
4.3 Executive Summary 64
4.4 Initial Design and Low-Fidelity Analysis 65
4.4.1 Geometry Generation 65
4.4.2 Preliminary Stability Assessment 65
4.5 High-Fidelity CFD Analysis and Meshing 65
4.5.1 Meshing Workflow 66
4.5.2 Mesh Independence and Solver Setup 66
4.6 Aerodynamic Performance and Flow Analysis 66
4.7 Experimental Validation 67

4.7.1 Model and Setup . . . 67
4.7.2 Data Acquisition . . . 67
4.8 Validation Results and Final Conclusions . . . 67

5 Flight Dynamics Analysis **69**
5.1 Introduction . . . 69
5.2 The Principles of Aircraft Stability . . . 69
5.2.1 Static Stability . . . 70
5.2.2 Dynamic Stability . . . 70
5.2.3 The Critical Relationship: Static as a Prerequisite for Dynamic . . . 71
5.3 Introduction to Aerodynamic Derivatives . . . 72
5.3.1 Quantifying Stability . . . 72
5.3.2 Longitudinal Stability Derivatives (The Pitching Plane) . . . 72
5.3.3 Lateral-Directional Stability Derivatives (The Coupled Roll-Yaw Motion) 73
5.3.4 Damping Derivatives and Dynamic Stability . . . 74
5.4 Stability Analysis Methodology . . . 74
5.5 Stability Simulation Results . . . 75
5.6 Summary . . . 79

6 Prototype Fabrication **81**
6.1 Introduction . . . 81
6.2 A Comparative Overview of Traditional Methods . . . 82
6.3 Principles of Material Extrusion (FFF) . . . 84
6.4 Material Selection for High-Performance FFF . . . 85
6.4.1 Case Studies and Applications: ASA in Demanding Environments . . 87
6.5 Final Prototype Fabrication . . . 88
6.5.1 Slicer Configuration and Print Preparation . . . 88
6.6 Fabrication Results and Post-Processing . . . 89
6.7 Summary . . . 90

7 Conclusions and Future Work **91**
7.1 Conclusion . . . 91
7.2 Limitations of the Current Research . . . 92
7.3 Future Work . . . 93

References **95**

List of Figures

3.1 Flow chart for the Design framework 37

4.1 OpenVSP UI interface 46
4.2 3D openVSP UAV model 47
4.3 openVSP Simulation Results 48
4.4 Fluent Watertight Meshing Workflow Interface 50
4.5 Optimal Volume Mesh Section Views 52
4.6 Pressure Contours @ $\alpha = 0$ 54
4.7 Pressure Contours @ $\alpha = 11$ 55
4.8 Pressure Contours @ $\alpha = 25$ 55
4.9 3D Printed Scaled Model 57

6.1 3D Printed Scaled prototype 89

List of Tables

2.1 Seminal Studies in BWB Aerodynamic and Structural Design 13
2.2 Comparison of Lightweight Structural Concepts 21
2.3 Summary of Key Design Trade-offs 26

3.1 Airfoil Grading Part I 39
3.2 Airfoil Grading Part II 40
3.3 Final Scores: Part I 40
3.4 Final Scores: Part II 40
3.5 Preliminary Optimal Design Parameters 41
3.6 Final Optimal Design Parameters 42
3.7 Comparison of Preliminary and Final Optimal Design Configurations. 43

6.1 Comparative Analysis of Traditional UAV Manufacturing Methods 83
6.2 Comparison of Mechanical and Thermal Properties of Common FFF Filaments 86
6.3 Environmental Resistance Profile of Key Thermoplastics 87

Chapter 1

Introduction

1.1 Background and Motivation

The field of **unmanned aerial vehicle** has emerged as an exciting segment of the aerospace industry and due to recent technological advances, customer acceptance has risen quite substantially which led to a widespread deployment of these systems, this recent growth in demand has highlighted the importance of UAVs capable of extended endurance, medium to high altitude operations and high payload capacities.

An **unmanned aerial vehicle** is defined by the U.S department of defense as a "A powered aerial vehicle that does not carry a human operator, uses aerodynamic forces to provide vehicle lift, can fly autonomously or be piloted remotely, can be expendable or recoverable, and can carry a lethal or non-lethal payload" [1]. Nonpowered aircraft like gliders can be considered UASs/UAVs, if they have flight controls, navigation, and carry payloads, tethered aerostats and traditional balloons are typically not considered UASs as they are not powered or guided in a traditional sense. [2]

UAVs are divided into different types and categories based on specific attributes such as weight, size, mission altitude, survivability, design approach and mission, the following are some categories most relevant to this paper :

- **Micro Air Vehicles (MAV):** Micro Unmanned Aircraft (MAVs) are the smallest size class of unmanned aircraft, although precise size definitions can vary they are typically under 0.5 pounds, with wingspans ranging from 6 inches to about 2.5 feet. Operating in a challenging low-Reynolds-number flight regime, MAVs experience poor aerodynamic efficiency. MAVs are characterized by stringent Size, Weight, and Power

(SWAP) constraints, which demand the use of miniature, performance-constrained systems. Due to their low mass and speed, MAVs are highly susceptible to environmental disturbances that have a propensity to negatively influence sensor stability and data quality, requiring advanced processing. [2]

Despite the above limitations, MAVs enable significant utility to specific missions by leveraging their compactness and mobility, such as close-range tactical imaging, city or indoor-based operations, and swarm operations, with the added potential of having low unit manufacturing costs, enabling multiple unit usage. [2]

- **Small Unmanned Aircraft (SUAS):** Small Unmanned Aircraft Systems (SUAS) or Mini UAS is a category that typically weighs between 1 to 55 pounds, landing between the Micro Air Vehicles and small tactical UAS and while the lower end typically comprises hand-launched electric vehicles with low endurance (0.5-2 hours), the upper weight range includes longer endurance systems for low-altitude operations, with an increasing capability to take over missions from aging tactical platforms. [2]

  Although SUAS are the largest category due to low cost and technological barriers, often evolving from hobbyist platforms, miniaturization advances have made them operationally significant. Key technologies like lightweight GPS autopilots, small gimbaled cameras (1-5 pounds), and high-bandwidth line-of-sight communications (10-100 kilometers range) make SUAS capable of carrying useful payloads and performing tasks, such as surveillance and data relay, that previously have necessitated much larger systems. heavier variants, assuming more of the missions of older tactical UAS. [2]

- **Medium-Altitude Long Endurance (MALE):** Medium-Altitude Long-Endurance (MALE) Unmanned Aerial Systems (UAS) offer far more mission capability than small systems, typically with gross weights between 500 and 1,000 kilograms and payload capacity between 90 and 500 kilograms, capable of offering an endurance of 12 to 40 hours and flying at altitudes between 4,500 and 15,000 meters, depending on the engine. [2]

  Widely utilized in the military sector with common missions including Intelligence, Surveillance, and Reconnaissance (ISR), Signals Intelligence (SIGINT), and strike missions, facilitated by the ability to carry high-bandwidth satellite communications and external weapons payloads. [2]

MALE systems' size and payload flexibility make them frequently the initial platforms to carry new mission technologies. However, this large scale demands conventional runway operations, hangar facilities, and heavy ground support equipment to transport and maintain. [2]

- **High-Altitude Long Endurance (HALE):** High-Altitude Long-Endurance (HALE) Unmanned Aerial Systems (UAS) are characterized as advanced, high-end unmanned aircraft systems designed for flight operations typically above 15,000 or 18,000 meters. Such systems usually possess an endurance of more than 24 hours and a gross weight that is usually in excess of 2,000 kilograms. [2]

  Historically classified under Tier II+ (mid-1990s), Northrop Grumman's RQ-4 Global Hawk presents as the central example and the sole U.S. HALE system. The characteristics position HALE UAS as the primary tool for rigorous long-endurance strategic operations. [2]

- **Ultra Long Endurance (ULE):** Ultra Long Endurance (ULE) Unmanned Aerial Systems (UAS) is an emerging category brought about by the technological convergence of propulsion, structures, and aerodynamics, with the aim of achieving flight durations greater than five days. Such systems fly at 7,000 meters or higher, with the potential of spanning both MALE as well as HALE operational categories, and typically delivering payloads greater than 200 kilograms. Despite not yet entering operational use, development programs include the heavy-fuel Aurora Orion and hydrogen-powered platforms, including the Boeing Phantom Eye and the AeroVironment Global Observer. [2]

  The primary deciding factor among non-solar designs is propulsion, which is based on high-efficiency heavy fuel engines or power derived from hydrogen fuel cells or engines. Their ability to provide extreme endurance implies potential applications in highly persistent surveillance or long-term communications relay missions. [2]

- **Solar-Powered:** Solar aircraft represent a unique category of Unmanned Aerial Systems (UAS) primarily defined by the aim of achieving prolonged flight for numerous day-night cycles ("eternal flight"), a long-sought after goal plagued by technical issues like flight at high latitudes, in unfavorable winds, and ensuring long-term system reliability. [2]

Solar aircraft typically incorporate low wing loading to minimize flight power loads and maximize wing area for solar power collection, necessitating light, high-performance composite ("gossamer") structures, key technological drivers that led to further research in this category include solar cell efficiency and round-trip efficiency of onboard energy storage. [2]

This technology has been in development for decades, with examples including early demonstrators like Astro Flight's Sunrise family, AeroVironment's Pathfinder-to-Helios series, and smaller systems like QinetiQ's Zephyr intended for uses such as extended communications relay, as well as extensive research efforts like the DARPA Vulture program. [2]

UAV projects undertaken within the academic environment are generally classified as small or small tactical categories due to pragmatic limitations such as short program durations (generally a single or two semesters for competitions, a maximum of four years for graduate school) and constrained finances. Their missions are generally within the confines of student competitions (like the AIAA Design Build Fly competition), payload demonstration, scientific testing or specific flight research topics. [2], However, strategic cooperation between national organizations and universities can enable more ambitious academic projects to address certain specific operational needs that help with growing critical industries. This thesis relates to such a project, which was realized through a partnership with the Algerian Space Agency (ASAL), specifically with its Satellite Development Center (CDS) in Oran.

This collaboration established CDS' requirement for a general-purpose and modular, high-performance aerial test platform. Such a platform is required to test and qualify various potential satellite subsystems which can include various sensors, communications links, attitude control components, battery technologies or new imaging techniques under representative atmospheric flight conditions and for extended periods of operation while also acting as a vehicle for future academic research that can include short duration low to medium altitude missions, such capabilities are often outside of those available for typical small academic UAVs, which positions this project as a vital risk-reduction milestone prior to the costly integration of these technologies into space assets and a crucial tool to help the Algerian academic community mature to more experimental, industry-oriented projects.

The demands for long endurance at low to medium altitudes clearly and naturally point towards the MALE (Medium-Altitude Long-Endurance) category of UAVs/UASs, and require

novel approaches and techniques.

Successfully realizing such a demanding platform motivates the exploration of advanced aerospace technologies. Meeting the combined requirements for endurance, altitude, payload capacity, and operational flexibility necessitates innovations in aerodynamic efficiency, power systems, and structural design. Therefore, state-of-the-art configurations and technologies investigated herein, such as the Blended-Wing-Body (BWB), additive manufacturing, advanced hybrid additive-composites, and novel lattice structures, as well as the use of solar power, present themselves as key enabling elements for developing this MALE UAV to achieve such ambitious endurance and performance goals.

1.2 Problem Statement

The ever-increasing degree of complexity and miniaturization in satellite technology, which ranges from sophisticated Earth observation sensors and high-bandwidth communication arrays to increasingly integrated power systems, necessitates similarly advanced and well-thought-out pre-flight validation methodologies.

Launching immature or inadequately tested systems entails unacceptably high risks of failure, which potentially can jeopardize costly missions and cause substantial delays of commercial or scientific objectives by way, of which the latter simply cannot exist without obtaining real-world measurements and data. While ground simulations and environmental testing provide preliminary foundational data, they cannot fully reproduce the dynamic effects of operating at altitude, atmospheric conditions, and sustained flight dynamics.

Flying test platforms capable of tackling a wide range of altitudes are thus a precious commodity for high-fidelity testing. Nevertheless, established options like stratospheric balloons, while attaining relevant altitudes, offer limited versatility and flight path controllability and persistence at a specific target altitude, often dictated by prevailing wind patterns.

Sounding rockets provide only fleeting moments in the desired environment at a considerably high cost. Consequently, the concept of a Low to Medium-Altitude, Long-Endurance (LALE/MALE) Unmanned Aerial Vehicle (UAV) manifests as an intriguing, potentially promising approach solution, promising a superior capacity for continuous, controlled, and relatively economical flight within relevant atmospheric conditions for subsystem shakedowns

and performance evaluation, as well as providing an essential scientific tool for follow-on ambitious activities and research.

Despite the theoretical promise, a significant gap exists between the ideal operating profile for effective satellite subsystem testing and the built-in capabilities of existing UAV systems under practical constraints. The specific set of requirements includes sustained operation at or above 3 km altitude ; an endurance of more than 14 hours to monitor long-term operational effects ; the ability to carry a non-negligible payload mass of 5 kilograms to allow for a variety of subsystem hardware and scientific measuring equipment ; adherence to a limited wingspan of less than 4 meters for operational and logistical convenience and simplicity ; and finally a modularity requirement to allow for maximum flexibility and mission optimization, these requirements establish a particularly challenging performance envelope, existing design paradigms for UAVs highlight severe trade-offs attempting to achieve these metrics simultaneously.

High-efficiency airframes typical of record-breaking endurance aircraft rely on extremely high aspect ratios and minimal wing loading; these structures, are inherently limited to small internal volumes which renders them unsuitable for accommodating large test articles, and their thin structures struggle to resist heavy point loads from payloads without considerable penalties in weight and structural complexity, particularly regarding wing root bending moments and torsional stiffness.

Conversely, heavy payload platforms inherently compromise aerodynamic efficiency through lower aspect ratio, thicker airfoils, or less streamlined fuselage, drastically curtailing their endurance potential and achievable service ceiling, it is extremely rare for deployable UAV systems currently available within the reach of non-military institutions to satisfy even two or three of the above four performance metrics simultaneously, displaying a fundamental limitation in conventional aircraft design practices when applied to this specific, demanding mission.

Exploring solutions beyond conventional design highlights highly advanced, highly integrated airframe concepts like the Blended Wing Body (BWB) configurations. BWBs offer the potential for substantial improvements in lift-to-drag ratio and internal volume fractions compared to traditional tube-and-wing aircraft. However, turning the advantages into reality involves navigating a complex labyrinth of challenging technical problems. The non-planar, smoothly varying geometry complicates accurate aerodynamic modeling, especially

in terms of stability, control, and low-speed performance. More importantly, the structural layout of a BWB represents a substantial challenge, especially when pursuing the extensive lightweighting demanded by the Medium Altitude Long Endurance mission profile.

Effectively distributing aerodynamic and payload-induced stresses throughout the integrated structure, while maximizing the material's use, requires complicated structural configurations that are difficult to achieve using traditional fabrication methods. Conventional aerospace manufacturing techniques—whether subtractive machining of metallic components or layup and curing of conventional composite materials in autoclaves—struggle to efficiently create these complex, doubly-curved surfaces and, more significantly, the intricate, optimized internal stiffening structures required to realize maximum structural efficiency without incurring excessive weight or manufacturing costs logically compel us to consider novel additive manufacturing methods.

And with the advancements of implicit modeling techniques, creating topology-optimized, load-path-aligned internal structures directly integrated in the complex BWB geometry is now a reality that can allow us to overcome the constraints of existing design philosophy and manufacturing technology.

There is, therefore, a critical and well-defined technological gap. It is specified not merely by the absence of an off-the-shelf UAV with the requisite specifications, but more fundamentally by the fact that there are no validated design principles and integrated computationally-based procedures available that can synergistically optimize the aerodynamics, structure, and manufacturability of a BWB specially created for the requirements of a versatile long-endurance, payload-carrying platform.

The difficulty exists at the complex intersection of advanced aerodynamics, structural mechanics, materials science, and novel manufacturing techniques, namely in the context of realizing ultra-lightweight structures for non-conventional airframe geometries in the MALE domain, the inability to effectively bridge this gap currently represents a significant roadblock, hindering the development of next-generation UAVs and thus slowing the pace of market adoption of the previously mentioned technologies.

1.3 Thesis Objectives

The primary objective of this thesis is to develop and validate an integrated design methodology for a new Medium-Altitude Long-Endurance (MALE) Unmanned Aerial Vehicle (UAV) airframe, specifically intended to act as a testing platform for various technologies and satellite subsystems, this involves bridging the identified technological gap by synergistically balancing structure, aerodynamics, and manufacturability for a challenging set of performance requirements.
This thesis aims to achieve the following objectives :

- **Design an Aerodynamically Efficient Blended Wing Body Airframe :** Develop a BWB airframe optimized for high L/D at target operational flight envelope to enable long endurance capabilities.
- **Achieve Extreme Structural Lightweighting and Investigate Lattice Structure Integration :** Design a minimal mass BWB through strategic and effective integration of lattice structures and advanced materials while ensuring structural integrity under flight loads and the specified 5 kilogram payload requirements.
- **Develop a Repeatable Computational Workflow :** Establish and utilize a fully repeatable computationally-driven workflow, leveraging open source software and code as well as modern implicit modeling techniques.
- **Produce a Validated Prototype Airframe Design :** Deliver a detailed scaled prototype that validates aerodynamic and performance targets while highlighting the modularity and payload integration considerations, and ensure upgradability and future proofing.

1.4 Scope of Research

This thesis focuses specifically on the aerodynamic and structural design and optimization through the integration of lattice structures in the airframe for the previously described MALE UAV testing platform.
The scope encompasses the following aspects :

- **Airframe Design through Computational Workflows:** Detailed design and development of the blended wing body (BWB) configuration through the application of parametric/implicit modeling techniques.

- **Aerodynamic Analysis:** Computational Fluid Dynamics (CFD) simulations to analyze and optimize the aerodynamic performance (lift, drag, stability characteristics) of the BWB shape at relevant flight conditions.
- **Structural Design and Lightweighting Techniques:** Detailed design of the primary and secondary airframe structures, and investigation, implementation and analysis of lightweighting strategies with a focus on internal lattice structures and advanced ribbing.
- **Material and Manufacturing:** Consideration and selection of appropriate materials and investigation of polymer-composites suitable for hybrid additive-composite manufacturing approaches for stiff, complex yet lightweight structures.
- **Payload Accommodation and Future Proofing:** Detailed designed approach for a modular airframe able to accommodate the required 5 kilograms payload mass and volume, including defining potential mounting locations and ensuring structural load paths and ease of future solar power integration.
- **Performance Verification and Prototype Development:** Verification of the final design's aerodynamic performance and structural integrity through prototype development and flight testing.

The following aspects are considered outside the scope of this specific thesis:

- Design, analysis, integration, and testing of the solar power generation and storage system.
- Design, development, implementation, and testing of the flight control system, avionics, sensors (excluding those considered payload), and communication systems.
- Detailed design of payload-specific integration hardware or ground support equipment.
- Mission planning, operational procedures, or regulatory compliance analysis.

1.5 Contributions

As previously mentioned this thesis presents the validation, integration and the design methodology for a high-endurance modular test platform enabled by investigating novel and ambitious technologies, the primary contributions of this thesis are :

- **Development of an Integrated Computational Design Workflow:** Established and demonstrated a computationally driven, repeatable workflow leveraging parametric/implicit modeling, Finite Element Analysis (FEA), and Computational Fluid Dynamics (CFD). This workflow enables a synergistically optimized BWB aerodynamics and complex internal structures, addressing a critical gap required for highly integrated airframe design.

- **Novel Application of Lattice Structures for BWB Lightweighting:** Designed and experimentally validated the strategic integration of lattice structures within a blended-wing-body (BWB) airframe in an effort to achieve extreme lightweighting. This work examines ambitious approaches towards lattice structure integration, specially designed for complex geometries and distributed loading paths typical of BWB designs, outside conventional structural design paradigms.

- **Design Framework for Additive Manufacturing:** Explored design considerations aimed at allowing for the use of additive manufacturing techniques, such as this method tackles manufacturability problems related to the sophisticated blended wing body (BWB)B geometries and internal lattice structures, providing a path towards market adoption and future integrations in existing projects.

Chapter 2

Literature Review

2.1 Context and Motivation

The strategic importance of Medium-Altitude, Long-Endurance (MALE) UAV/UAS has grown substantially in recent decades. As previously mentioned such platforms serve as critical assets for a diverse range of persistent missions, including intelligence, surveillance, and reconnaissance (ISR); communications relay; environmental and agricultural monitoring; and disaster response or as test platforms and for such applications, the primary figure of merit is endurance which is defined as the ability to remain aloft for extended periods—days or even weeks—dramatically enhances operational effectiveness and reduces logistical burdens. However, the endurance of current MALE UAVs is fundamentally constrained by onboard energy storage, whether in the form of conventional fossil fuels or batteries and overcoming this burden is paramount to the future success of these systems.

2.2 The Proposed Technological Convergence

A paradigm shift in MALE UAV performance may be achievable through the synergistic integration of three distinct and advanced technological pillars. Each pillar offers a significant performance advantage, but their combination presents a complex, multidisciplinary design challenge riddled with conflicting requirements. The three pillars are:

- **Blended-Wing-Body (BWB) Airframes:** This novel aircraft configuration, where the wing and fuselage are seamlessly integrated into a single lifting surface, offers a foundation of superior aerodynamic efficiency compared to traditional tube-and-wing designs. [3]

- **Solar Power Systems:** The integration of high-efficiency photovoltaic (PV) cells and advanced energy storage systems provides a means to harvest energy in-flight, offering the potential to extend endurance far beyond the limits of conventional fuels and even enable "perpetual" flight under the right conditions. [1]

- **Lattice Structures:** Fabricated via Additive Manufacturing (AM), these computationally designed structures promise radical lightweighting. This is not merely an incremental improvement but a critical enabling technology, necessary to offset the inherent weight penalties of the other two pillars and make the entire concept viable. [4]

2.3 Scope and Structure of the Review

This review critically evaluates the state-of-the-art literature within each of these three domains before synthesizing the findings to shed light on the profound multidisciplinary challenges and opportunities at their intersection. The objective is to analyze the inherent design conflicts and trade-offs that arise when attempting to merge these technologies into a single system.

The review is structured to guide the reader through this complex design space, beginning with the foundational BWB platform, moving to the integration of the solar power ecosystem and the advanced structural design paradigm of lattices, and culminating in a synthesis that identifies critical research gaps and proposes compelling directions for future work. The overarching goal is to provide a comprehensive scholarly foundation for research into a novel design methodology for this next-generation aircraft concept.

2.4 The Blended-Wing-Body Platform

The Blended-Wing-Body (BWB) represents a departure from the conventional tube-and-wing aircraft architecture that has dominated aviation for nearly a century. Its selection as the airframe for a high-endurance UAV is predicated on its promise of exceptional aerodynamic efficiency, though this benefit is coupled with significant challenges in stability, control, and structural design.

2.4.1 Aerodynamic Superiority and Historical Context

The modern BWB concept was pioneered in the 1990s through the seminal work of R. H. Liebeck and his collaborators at McDonnell Douglas (later Boeing), in partnership with NASA. [3] These foundational studies established the BWB as a credible and potentially revolutionary configuration for subsonic transport aircraft.

he core principle of the BWB is that the entire airframe—not just the wings—functions as a lifting surface, this integration minimizes the wetted area-to-lifted volume ratio and reduces interference drag between the wing and body, resulting in a substantially higher lift-to-drag (L/D) ratio.

Numerous studies, spanning from large transport concepts to smaller UAVs, have consistently validated this aerodynamic advantage. Performance comparisons predict improvements in L/D of 15% to 30% over equivalent conventional aircraft [5]. For an energy-limited platform like a solar-powered UAV, this is a critical advantage, as the power required for level flight is inversely proportional to the L/D ratio.

This aerodynamic gain translates directly into significant reductions in required power (or fuel burn in conventional aircraft, with savings up to 27% reported), lower takeoff weight, and the ability to carry a larger payload or more energy storage for a given airframe size [5], Recognizing these benefits, researchers have increasingly adapted the BWB concept for MALE UAV applications, where its high aerodynamic efficiency and large internal volume for payloads and systems are particularly attractive. Table 1 summarizes several key studies that have shaped the understanding of BWB platforms.

Table 2.1: Seminal Studies in BWB Aerodynamic and Structural Design

Author(s) & Year	**Publication /Affiliation**	**Key Contribution/Finding**	**Platform Focus**
Liebeck (2004)	Journal of Aircraft / Boeing	Foundational paper detailing the BWB concept, predicting a 27% fuel burn reduction and outlining core design challenges.	Large Transport

Continued on next page

Table 2.1: Seminal Studies in BWB Aerodynamic and Structural Design (Continued)

Author(s) & Year	**Publication /Affiliation**	**Key Contribution/Finding**	**Platform Focus**
Panagiotou et al. (2017)	AIAA Conference / Aristotle University	Conducted a parametric aerodynamic study of BWB platforms at low subsonic speeds, establishing key design parameter sensitivities for UAV applications.	UAV
Kapsalis et al. (2022)	AIAA SciTech Forum	Presented a Design of Experiments (DOE) based optimization of a tactical BWB UAV, highlighting the trade-offs between performance and stability.	UAV
An et al. (2019)	MATEC Web of Conferences / UiTM	Used CFD and wind tunnel data to demonstrate the necessity of horizontal stabilizers for achieving longitudinal stability in a BWB UAV prototype.	UAV

Continued on next page

Table 2.1: Seminal Studies in BWB Aerodynamic and Structural Design (Continued)

Author(s) & Year	**Publication /Affiliation**	**Key Contribution/Finding**	**Platform Focus**
Gudmundsson (2005)	AIAA Paper / NASA	Detailed the severe structural challenges of the BWB's non-cylindrical pressurized cabin, highlighting the high bending stresses compared to conventional fuselages.	Large Transport

2.4.2 The Stability and Control Conundrum

The BWB's elegant, integrated shape is also the source of its greatest aerodynamic challenge. The absence of a conventional empennage (tail) deprives the aircraft of the large moment arm used for stabilization, leading to inherent longitudinal and directional instability [6]. This is not merely a theoretical concern; flight tests of early BWB UAV prototypes have vividly demonstrated this issue, with some aircraft experiencing a dangerous "overturning condition" at certain angles of attack when flying without corrective measures [5]. The literature presents a clear conflict in how to mitigate this instability. One school of thought, stemming from early transport studies, involves the careful design of reflexed airfoils in the center-body to provide the necessary nose-up pitching moment for trim without adding separate control surfaces [3], however, for many UAV applications, a more common approach is to add control surfaces that functionally replace the tail. This includes vertical stabilizers or winglets to provide directional stability (i.e., a positive weathercock stability derivative, $C_{n\beta}$) [7] and, critically, horizontal stabilizers to manage longitudinal stability. A study by An et al. (2019) showed through both CFD and wind tunnel experiments that adding horizontal stabilizers—particularly larger ones placed further aft—significantly improved static stability by creating a steeper, more negative pitching moment slope ($dC_m/d\alpha$) [5]. A steep negative slope ensures a strong restorative nose-down moment when the angle of attack increases, preventing pitch-up and stall.

This solution, however, introduces a fundamental design conflict. The very additions that enhance stability—the stabilizers—also increase the aircraft's wetted area and create in-

terference drag, which can partially erode the BWB's core aerodynamic advantage [5], this creates an intricate trade-off between aerodynamic efficiency and flight stability that is a central theme in BWB design [6], navigating this trade-off represents a critical multidisciplinary design optimization (MDO) problem. The challenge is compounded by the limitations of design tools. Low-fidelity analysis methods, while computationally fast, may fail to accurately capture the subtle drag penalties associated with stability-enhancing features, leading to overly optimistic and potentially flawed performance predictions in the conceptual design phase. Conversely, high-fidelity CFD, which can capture these effects, is often too computationally expensive to be used within a broad MDO loop and this "fidelity gap" highlights a need for advanced, multi-fidelity optimization strategies that can efficiently and accurately balance these competing requirements.

2.4.3 Unique Structural and Integration Demands

The BWB's unconventional shape poses unique structural challenges that distinguish it from traditional aircraft. In a conventional airliner, the cylindrical fuselage is an exceptionally efficient structure for handling cabin pressurization loads, which are resisted primarily through uniform membrane (hoop) stresses in the skin however, the BWB's wide, flat, box-like center-body behaves very differently, a fact that has been detailed in a NASA study by Gudmundsson (2005), internal pressure loads on this non-cylindrical shape are resisted primarily through bending, which can result in stress levels an order of magnitude higher than the membrane stresses in a comparable cylindrical fuselage [8] which necessitates a much heavier structure to prevent failure or excessive deformation that could compromise the aerodynamic shape.

While a MALE UAV is typically unpressurized, the underlying structural principle remains highly relevant. The wide, flat center-body must still serve as the primary load-bearing structure, transferring the immense bending moments from the high-aspect-ratio wings across its span. A conventional semi-monocoque design, consisting of skin, stringers, and frames, may not be the most mass-efficient solution for this unique load path, early BWB studies explored alternative concepts like vaulted ribbed shells and deep honeycomb sandwich panels, but these were often found to be heavy, complex to manufacture, or difficult to maintain [8] This inherent structural inefficiency of the BWB shape becomes a powerful "pull factor" for the adoption of non-conventional structural solutions. It suggests that the application of novel concepts like topology-optimized lattice structures is not merely a generic lightweighting exercise. Rather, it is a targeted strategy to address a fundamental, inherent weakness of the BWB platform by providing exceptionally high, tailorable stiffness-to-weight ratios,

such advanced structures could potentially solve the BWB's structural conundrum, stiffening the center-body against bending loads without the prohibitive mass penalty of conventional approaches.

The successful marriage of the BWB's aerodynamic form with an advanced, lightweight structural system could therefore unlock a level of performance that neither technology could achieve in isolation.

2.5 Solar Power Systems for Extended-Endurance Flight

To transcend the endurance limits of chemical fuels or batteries, the UAV must become an energy harvester. The integration of a solar power system transforms the aircraft into a self-sustaining platform, but introduces a new layer of multidisciplinary complexity centered on a delicate, 24-hour energy balance.

2.5.1 The Energy Balance Imperative for Perpetual Flight

The concept of solar-powered flight has a rich history, with pioneers like Paul MacCready demonstrating its feasibility with aircraft like the Solar Challenger, which crossed the English Channel in 1981 using only solar power with no battery storage, for a modern MALE UAV, the objective is far more demanding: achieving "perpetual endurance" or "eternal flight," which necessitates continuous operation through day and night cycles.

The foundational principle governing this capability is a strict 24-hour energy balance, which can be stated simply: the total solar energy collected during daylight hours must equal or exceed the total energy consumed by the aircraft over a full 24-hour period, achieving this positive energy balance is a formidable challenge, heavily dependent on a range of mission and environmental parameters, some of the key influencing factors include the geographical location of operation (latitude dictates solar intensity and the length of the day), the time of year, and the flight altitude and while higher altitudes are generally favorable, offering more intense and consistent solar radiation above most cloud cover, they also introduce a harsh thermal environment with extremely low temperatures that can degrade battery performance [9].

A significant body of research has been dedicated to developing sizing methodologies and MDO codes, such as SD2020 and ASWING, to model this complex interplay of factors. These computational tools take mission requirements as inputs to perform a top-level sizing of the

aircraft, determining the necessary wingspan, solar array area, and battery mass required to close the energy balance [10]

2.5.2 Integration of Energy Systems: Harvesting and Storage

The solar power system itself consists of two primary subsystems: energy harvesting and energy storage.

- **Solar Cell Technology:** The performance of the energy harvesting system is dictated by the efficiency and weight of the photovoltaic (PV) cells. The technology has evolved significantly since the early days of solar flight with photovoltaics that could hit efficiencies around 10-14%. Modern solar UAVs leverage high-efficiency (>22%), lightweight, and semi-flexible cells that maximize the power-to-weight ratio and can be more easily integrated onto the curved surfaces of an airfoil [11], looking forward, emerging technologies like flexible perovskite-organic tandem cells are showing revolutionary potential. Recent lab results have demonstrated efficiencies over 26%, with a theoretical potential to exceed 30%, promising a massive leap in power generation for a given surface area and making them an ideal candidate for future UAVs [12]

- **Energy Storage Technology:** To operate through the night or periods of low sun, a robust energy storage system is non-negotiable. The literature shows a clear and enduring consensus on the use of lithium-based battery chemistries due to their superior specific energy density (Wh/kg). Lithium-Ion (Li-Ion) and Lithium-Polymer (Li-Po) batteries are the most common choices for current UAV designs [11]. For high-performance HALE platforms like the QinetiQ Zephyr, more advanced, high-power Lithium-Sulphur batteries have been employed to further push the endurance envelope.

- **Power Management:** The brain of the power system is a sophisticated suite of electronics. A Maximum Power Point Tracking (MPPT) controller is essential to continuously adjust the electrical load on the solar array to ensure it is always operating at its peak power output, even as illumination conditions change. This is coupled with an overarching Energy Management System (EMS) and a Battery Management System (BMS), which are critical for intelligently routing power, managing the state of charge of the batteries, and ensuring their health and safety by preventing conditions like overcharging or thermal runaway [11].

2.5.3 The Weight Penalty and Performance Trade-offs

A fundamental conflict in the design of any solar-powered aircraft is the mass of the power system itself. To increase endurance, one must add more solar cells and batteries. However, this added mass increases the aircraft's total weight, which in turn requires more power to maintain flight [13]. This increased power demand necessitates an even larger solar array and more batteries, creating a "vicious cycle" or "death spiral" that can quickly lead to an unfeasible design if not carefully managed through rigorous optimization [13].

This trade-off extends beyond a simple power-to-weight calculation and has profound multidisciplinary consequences. The physical integration of solar cells onto the wing surface, for example, can alter the aerodynamic profile. If not integrated seamlessly, the cells can introduce surface roughness or steps that trip the boundary layer from smooth laminar flow to turbulent flow, increasing skin friction drag and degrading aerodynamic performance.[11] The mass and placement of the batteries are also critical, directly impacting the aircraft's structural design, its center of gravity, and consequently its stability and control characteristics [14] This deep coupling of disciplines makes an integrated design approach, where the airframe, propulsion, and energy systems are co-optimized, an absolute necessity.

Studies have shown that achieving a precise match between the airframe's aerodynamic characteristics and the power system's output is critical to maximizing the overall efficiency of the aircraft, the integration of a solar power system fundamentally changes the design philosophy of the aircraft. A conventional aircraft is designed to perform optimally at a few key, relatively static flight conditions (e.g., cruise, loiter, takeoff), in contrast, a solar-powered aircraft operates as a dynamic energy ecosystem. Its performance is not a fixed value but a continuous function of time of day, time of year, latitude, and weather.

The aircraft is in a constant state of harvesting, storing, and expending energy. This shifts the primary optimization objective from a narrow goal like "minimize drag at cruise" to a much broader one: "maximize net energy gain over a 24-hour cycle." This can lead to counter-intuitive design choices and operational strategies. For instance, the optimal flight path may be determined not by the shortest distance but by the route with maximum solar exposure, The aircraft might even be programmed to enter a controlled glide to charge its batteries when power generation exceeds the power required for level flight, this elevates the Energy Management System (EMS) to a flight-critical component, on par with the flight control system, as it must make real-time decisions about power allocation that directly affect the aircraft's ability to survive the night. Furthermore, the BWB platform presents

a unique conflict between two of its primary advantages when considering solar integration, on one hand, its vast, continuous upper surface appears to be an ideal canvas for mounting a large solar array. On the other hand, the BWB's high aerodynamic efficiency is predicated on maintaining smooth, uninterrupted airflow over its carefully designed lifting surfaces which in turn makes physical act of attaching solar cells, even thin, flexible ones, inevitably introduces seams, edges, and slight surface imperfections. These features can be sufficient to "trip" the boundary layer from a low-drag laminar state to a high-drag turbulent state, thereby compromising the very aerodynamic efficiency that made the BWB an attractive choice in the first place [11] and it creates a direct conflict: maximizing the use of the BWB's surface area for power generation could degrade its aerodynamic performance implying that a critical area for research is not merely the placement of solar cells, but the development of advanced materials science and manufacturing techniques to embed the PV cells so seamlessly within the composite wing skin that the aerodynamic penalty is minimized to a negligible level.

2.6 Lightweighting Through Additive Manufacturing and Novel Lattice Structures

To counteract the significant mass of the solar power system and the inherent structural inefficiency of the BWB shape, a radical approach to structural design is required. This third pillar of technology moves beyond conventional composite construction and into the realm of computationally designed lattice structures enabled by additive manufacturing.

2.6.1 A New Paradigm in Structural Design: Lattice Structures

Lattice structures are a class of porous, cellular materials composed of a three-dimensional, ordered array of interconnected struts or beams [4], they represent a significant evolution from other cellular solids like foams, which have a random and stochastic cell structure, and honeycombs, which are essentially 2D prismatic extrusions. The ordered, 3D architecture of lattices allows for their mechanical properties to be precisely tailored to meet specific loading requirements [4], for aerospace applications, their most compelling advantages are exceptionally high stiffness-to-weight and strength-to-weight ratios, superior energy absorption capabilities, and the potential for multifunctionality [4] and when properly designed, lattice structures have been shown to possess compressive and shear strength superior to foams and honeycombs of equivalent density [4].

The introduction of gyroid structures and additively manufactured parts with their incredible stiffness to weight ratios highlights the immense potential when moving away from traditional structural philosophies. Table 2 provides a comparative overview of different lightweight structural concepts.

Table 2.2: Comparison of Lightweight Structural Concepts

Structural Concept	**Basic Principle**	**Key Advantages**	**Key Disadvantages/ Challenges**	**Primary Application**
Semi-Monocoque (Al/Composite)	A thin outer skin is supported by longitudinal stringers and transverse frames/ribs to carry loads.[23]	Mature, well-understood design and manufacturing; good damage tolerance.	Not weight-optimal for complex or non-uniform load paths like those in a BWB.	Conventional fuselages and wings.
Composite Sandwich Panel	Two thin, stiff skins are bonded to a thick, lightweight core (e.g., honeycomb, foam).[43]	Very high bending stiffness-to-weight ratio; smooth aerodynamic surfaces.	Susceptible to core-skin debonding, moisture ingress into the core, and impact damage.	Control surfaces, fairings, some wing structures.

Continued on next page

Table 2.2: Comparison of Lightweight Structural Concepts (Continued)

Structural Concept	**Basic Principle**	**Key Advantages**	**Key Disadvantages/ Challenges**	**Primary Application**
Geodesic/Lattice (Pro-Composite)	A grid of unidirectional composite ribs carries the primary tensile and compressive loads.[42]	Highly weight-efficient by aligning fibers with load paths; high allowable stresses.	Manufacturing complexity of joints; requires protective outer skin.	Advanced fuselage and wing structures.
TO-Generated Lattice (AM)	A porous structure of interconnected struts is computationally optimized for a specific load case.[s]	Highest theoretical stiffness-to-weight; properties can be tailored locally; enables multifunctionality.	Severe manufacturing scale and quality limitations; lack of characterization data; certification pathway is undefined.[44]	Next-generation lightweight components.

2.6.2 Enabling Technologies: Topology Optimization and Additive Manufacturing

The practical realization of advanced lattice structures is made possible by the powerful synergy between two key technologies :

- **Topology Optimization (TO):** Serving as the "brain" of the design process, TO is a computational methodology that automatically determines the optimal distribution of material within a given design volume, subject to a set of loads and constraints, it gen-

erates highly efficient, often organic-looking, lightweight structures that are frequently counter-intuitive and difficult to conceive using traditional design approaches.

- **Additive Manufacturing (AM):** Acting as the "hands," AM (also known as 3D printing) is the fabrication technology that brings TO designs to life. By building parts layer-by-layer directly from a digital model, AM can create the complex internal geometries, intricate features, and freeform shapes characteristic of TO-generated lattices—designs that are often impossible to produce using conventional subtractive (machining) or formative (molding, forging) methods.

This combination has spurred the development of advanced design techniques, including multi-scale optimization, which simultaneously optimizes the overall macro-scale shape of a component and the micro-scale topology of the lattice unit cells within it, Further innovation is seen in bionic or nature-inspired design methods, which use different algorithms to simulate the growth patterns of natural structures (e.g., plant leaves, insect wings) to generate highly efficient stiffener layouts for wing surfaces, achieving significant improvements in buckling resistance and weight reduction.

2.6.3 Application and Challenges in Aerospace Structures

The literature demonstrates a rapidly growing interest in applying these techniques to primary aircraft structures, moving beyond small, secondary components. Research has explored replacing conventional ribs and spars in aircraft wings with optimized lattice-infilled structures, promising significant weight savings over even advanced composite designs.9 However, the path from theoretical potential to flight-certified reality is laden with significant manufacturing and qualification challenges.

- Scale and Size Limitations: A major hurdle is the build volume of current AM machines, which makes the fabrication of large, monolithic aircraft components, such as a full-span MALE UAV wing, difficult or impossible.44

- Quality, Consistency, and Defects: Achieving consistent geometric accuracy and material properties across large builds is a significant challenge. AM processes can introduce defects like porosity, high surface roughness, and significant internal residual stresses, all of which can severely degrade the mechanical performance, particularly the fatigue life, of the finished part.45

- Post-Processing: AM-produced parts, especially complex lattices, often require extensive and costly post-processing steps. These can include the removal of support

structures, surface finishing (e.g., sandblasting, chemical polishing) to improve surface quality, and heat treatment to relieve residual stresses and optimize the material's microstructure.8

- Design for Additive Manufacturing (DfAM): A critical need exists for the maturation of DfAM principles. This involves integrating the specific constraints of the AM process—such as minimum feature size, maximum unsupported overhang angles, and powder removal from internal cavities—directly into the topology optimization algorithm. This ensures that the resulting design is not only optimal in theory but also practically manufacturable without significant redesign.41

The integration of topology optimization and additive manufacturing represents a fundamental change in engineering philosophy. It is a shift from "designing with materials" to "designing the material itself." In traditional design, an engineer selects a material like aluminum or a specific carbon fiber layup, whose properties are well-documented, standardized, and largely uniform. With TO-generated lattices, the structure is the material. Its mechanical properties, such as stiffness and strength, are not uniform; they are heterogeneous and anisotropic, meticulously tailored to the local stress field.55 Furthermore, these properties are not intrinsic but are instead a direct consequence of the AM process parameters, the chosen material, the feature size, and the surface finish.46 A lattice printed on one machine may exhibit different mechanical behavior than the exact same design printed on another. This reality invalidates the traditional handbook-based approach to material properties and creates a massive characterization and validation gap. Each optimized component is, in effect, a novel, uncharacterized metamaterial. This raises a profound third-order challenge: how can an aircraft structure be certified for flight when its constituent material properties are not only complex and anisotropic but are also inextricably linked to the unique manufacturing process that created them? This points to an urgent need for new qualification frameworks that tightly integrate process modeling, in-situ monitoring, and advanced non-destructive testing. Compounding this issue is the extreme computational cost associated with high-fidelity, multi-scale lattice optimization. A full Finite Element Analysis (FEA) that resolves every single strut in a large-scale lattice structure is computationally prohibitive for use within an iterative optimization loop.54 To make the problem tractable, designers often rely on homogenization techniques, where the lattice is mathematically abstracted and represented as a continuum with "effective" or "smeared" properties.8 While computationally efficient, these homogenized models can fail to capture critical, localized failure modes, such as the elastic buckling of individual struts, which may be the very mechanism that governs the ultimate failure of the entire structure.8 This forces designers into

a difficult compromise: using a fast but potentially inaccurate homogenized model for the optimization process, and then relying on a slow, high-fidelity analysis for a few single-point validation checks. This reveals a critical gap in computational mechanics and points to the need for new, highly efficient, and accurate modeling techniques—such as advanced model order reduction or machine learning-based surrogate models—that can bridge the fidelity gap between micro-scale lattice physics and macro-scale component optimization.

2.7 Synthesis : Multidisciplinary Conflicts, Gaps, and Future Directions

The convergence of BWB aerodynamics, solar power systems, and additively manufactured lattice structures creates a design space of immense potential but also of profound complexity. A synthesis of the literature reveals critical conflicts, significant gaps in knowledge, and clear directions for future research that must be pursued to realize this advanced UAV concept.

2.7.1 Conflicting Viewpoints and Ongoing Debates

Across the literature, several key tensions and debates emerge that define the primary challenges in this field. A central, recurring theme is the trade-off between the fidelity of the analysis methods used during design and the associated computational cost.14 Conceptual design benefits from the rapid exploration of a wide design space, which favors low-fidelity tools like panel methods for aerodynamics and beam theory for structures. However, these tools may be insufficient to capture the critical multi-physics interactions inherent to this concept, such as the subtle aerodynamic drag penalties of stability-enhancing features or the local buckling modes of a lattice structure. High-fidelity MDO using CFD and detailed FEA is often computationally intractable, creating a "fidelity gap" that complicates the design process. A second debate centers on structural philosophy. Should designers pursue an evolutionary path, optimizing traditional composite semi-monocoque structures 23, or a revolutionary one, adopting the more radical lattice structure paradigm? While lattices offer the highest theoretical performance 42, they are a less mature technology, carrying significant manufacturing, characterization, and certification risks.44 Advanced composites, while perhaps less optimal, are a known quantity with established design and qualification pathways.43 Finally, the BWB platform enables novel system integration strategies that present their own set of trade-offs. The literature discusses concepts like distributed electric propulsion (DEP), which can offer aero-propulsive benefits by ingesting the boundary layer but adds significant system complexity.57 Similarly, the placement of batteries presents a

choice: they can be consolidated near the center of gravity for easier management, or they can be distributed throughout the wing structure, where their mass can be used to alleviate wing bending loads, effectively making them part of the load-bearing structure.37 This latter approach offers structural efficiency but complicates thermal management and electrical wiring. These fundamental trade-offs are summarized in Table 3.

Table 2.3: Summary of Key Design Trade-offs

Trade-off	**Conflicting Parameters**	**Key Influencing Factors**
Endurance vs. Payload	Flight Time vs. Mission Equipment Mass	Solar cell efficiency, battery specific energy, structural weight fraction.
Aerodynamic Efficiency vs. Stability	Lift-to-Drag Ratio (L/D) vs. Static/Dynamic Stability	BWB's tailless configuration requires control surfaces (e.g., stabilizers, winglets) that add drag.
Structural Weight vs. Manufacturing Risk	Mass Reduction vs. Technology Readiness Level	Radical lightweighting with AM lattices offers high performance but carries significant manufacturing and certification risk compared to mature composites.
Power Generation vs. Aerodynamic Performance	Solar Array Area vs. Skin Friction Drag	Covering wings with solar cells increases available power but can disrupt smooth laminar flow, increasing aerodynamic drag.
Operational Altitude vs. System Constraints	Solar Irradiance vs. Thermal/Pressure Environment	High altitude provides better solar radiation but imposes extreme low-temperature and low-pressure conditions on batteries and electronics.

2.7.2 Gaps in the Current Literature

A critical analysis of the existing research reveals several significant gaps that currently impede progress:

- **Gap 1: Lack of a Holistic, Multi-Scale, Multi-Physics MDO Framework;**

The most profound gap is the absence of a truly unified MDO framework capable of concurrently optimizing the key interacting disciplines. Current approaches tend to optimize BWB aerodynamics, the time-variant solar energy ecosystem, and the anisotropic, process-dependent mechanics of AM lattice structures in a sequential or loosely coupled manner. This approach inherently misses crucial cross-disciplinary trade-offs and synergies, likely leading to sub-optimal global designs.

- **Gap 2: Scarcity of Experimental Data for Large-Scale Aerospace Lattice Structures.** While numerous studies analyze the mechanical properties of small, coupon-sized lattice samples fabricated via (AM) there is a stark lack of published experimental data on the manufacturing and testing of large-scale (i.e., meter-span) primary aerospace structures, such as a representative UAV wing box, built with topology-optimized lattices. The performance of such structures under realistic flight loads—including fatigue, vibration, thermal cycling, and damage—is largely unknown. The discrepancy between the performance predicted by idealized computational models and the actual performance of as-built structures represents a major area of uncertainty.

- **Gap 3: Insufficient Research into Multifunctional Lattice Structures.** The literature focuses overwhelmingly on the mechanical (load-bearing) properties of lattice structures. However, their inherent porosity offers tantalizing potential for multifunctionality. A clear gap exists in research that explores the design of lattices that are optimized to simultaneously provide structural support while also performing other functions, such as acting as integrated heat sinks for the thermal management of batteries and electronics 59, providing tailored vibration damping to protect sensitive payloads [4], or housing embedded sensors.

2.8 Conclusion

2.8.1 Summary of Findings

This review has explored the nexus of three innovative technologies—Blended-Wing-Body aerodynamics, solar propulsion, and additively engineered lattice structures—as a possible way to a novel new generation of Medium-Altitude, Long-Endurance UAVs with unmatched persistence. The literature confirms the extensive theoretical potential in this method. The BWB airframe offers a a basis for aerodynamics that is well beyond traditional designs. Solar power provides a strategy to harness power in-flight, breaking the shackles of fuel-limited endurance. Finally, topology-optimized lattice structures possess a game-changing

lightweighting capability, which is key to the viability of the overall concept by offsetting the great mass drawbacks of the solar power system and the special structural requirements of the BWB.

2.8.2 Reinforcement of Core Challenges

Yet the process of achieving this potential is fraught with significant multidisciplinary hurdles. challenges. Its aerodynamic grace is compromised by its intrinsic instability and inefficient structural load paths. The goal of sustained solar flight is trapped in a "vicious cycle." in relation to weight and power, whereby the systems used for endurance also maximize the power output critical to flight. We are primarily interested in the novel lattice structures offering weight Problems are constrained by significant factors in manufacturing, modeling, and certification. Challenges. The complexity of these interlinked systems renders a design space in which sequential or loosely coupled optimization is bound to fail.

2.8.3 Justification for Thesis Work

The issue laid out in Chapter 1 sets a clear and real technology gap: conventional aircraft design is not adequate to meet the multifaceted and wide-ranging demands stipulated by the Satellite Development Center (CDS) for a multi-mission MALE testbed. The extensive literature review created in Chapter 2 reinforces the justification of why the gap remains. The results suggest that while a promising solution arises at the confluence of Blended-Wing-Body aerodynamics, solar energy harvesting, and the use of additively manufactured lattice structures, its realization is currently thwarted by substantial, interdisciplinary conflicts.

This thesis is therefore justified as a direct and necessary response to the critical shortcomings identified in the literature. It directly confronts the main challenge—the lack of an integrated, multi-physics multidisciplinary design optimization (MDO) framework (Gap 1)—by creating and validating a unified computational strategy that can handle the complex trade-offs involved between aerodynamic efficiency, weight, and mission duration. This work goes beyond theoretical deliberations by creating a tangible, optimized design basis specific to the given mission profile.

With this project, the present thesis establishes a fundamental prerequisite for tackling the following challenges concerning overall structural realization and empirical validation (Gap 2). It provides a clear and step-by-step way from the initial concept to a tangible prototype that is able to produce the vast experimental data that are presently lacking in the discipline.

This work is more than an incremental advance; it is, rather, a conceptual contribution that delivers the supported design principles necessary to close the theoretical capabilities and the physical, high-performance flying platform essential to furthering national scientific and technological missions.

Chapter 3

Design Methodology

3.1 Introduction

The conceptual design of an aircraft represents a difficult engineering challenge, characterized by a complicated network of complex and often conflicting interactions between multiple disciplines and objectives such as aerodynamics, structures, propulsion, and performance.

Historically, design proceeded sequentially, with decisions in one discipline passed "over the wall" to the next in a feedback loop, this approach, however, often leads to suboptimal outcomes with long lead times, as it fails to capture the synergistic or antagonistic relationships between disciplines and for that Multidisciplinary Design Optimization (MDO) has emerged as an indispensable methodology to address this complexity, providing a formal, mathematical framework for exploring the design space in a holistic manner, by considering all relevant disciplines simultaneously.

MDO enables the discovery of superior designs that exploit these interdisciplinary couplings, leading to solutions that are difficult or impossible to achieve through the traditional sequential optimization which gave this integrated approach a significant and pronounced presence in the conceptual design phase, and while this early stage accounts for a small fraction of the total program expenditure, the decisions made here commit the vast majority of the aircraft's lifecycle cost, consequently, the ability to conduct robust analysis, explore a wide range of alternatives, and make informed trade-offs at this juncture is of paramount importance.

This chapter presents a detailed examination of a custom computational framework, developed entirely in the Python programming language, for the initial design and optimization

of the UAV. It provides a comprehensive deconstruction of the framework's architecture, the analytical fidelity of its core disciplinary models, and its application in a multi-objective optimization study, this framework utilizes a Non-dominated Sorting Genetic Algorithm II (NSGA-II) to navigate the intricate design space and identify a set of globally optimal aircraft configurations that balance competing performance objectives, but in our case and our study endurance will be given top priority in our choice

3.2 Optimization Methodology and Framework Architecture

The successful navigation of the complex and constrained design space described in the introduction necessitates a sophisticated optimization strategy. To this end, the core of the design methodology is a Multi-objective Evolutionary Algorithm (MOEA), specifically the Non-dominated Sorting Genetic Algorithm II (NSGA-II). The selection of NSGA-II is predicated on its proven efficacy in solving non-linear, multi-modal, and constrained problems characteristic of conceptual aircraft design. Its architecture is built upon several key mechanisms that collectively ensure both convergence towards the true set of optimal solutions and a comprehensive mapping of the inherent design trade-offs.

The operational principles of the NSGA-II algorithm can be deconstructed into three fundamental components:

- **Non-Dominated Sorting:** The algorithm's primary innovation is its method for ranking solutions in a multi-objective landscape. In such a landscape, the notion of a single "best" solution is often ill-defined. Instead, solutions are evaluated using the concept of Pareto dominance. A design solution **A** is said to dominate solution **B** if it is superior or equal to **B** across all objectives and strictly superior in at least one. NSGA-II begins by sorting the entire population of candidate designs into a hierarchy of non-dominated "fronts." The first front, designated F_1, comprises the set of Pareto-optimal individuals—those that are not dominated by any other solution in the population. The second front, F_2, contains solutions that are only dominated by individuals in F_1, and this sorting continues until the entire population is ranked.

- **Elitism:** NSGA-II is an elitist algorithm, a critical feature that guarantees the preservation of high-performing solutions across generations. At each iteration, the parent population and its generated offspring are combined. The non-dominated sorting procedure is then applied to this combined, larger population. The best individuals—those

residing in the highest-ranked fronts (F_1, F_2, etc.)—are selected to form the parent population for the subsequent generation. This mechanism prevents the loss of elite solutions due to stochastic sampling effects and promotes a steady convergence toward the true Pareto-optimal front.

- **Diversity Preservation via Crowding Distance:** A significant challenge in multi-objective optimization is avoiding premature convergence to a small, clustered region of the Pareto front. To ensure the final set of solutions represents the full spectrum of available trade-offs, NSGA-II employs a diversity preservation mechanism known as the **"crowding distance."** For all solutions within the same non-dominated front, the algorithm calculates the average distance of a solution to its nearest neighbors along each objective axis. This metric quantifies the density of solutions in the objective space. When selecting individuals from a front to carry over to the next generation, preference is given to those with a higher crowding distance (i.e., those located in sparser regions). This process actively encourages exploration and results in a well-distributed set of optimal solutions.

The exploration of the design space is driven by genetic operators, specifically Simulated Binary Crossover (SBX) and Polynomial Mutation (PM), which are adept at handling the continuous, real-valued variables typical of engineering problems. A crucial aspect of the implemented methodology is its adaptation of the standard NSGA-II output. Whereas the algorithm is designed to generate a Pareto front representing a set of optimal trade-off solutions, this study automates the selection process to align with its primary research objective.

Upon the termination of the optimization run, the framework does not present the full Pareto set to the designer. Instead, it systematically interrogates the final population and programmatically extracts the single design configuration that demonstrates the maximum calculated endurance.

This hybrid approach uniquely harnesses the robust exploratory power of a multi-objective search to thoroughly map the solution space, yet delivers a deterministic, single-point solution optimized explicitly for the most critical performance metric.

3.3 The Integrated Computational Framework

The NSGA-II algorithm serves as the engine for a broader, integrated computational framework developed to execute this MDO study. This framework automates the entire conceptual design loop, from the generation of a candidate design to its multi-faceted performance evaluation. The architecture is built upon two foundational pillars: a parametric definition of the aircraft and a series of interconnected disciplinary analysis modules.

3.3.1 Parametric Vehicle and Mission Representation

The aircraft is not defined by a fixed geometry but is instead represented by a vector of 16 design variables that serve as the genetic code for the optimization algorithm. These variables define the aircraft's geometry, its propulsion system and energy storage system, performance metrics and some safety metric related to thermal management, allowing for a comprehensive exploration of the design space. The variables include:

- **Geometric Parameters:** Wing span defined in the code as **`(b_wing_span)`**, wing area **`(s_wing_area)`**, and mean geometric chord **`(MGC_wing)`**, scale factor **`sf_scale_factor`**
- **Propulsion and Power System Parameters:** Motor Kv rating **`(kv_motor_rpm_volt)`**, propeller diameter **`(Prop_D_propeller)`**, and the battery system configuration **`(num_cells_series_batt, C_cells_parallel)`**.
- **Performance Metrics:** Target cruise true air speed **`(u_aircraft_velocity)`**, rate of climb **`(u_vertical_climb_target)`**, and liftoff velocity **`(u_liftoff)`**

3.3.2 Disciplinary Analysis Modules

For each unique design vector generated by the algorithm, a sequence of analysis modules evaluates its viability and performance. These modules are composed of physics-based models that simulate the aircraft's behavior.

- **Weight & Sizing:** The aircraft's gross takeoff weight is dynamically calculated. The weight of the battery system, a function of the number and capacity of its cells, is added to the baseline structural and payload weights. This ensures that the performance cost of a larger energy store is rigorously accounted for
  the equation is represented as follows :
  $W_{\text{aircraft}} = (W_{\text{structural}} + (C_{\text{cells_parallel}} \cdot N_{\text{cells_series}}) \cdot 0.049 + ((C_{\text{cells_parallel}} \cdot N_{\text{cells_series}}) \cdot 0.049) \cdot 0.1 + W_{\text{payload}}) \cdot g$.

where the term $[(C_{\text{cells_parallel}} \cdot N_{\text{cells_series}}) \cdot 0.049]$ represents the battery weight, and the the value **0.049** represents the weight of a single Li-Ion cell, the same term is then multiplied by **0.1** and then add to the weight equation to account for wiring of the system.

- **Aerodynamics:** This module computes the aircraft's aerodynamic characteristics. The parasite drag coefficient (CD0) is estimated using a skin-friction-based approach dependent on the Reynolds number, augmented by empirical values for surface imperfections. The induced drag is calculated as a function of the lift coefficient, wing aspect ratio, and the Oswald efficiency factor and they were governed by the following equations :

$$Re_{\text{cruise}} = \frac{\rho_{\text{cruise}} \cdot u_{\text{aircraft}} \cdot \text{MGC}}{\mu_{\text{cruise}}} \tag{3.1}$$

$$C_{f_{\text{cruise}}} = \begin{cases} \frac{1.328}{\sqrt{Re_{\text{cruise}}}} & \text{if } Re_{\text{cruise}} < 5 \times 10^5 \\ \frac{0.455}{(\log_{10}(Re_{\text{cruise}}))^{2.58}} & \text{if } Re_{\text{cruise}} \geq 5 \times 10^5 \end{cases} \tag{3.2}$$

$$FF = 1 + 2(t/c) + 60(t/c)^4 \tag{3.3}$$

$$AR = \frac{b^2}{S} \tag{3.4}$$

$$e = (1.78(1 - 0.045 \cdot AR^{0.68}) - 0.64) \cdot e_{\text{correction}} \tag{3.5}$$

$$k = \frac{1}{\pi \cdot e \cdot AR} \tag{3.6}$$

$$S_{\text{wet}} = 2S(1 + 0.2(t/c)) \tag{3.7}$$

$$C_{D0} = C_{f_{\text{cruise}}} \cdot FF \cdot \frac{S_{\text{wet}}}{S} + C_{D0_{\text{imperfections}}} \tag{3.8}$$

$$C_D = C_{D0} + C_{Di} \tag{3.9}$$

Note that $e_{\text{correction}}$ and $C_{D0_{\text{imperfections}}}$ are corrective values added into the algorithm after experimental validation to increase the fidelity of the framework.

- **Propulsion & Power System:** A detailed powertrain model simulates the energy flow from the battery to the propeller. It calculates the motor's shaft power, torque, and efficiency based on its Kv rating, internal resistance, and operating current. The energy consumed during the takeoff and climb phases is calculated via time-stepped simulations **`(energy_for_takeoff, energy_for_climb)`**, and this value is subtracted from

the total battery capacity to determine the energy available for the cruise segment, for the cruise and climb phases the following equations were used to model the power :

$$K_t = \frac{9.5493}{K_v} \tag{3.10}$$

$$K_e = \frac{60}{2\pi K_v} \tag{3.11}$$

$$Q_m = K_t(I_{\text{total}} - I_0) \tag{3.12}$$

$$\omega = \frac{V_{\text{bemf}}}{K_e} \tag{3.13}$$

$$P_{\text{shaft}} = Q_m \cdot \omega \tag{3.14}$$

$$P_{\text{elec}} = V_{\text{batt}} \cdot I_{\text{total}} \tag{3.15}$$

$$\eta_{\text{motor}} = \frac{P_{\text{shaft}}}{P_{\text{elec}}} \tag{3.16}$$

then thrust to weight required was calculated using an equation from general aviation design [15], which will then allow us to determine the propulsive power required and the propeller efficiency, which will be used to calculate the energy used consumed

$$\frac{T}{W} = \frac{V_v}{V} + \frac{q}{W/S} C_{D_{\min}} + \frac{k}{q}\left(\frac{W}{S}\right) \tag{3.17}$$

$$T_{\text{req}} = \left(\frac{T}{W}\right)_{\text{req}} \cdot W \tag{3.18}$$

$$P_{\text{prop}} = T_{\text{req}} \cdot V_{\text{climb}} \tag{3.19}$$

$$\eta_{\text{prop}} = \frac{P_{\text{prop}}}{P_{\text{shaft}}} \tag{3.20}$$

$$P_{\text{elec}} = \frac{P_{\text{prop}}}{\eta_{\text{total}}} \tag{3.21}$$

and for the takeoff phase the same power calculations were used, but the difference in calculation is in the thrust required, since the UAV will start from 0 velocity modeling the transition from static to dynamic thrust is required and it was achieved using the following equations :

$$T_{\text{ideal_static}} = (P_{\text{shaft}})^{2/3}(2\rho_0 A_{\text{prop}})^{1/3} \tag{3.22}$$

$$T_{\text{static}} = T_{\text{ideal_static}} \cdot \text{FoM} \tag{3.23}$$

$$f_v = \begin{cases} \left(\frac{V}{V_{\text{liftoff}}}\right) V_{\text{factor_max}} & \text{if } V_{\text{liftoff}} > 0 \\ 0 & \text{otherwise} \end{cases} \tag{3.24}$$

$$T_{\text{avail}} = T_{\text{static}} \left(1 - \min(f_v, V_{\text{factor_max}})\right), \quad \text{where } T_{\text{avail}} \geq 0 \tag{3.25}$$

- **Performance & Mission Simulation:** The framework evaluates key performance metrics and ensures compliance with mission requirements. This includes a simulation of the takeoff ground roll **`(sg_calc)`** and a check of the aircraft's ability to achieve the desired rate of climb. The primary endurance objective is calculated based on the remaining battery energy and the power consumption during cruise, the equation used to estimate the endurance of the aircraft was taken from a 2011 article on the range and endurance estimation of battery powered aircraft [16] :

$$E_{\text{max}} = \left(\frac{E_{\text{avail}}}{\frac{1}{2}\rho u^3 S C_{D_{\text{min}}} + \frac{2W^2 k}{\rho u S}}\right)^{1.2} \tag{3.26}$$

  where the power term is the a coefficient for Li-Ion batteries which accounts for high capacity batteries' discharge rate.

3.3.3 Formulation of the Optimization Problem

The design challenge is formally posed as a constrained, multi-objective optimization problem. The framework seeks to simultaneously optimize four competing objectives, with a search that is governed by 25 inequality constraints that enforce physical and operational limits, such as ensuring a safe stall margin, preventing propeller tips from exceeding a critical Mach number, limiting motor current to prevent overheating, and ensuring the takeoff distance is within a specified maximum.

This complete problem formulation provides a robust mathematical basis for the NSGA-II algorithm to systematically explore the design space. Although four objectives are used to guide the search and ensure a well-rounded exploration of design trade-offs, the process

culminates in the automated extraction of a single solution. From the final population of the optimization run, the framework identifies and outputs the specific design configuration that yields the maximum calculated endurance, thereby directly addressing the primary goal of this investigation the following image is a flow chart that represents the aforementioned process :

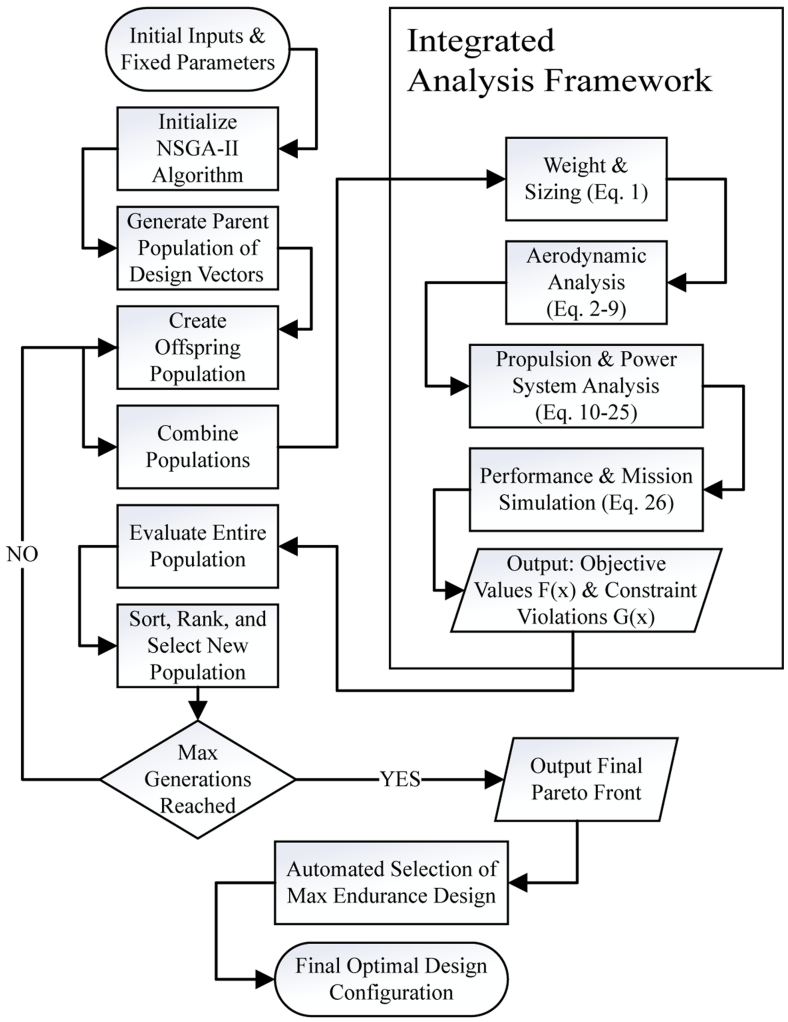

Figure 3.1: Flow chart for the Design framework

3.4 Airfoil Selection

The selection of an appropriate airfoil is a cornerstone of aircraft design, as it fundamentally governs the aerodynamic efficiency and, consequently, the endurance of the aircraft. For a long-endurance UAV, where flight time is the primary performance metric, an airfoil must be chosen that maximizes the lift-to-drag ratio (L/D) at the intended cruise flight condition, while also ensuring safe and predictable behavior across the entire flight envelope.

To navigate the trade-offs between multiple competing airfoil characteristics, this study adopted a structured evaluation methodology highlighted by Dr. Snorri Gudmundsson [15]. This approach utilizes a semi-quantitative grading system to provide a decisive and objective comparison between several candidates based on a set of desired parameters. For this design, six promising airfoils were identified as candidates: LW109A, NACA23015, NACA65(2)-415, NACA65(2)-415 with a=0.5, NACA66(3)-418, and NACA747A415.

Each candidate was evaluated against a set of critical aerodynamic and performance criteria relevant to a long-endurance mission:

- **Maximum Lift Coefficient** ($C_{l_{max}}$)**:** A higher value is desirable as it contributes to better takeoff performance and a wider stall margin at cruise.
- **Maximum Lift-to-Drag Ratio** $(C_l/C_d)_{max}$**:** This is arguably the most critical parameter for endurance. A higher ratio signifies greater aerodynamic efficiency, directly translating to lower power consumption during cruise. The NACA65(2)-415 (a=0.5) showed the highest value at 128.
- **Minimum Drag Coefficient** ($C_{d_{min}}$)**:** A lower value is preferred to minimize parasite drag.
- **Stall Characteristics:** A "Smooth" stall is a crucial safety feature, as it provides the pilot or autopilot with adequate warning and maintains controllability. An "Abrupt" stall, as seen with the NACA23015, is undesirable.
- **Pitching Moment Coefficient** (C_m)**:** A value closest to zero is ideal to minimize the trim drag required from the control surfaces to maintain level flight.
- **Drag Bucket:** It is highly advantageous for the aircraft's cruise lift coefficient to fall within the airfoil's low-drag "bucket" to ensure flight occurs at peak efficiency.

- **Sensitivity to Surface Quality:** Airfoils that are less sensitive to surface imperfections (dirt, bugs, manufacturing flaws) are more robust for real-world operations.

The six candidates were graded against these criteria, and their performance is summarized in Tables 1.4 and 1.5. The final scores, presented in Tables 1.6 and 1.7, quantify the overall suitability of each airfoil for the mission.

Upon final evaluation, the LW109A airfoil was selected, having achieved the highest score of 6.5. While other airfoils like the NACA65(2)-415 variants showed a higher maximum lift-to-drag ratio, the LW109A presented the best overall balance of characteristics. Its selection was justified by its favorable cruise efficiency (with both cruise and best ROC C_l in the drag bucket), smooth stall characteristics, and a relatively high ($C_{l_{max}}$) of 1.23 as well as it's thickness, making it the most robust and well-rounded choice to maximize the primary objective of flight endurance.

Table 3.1: Airfoil Grading Part I

Parameter	**LW109A**	**NACA23015**	**NACA65(2)-415**
Thickness Ratio	**18.71** %	15 %	15 %
Sensitive to surface quality?	Yes	**No**	Yes
C_l at $\alpha = 0$[a]	0.019	0.12	0.35
$C_{l,\max}$[b]	1.23	**1.62**	1.365
α at $C_{l,\max}$ (deg)[b]	**19**	16	16
Stall characteristics	**Smooth**	Abrupt	**Smooth**
$C_{d,\min}$[c]	0.0078	0.0069	**0.0065**
$(C_l/C_d)_{\max}$[b]	76	90	**115**
α at $(C_l/C_d)_{\max}$ (deg)[c]	5	9	**4.5**
Cruise C_m[d]	0.027	**-0.008**	-0.078
Is cruise C_l in drag bucket?	**Yes**	No	**Yes**
Is best ROC C_l in drag bucket?	**Yes**	No	**Yes**

[a] Closest to cruise C_l is best. [b] Highest is best. [c] Lowest is best. [d] Closest to zero is best.

Table 3.2: Airfoil Grading Part II

Parameter	**NACA65(2)-415 a=0.5**	**NACA66(3)-418**	**NACA747A415**
Thickness Ratio	15 %	**18** %	15 %
Sensitive to surface quality?	Yes	Yes	Yes
C_l at $\alpha = 0$[a]	0.3	0.35	0.217
$C_{l,\max}$[b]	**1.33**	1.268	1.278
α at $C_{l,\max}$ (deg)[b]	17	18	**19**
Stall characteristics	Smooth	Smooth	Smooth
$C_{d,\min}$[c]	0.0067	0.0072	**0.0064**
$(C_l/C_d)_{\max}$[b]	**128**	116	113
α at $(C_l/C_d)_{\max}$ (deg)[c]	5.5	**5**	6.5
Cruise C_m[d]	-0.057	-0.077	**-0.027**
Is cruise C_l in drag bucket?	No	**Yes**	**Yes**
Is best ROC C_l in drag bucket?	Yes	Yes	Yes

[a] Closest to cruise C_l is best. [b] Highest is best. [c] Lowest is best. [d] Closest to zero is best.

Table 3.3: Final Scores: Part I

Airfoil	**LW109A**	**NACA23015**	**NACA65(2)-415**
Score	**6.5**	4	4.5

Table 3.4: Final Scores: Part II

Airfoil	**NACA65(2)-415 a=0.5**	**NACA66(3)-418**	**NACA747A415**
Score	3	4.5	**6**

3.5 Optimization Results

The computational framework was executed to yield an optimal design point. The process involved two principal stages: an initial optimization based on theoretical aerodynamic data, followed by a final optimization incorporating experimental data. This iterative approach demonstrates the framework's ability to adapt to increasing levels of fidelity in its disciplinary models.

3.5.1 Preliminary Design Configuration (Theoretical CLmax)

The first optimization run was conducted using a theoretical maximum lift coefficient (CLmax) for the selected airfoil, derived from 2D aerodynamic computational tools. This run produced a preliminary design point optimized for maximum endurance under these idealized conditions. The key parameters of this configuration are summarized in the following table :

Table 3.5: Preliminary Optimal Design Parameters

Parameter	**Value**
Performance	
Optimized Endurance	9.61 hours
Total Aircraft Weight	15.58 kg
Cruise Speed	13.45 m/s
Geometry	
Wing Span	4.00 m
Wing Area	2.20 m^2
Aspect Ratio	7.28
Propulsion System	
Battery Capacity	87.53 Ah
Motor Kv Rating	185 RPM/Volt
Aerodynamics (Cruise)	
Cruise Lift Coefficient (C_L)	0.905
Parasite Drag Coefficient (C_{D0})	0.0215

3.5.2 Final Design Configuration (Corrected CLmax)

Following the preliminary design, wind tunnel testing was conducted on a scaled model to determine the actual three-dimensional CLmax of the aircraft configuration. This experimentally-derived value, which accounts for 3D effects and potential manufacturing imperfections, was lower than the theoretical 2D value. The optimization framework was executed a second time with this corrected, higher-fidelity aerodynamic input. The resulting final design configuration is detailed in following table :

Table 3.6: Final Optimal Design Parameters

Parameter	**Value**
Performance	
Optimized Endurance	7.40 hours
Total Aircraft Weight	12.84 kg
Cruise Speed	13.61 m/s
Geometry	
Wing Span	4.00 m
Wing Area	2.49 m^2
Aspect Ratio	6.41
Propulsion System	
Battery Capacity	59.57 Ah
Motor Kv Rating	531 RPM/Volt
Aerodynamics (Cruise)	
Cruise Lift Coefficient (C_L)	0.642
Parasite Drag Coefficient (C_{D0})	0.0216

A comparison of the two results reveals the significant impact of incorporating higher-fidelity experimental data. The more realistic (and lower) CLmax forced the optimizer to find a fundamentally different solution to maximize endurance. The final design is notably lighter (12.84 kg vs. 15.58 kg), achieved primarily by reducing the battery capacity by over 30%.

To compensate for the reduced lift capability and maintain flight, the wing area was increased, resulting in a lower wing loading and a lower aspect ratio. The propulsion system was also drastically altered, shifting to a much higher Kv motor. This adaptation, while logical from a multidisciplinary perspective, resulted in a 23% reduction in the achievable endurance.

This outcome underscores the critical importance of iterative design refinement and the value of integrating experimental data within an MDO framework to converge on a feasible and realistic solution.

Table 3.7: Comparison of Preliminary and Final Optimal Design Configurations.

Parameter	**Preliminary**	**Final**	**Change (%)**
Performance			
Endurance (hours)	9.61	7.40	−23.00
Total Weight (kg)	15.58	12.84	−17.60
Cruise Speed (m/s)	13.45	13.61	1.20
Geometry			
Wing Span (m)	4.00	4.00	0.00
Wing Area (m^2)	2.20	2.49	13.20
Aspect Ratio	7.28	6.41	−12.00
Propulsion System			
Battery Capacity (Ah)	87.53	59.57	−31.90
Motor Kv (RPM/Volt)	185.00	531.00	187.00
Aerodynamics (Cruise)			
Lift Coefficient (C_L)	0.91	0.64	−29.10
Parasite Drag (C_{D0})	0.02	0.02	0.50

3.6 Summary

This chapter detailed the development and application of a custom Multidisciplinary Design Optimization (MDO) framework for the conceptual design of a long-endurance Blended Wing Body UAV. The methodology was architected around the Non-dominated Sorting Genetic Algorithm II (NSGA-II), which was coupled with a series of physics-based disciplinary modules to evaluate aircraft weight, aerodynamics, and powertrain performance. Prior to optimization, a critical design choice was made through a structured airfoil selection process. Following a grading methodology that evaluated six candidates on key performance metrics, the LW109A airfoil was chosen for its balanced characteristics suitable for long-endurance flight.

The framework was then used to automate the exploration of a complex, 16-variable design space and programmatically select an optimal configuration based on the primary objective of maximizing flight endurance. The results were presented in a two-stage process that highlights the importance of iterative design refinement. An initial, preliminary design was generated using theoretical aerodynamic data, yielding a predicted endurance of 9.61 hours. This design was then refined in a second optimization run that incorporated a lower, experimentally-derived maximum lift coefficient (CLmax) obtained from wind tunnel testing.

The comparison between the two configurations revealed the significant impact of integrating higher-fidelity data. The final, more realistic design was fundamentally different, featuring a 17.6% reduction in total weight and a 13.2% increase in wing area to compensate for the reduced lift capability. This necessary adaptation, driven by real-world constraints, resulted in a final achievable endurance of 7.40 hours. This outcome underscores the critical value of the MDO framework as a tool for navigating complex design trade-offs and demonstrates that integrating experimental data is essential for converging on a feasible and realistic aircraft design.

Chapter 4

Integrated Design, Analysis, and Validation

4.1 Introduction

The successful multidisciplinary optimization detailed in Chapter 3 provided a set of refined design parameters for a high-endurance BWB UAV. However, these parameters represent a theoretical optimum. This chapter documents the critical process of translating that theoretical solution into a physically realizable, aerodynamically stable, and structurally sound aircraft, ready for prototyping. It details a rigorous, iterative workflow that bridges the gap between computational optimization and real-world performance.

The methodology described herein deviates from a linear design sequence, instead adopting a modern, iterative loop of computational analysis, experimental validation, and design refinement. This chapter will first detail the aerodynamic and stability validation process, beginning with geometry generation in OpenVSP and progressing through Vortex Lattice Method (VLM) analysis, high-fidelity Computational Fluid Dynamics (CFD) in Ansys Fluent, and crucial validation against wind tunnel data.

Following this aerodynamic validation and a final design re-optimization, the focus shifts to the core structural challenge: the design of an ultra-lightweight airframe using novel lattice structures. This process, executed in nTop for lightweighting. It details the generation of the gyroid lattices designed to achieve both a strong yet lightweight structure as well as extract the proper moments of inertia of the aircraft to be used in the stability analysis of the aircraft. The chapter culminates with a structural validation using Finite Element

Analysis (FEA) based on a homogenization study of the lattice properties, finally a dynamic stability study was conducted and the final prototype manufacturing started

4.2 Aerodynamic Design and Iterative Validation Loop

The tailless nature of the BWB configuration necessitates a meticulous approach to ensure a well trimmed flight. This was achieved through an iterative process involving low- and high-fidelity computational tools, culminating in experimental validation.

4.2.1 Initial Geometry and Analysis

Based on the final parameters from the optimization framework in Chapter 3, the initial 3D geometry of the BWB airframe was generated using OpenVSP, an open-source parametric aircraft geometry tool. Its development was originally initiated by J.R. Gloudemans and others at NASA in the early 1990s. On January 10, 2012, OpenVSP was released as an open-source project under the NASA Open Source Agreement (NOSA), making it freely accessible to the public.

At its core, OpenVSP is designed for the conceptual design phase of aerospace vehicles. It allows users to create 3D models of aircraft using a parametric approach. This means that the geometry is defined by engineering parameters such as wing span, root and tip chords, sweep angle, and fuselage length and cross-section shape. This parametric nature enables rapid design iterations and trade studies, as modifications to the aircraft's form can be made by simply adjusting these parameters.

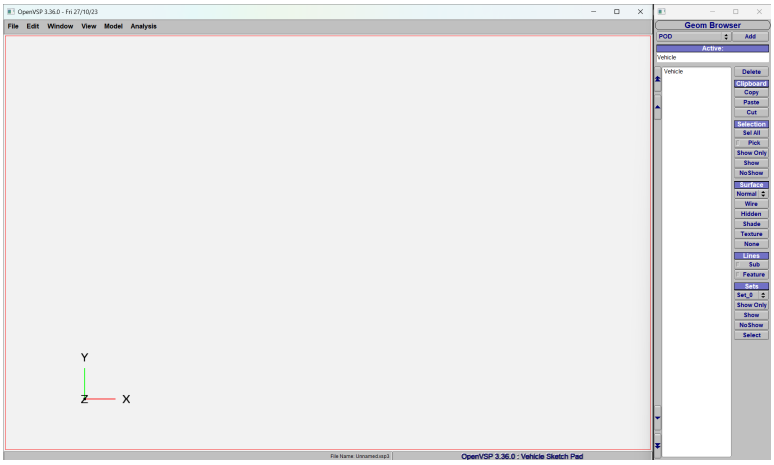

Figure 4.1: OpenVSP UI interface

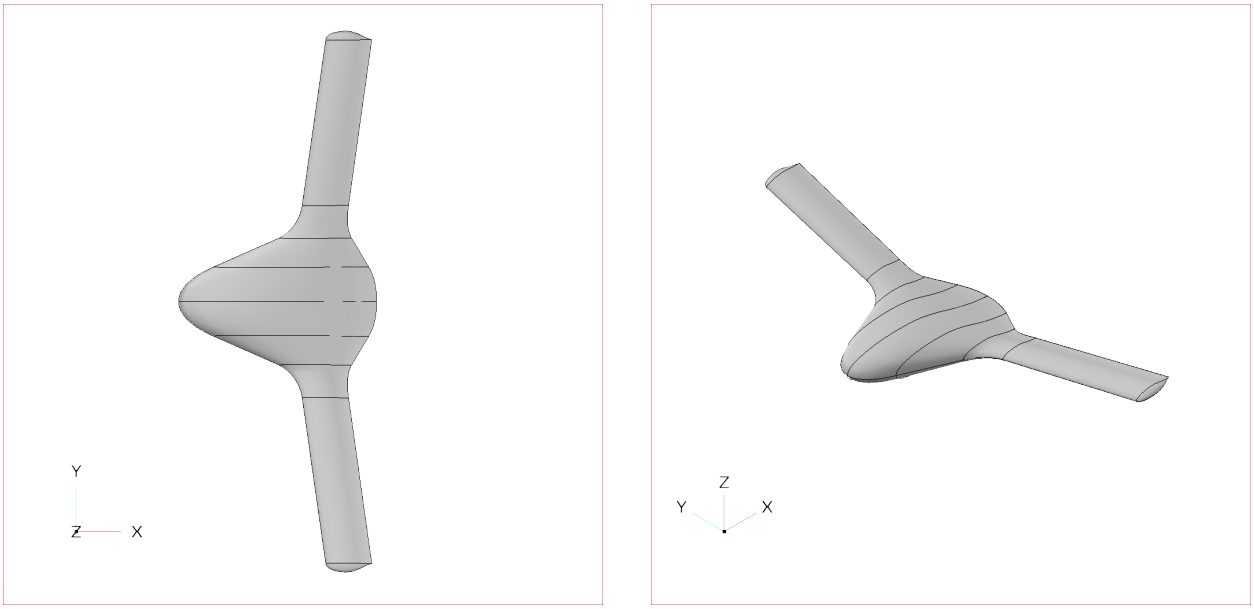

(a) Top View of the 3D UAV model (b) Isometric View of the 3D UAV model

Figure 4.2: 3D openVSP UAV model

OpenVSP is instrumental in establishing a rapid and iterative preliminary validation loop. This is primarily achieved through its integrated VSPAERO tool, which utilizes a low-fidelity but computationally inexpensive Vortex Lattice Method (VLM). This method is particularly well-suited for the conceptual design stage, as it allows for the quick assessment of aerodynamic derivatives, which are crucial for stability analysis which we will elaborate on more later.

The primary objective of this computational step was to determine the aircraft's neutral point—the aerodynamic center for the entire aircraft. The neutral point is a critical parameter for longitudinal static stability. For the aircraft to be inherently stable, its Center of Gravity (CG) must be located forward of the neutral point. The distance between these two points defines the static margin, which is a key measure of the aircraft's tendency to return to a trimmed state after a disturbance.

Using VSPAERO's VLM solver, multiple analyses were run to calculate the pitching moment coefficient (Cm) for a range of angles of attack. By identifying the location where the derivative of the pitching moment coefficient with respect to the angle of attack is zero, the neutral point was precisely located. This analysis allowed for the establishment of a target CG range that ensures a positive static margin, thereby guaranteeing a statically stable flight configuration.

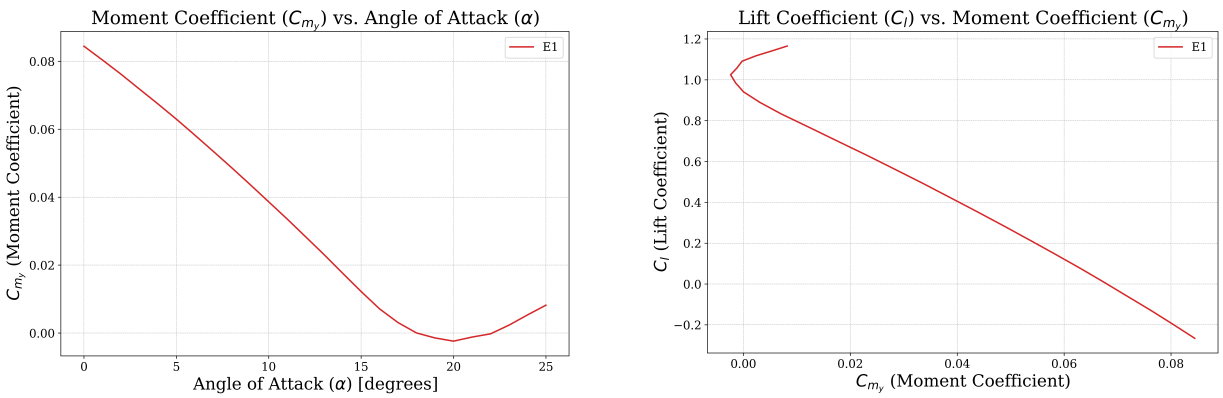

Figure 4.3: openVSP Simulation Results

4.2.2 High-Fidelity CFD Analysis

With a provisionally stable geometry defined and a 3d, the model was exported as a STEP file for high-fidelity aerodynamic analysis using Ansys Fluent. To streamline this computationally intensive process, a Python API script was developed to automate the CFD workflow, mainly physics setup to simulation execution and post-processing.

High-Fidelity Mesh Generation with the Ansys Fluent Watertight Workflow

The generation of a high-quality computational mesh is the foundation upon which reliable and accurate Computational Fluid Dynamics (CFD) simulations are built. The mesh discretizes the geometric domain into a finite number of cells where the governing equations of fluid motion are solved. Consequently, the quality, density, and topology of the mesh directly influence the accuracy, convergence stability, and computational speed of the simulation. Recognizing the critical and often time-consuming nature of this pre-processing step, Ansys has developed a suite of sophisticated meshing tools within its Fluent software. Among these are guided, task-based workflows designed to streamline the process for engineers.

The development of distinct meshing workflows within Ansys Fluent is not merely an addition of features; it represents a fundamental strategic approach to CFD pre-processing. This strategy acknowledges that engineers operate in two disparate realities defined by the quality of their input geometry. One reality involves idealized, "clean" CAD from a controlled and modern design process, while the other involves complex, "dirty" geometry originating from legacy systems, reverse engineering, or large, multi-component assemblies. The Watertight Geometry workflow is the embodiment of the "ideal path," designed to offer maximum speed

and automation when starting with geometrically perfect models.

The term "watertight" has its origins in the field of computer graphics, where it is used to describe a mesh that constitutes a single, perfectly closed surface. A watertight mesh has no holes, gaps, or self-intersections, and thus possesses a clearly defined interior and exterior volume. Formally, it is defined as a 2-manifold mesh where every edge is shared by exactly two faces, meaning there are no "boundary edges".

In the context of CFD, this concept is adopted directly. A watertight geometry is one that is considered "clean," "closed," and free of any leaks that would prevent it from holding a fluid if it were a physical container. This state is the ideal starting point for many CFD simulations because it removes ambiguity in defining the boundaries between fluid and solid domains. The alternative, an "unwatertight" mesh, preserves holes and gaps. While this is desirable for applications like reverse engineering or metrology where the as-is condition of a part must be captured, it is unsuitable for volumetric meshing required by CFD, where a closed domain is necessary to contain the mesh cells.

The Ansys Fluent user interface presents the Watertight Geometry workflow as a clear, sequential list of tasks in a dedicated pane. This guided structure is a key usability feature, as it logically orders the complex series of operations required to generate a high-fidelity mesh. Each task represents a major step in the process, and completing them in sequence ensures that all dependencies are met. For example, a surface mesh must be generated before boundary layers can be added. This task-based approach simplifies the user experience, provides a clear roadmap from start to finish, and helps prevent common errors, particularly for those new to CFD meshing.

The following steps outline the typical progression through the Watertight Geometry workflow, combining the conceptual tasks seen in the GUI with the underlying scriptable commands that can be accessed via PyFluent.

- **Import Geometry:** The process begins by importing the prepared, watertight CAD model into Fluent. Supported formats include native CAD files as well as Ansys-specific formats like .pmdb. At this stage, it is critical to specify the correct length unit (e.g., mm, in) to ensure the model is scaled properly.
- **Describe Geometry:** This crucial task informs Fluent about the nature of the model. The user specifies whether the geometry consists of only fluid regions, only solid regions, or a combination of both. This description dictates which subsequent tasks are

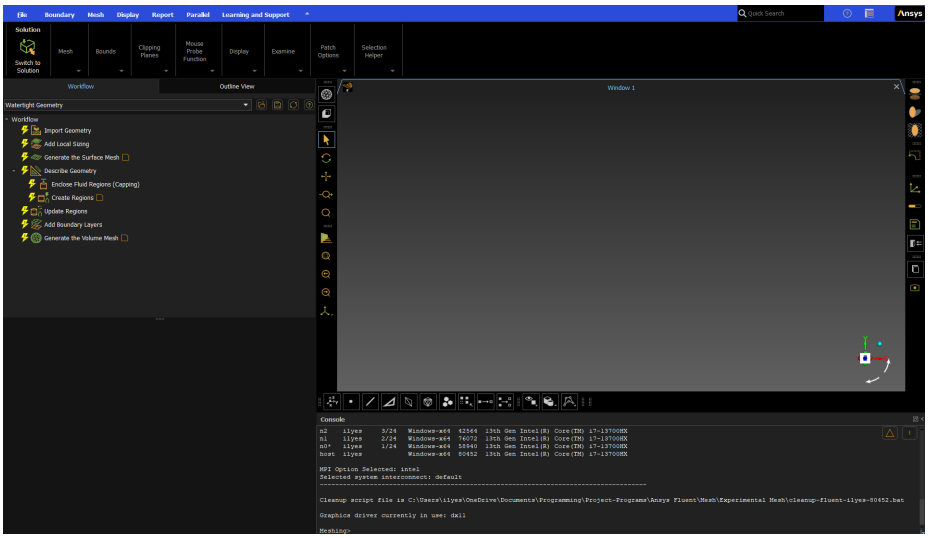

Figure 4.4: Fluent Watertight Meshing Workflow Interface

required. For example, if the user imports a solid body and describes the geometry as intended for an external flow simulation, Fluent will automatically add tasks for creating a fluid volume around the solid.

- **Update Boundaries and Regions:** Here, the various surfaces of the model are assigned physical types, such as `(velocity-inlet)`, `(pressure-outlet)`, or `(wall)`. This step is foundational for setting up the physics of the simulation later.

- **Add Local Sizing:** While global mesh settings provide a baseline cell size, local sizing controls are essential for achieving a high-quality mesh. This task allows the user to specify finer mesh resolutions in specific regions of high geometric complexity (e.g., small fillets, sharp corners) or in areas where high-resolution flow physics are expected (e.g., wakes, shear layers). This ensures that computational resources are focused where they are most needed.

- **Generate the Surface Mesh:** This task creates the two-dimensional mesh that discretizes all boundary surfaces of the domain. The quality of the volume mesh is highly dependent on the quality of this initial surface mesh; a good surface mesh is the foundation for a good volume mesh.

- **Add Boundary Layers:** To accurately capture the physics of wall-bounded turbulent flows, the boundary layer—the thin region near a solid surface where viscous effects are dominant—must be adequately resolved. This task generates highly-anisotropic prismatic or hexahedral cells (known as inflation or prism layers) that are stacked

normal to the wall. This is critical for the correct performance of turbulence models like k-omega SST.

- **Generate the Volume Mesh:** With the surfaces and boundary layers meshed, this task fills the remaining interior of the domain with three-dimensional cells. Ansys Fluent offers several advanced volume meshing technologies, including the Mosaic (poly-hexacore) meshing capability. Mosaic meshing intelligently combines high-quality hexahedral cells in the bulk flow region with conformal polyhedral elements that transition to the prism layers near the walls, providing an optimal balance of accuracy, cell count, and solver speed.

- **Switch to Solution:** Once the volume mesh is finalized and deemed of sufficient quality, this final action transitions the session from the meshing environment to the solver environment, where physics models and boundary conditions can be applied to the newly created mesh.

After going through the workflow, a mesh sensitivity study was conducted to find the optimal mesh prior to starting the simulation, the study was conducted at an AoA of 0, and at the cruise speed and altitude, both of which were extracted from the optimization that was done in Chapter 3, the result of the sensitivity study was the following :

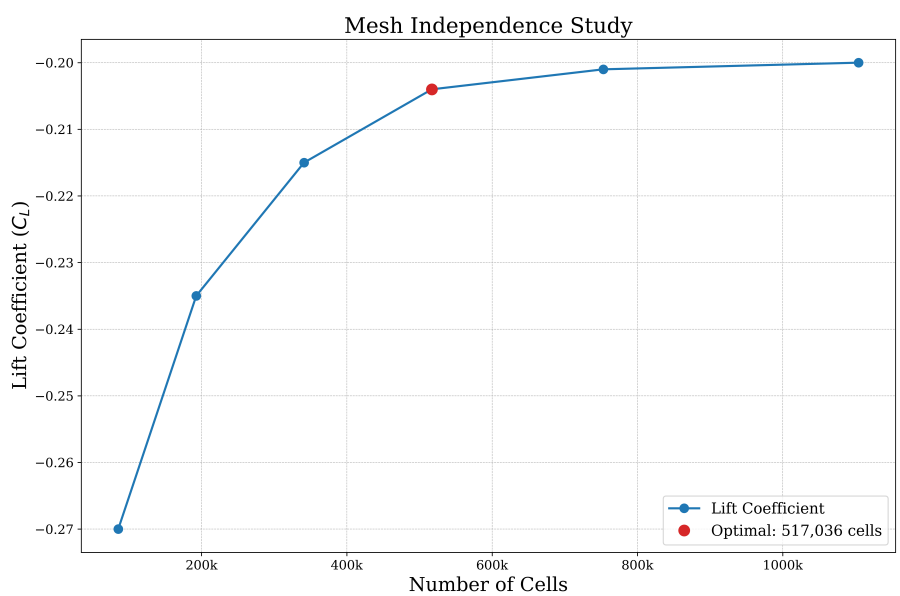

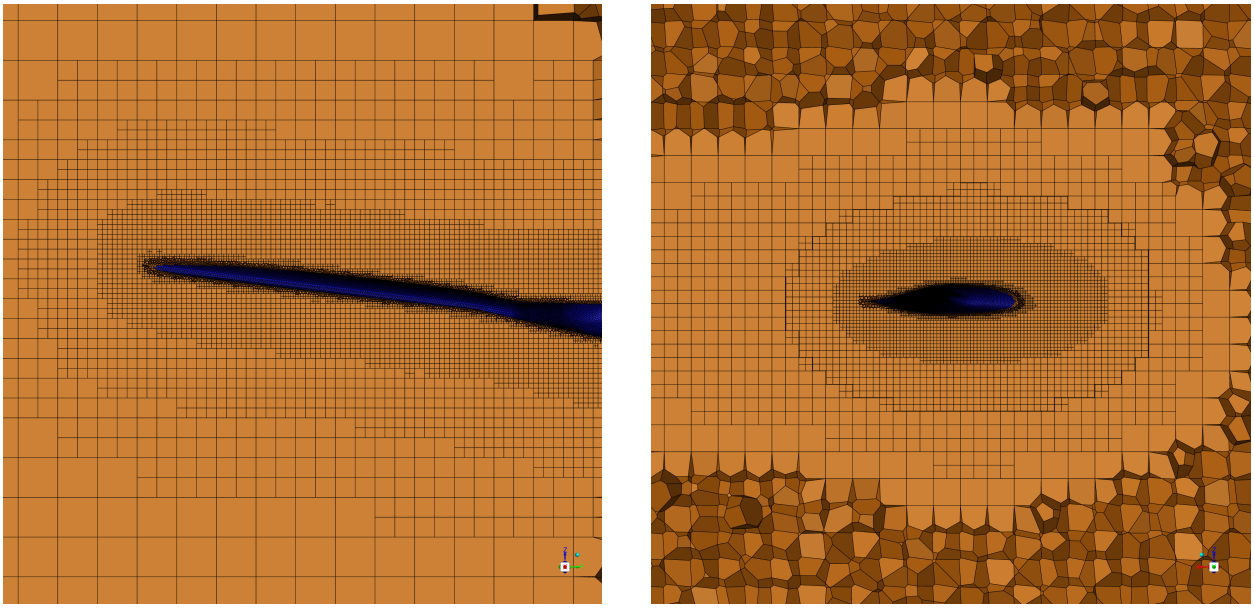

(a) Fontal Section View of The Optimal Volume Mesh

(b) Side Section View of The Optimal Volume Mesh

Figure 4.5: Optimal Volume Mesh Section Views

Having established a high-quality and mesh-independent computational grid, the process transitions from the pre-processing (meshing) phase to the solver setup phase. The finalized mesh, containing 517,036 cells, provides the discrete domain upon which the governing equations of fluid dynamics—the Reynolds-Averaged Navier-Stokes (RANS) equations—will be solved.

The next crucial step involves defining and setting up the physical models that characterize the flow that represent the aircraft's operating environment, and initializing the numerical solver and the most critical choice in this stage for external aerodynamic analysis is the selection of a the turbulence model.

CFD Analysis

As previously mentioned Ansys' API for fluent, (Pyfluent) was used to automate the simulation process, Spalart-Allmaras was used as a turbulence model, turbulence is a complex, chaotic fluid motion that remains one of the most significant challenges in CFD. Direct Numerical Simulation (DNS), which resolves all scales of turbulent motion, is computationally prohibitive for almost all engineering applications. Instead, the industry relies on turbulence models, which are mathematical approximations designed to predict the effects of turbulence

on the mean flow. The Reynolds-Averaged Navier-Stokes (RANS) equations are the most common framework for this, and a wide variety of models exist to provide closure for these equations.

Spalart-Allmaras' model design reflects a deliberate and highly successful engineering compromise. It consciously sacrifices the theoretical universality sought by more complex two-equation models in favor of exceptional robustness, computational economy, and specialized accuracy within its intended domain of wall-bounded aerodynamic flows. This targeted approach has established it as a foundational tool for aerodynamic design and analysis.

The model excels in the simulation of external aerodynamic flows, which is its intended domain. Its primary strength is the accurate prediction of attached wall-bounded flows, even in the presence of moderate adverse pressure gradients, a condition commonly found on the suction side of airfoils. This makes it a "workhorse" model in the aerospace industry.

Its application and validation are extensive, covering a wide range of flight regimes:

- **Subsonic and Transonic Flows:** It is widely used for analyzing airfoils, wings, and full aircraft configurations in subsonic and transonic flight, accurately predicting lift and drag for attached flow conditions.
- **Supersonic and Hypersonic Flows:** he model has been successfully implemented and validated for high-speed flows, including the simulation of ballistic missiles and hypersonic vehicles. It is capable of capturing key phenomena like shock-boundary layer interactions and the formation of fuselage vortices.
- **Turbomachinery:** It is also gaining popularity for turbomachinery applications, such as analyzing the flow over compressor and turbine blades, where wall-bounded effects are dominant.

Building upon the established strengths and widespread validation of the Spalart-Allmaras model within the aerospace industry, it was logically selected as the turbulence model for the high-fidelity CFD analysis of the Blended Wing Body (BWB) UAV. The specific characteristics of this project—namely, the need for accurate lift and drag predictions for an aircraft configuration dominated by attached, wall-bounded flows across a subsonic flight regime—align perfectly with the model's intended domain. Its computational efficiency and robustness were also critical factors, enabling a comprehensive analysis across a wide range of flight conditions without incurring prohibitive computational costs.

Leveraging the previously developed Python script for automating the CFD workflow with PyFluent, a series of simulations was systematically executed. This analysis campaign was designed to simulate the UAV's performance at its cruising speed and altitude, as determined by the optimization in Chapter 3, across a range of angles of attack from -3 to 25 degrees, with the primary objectives of obtaining high-fidelity values for the aerodynamic coefficients, validate the initial predictions from the lower-fidelity VLM analysis, and gain detailed insight into the complex flow phenomena, such as wingtip vortices and boundary layer development, inherent to the unique BWB airframe.

Following the execution of the automated simulation campaign across the specified range of angles of attack, a comprehensive dataset characterizing the BWB UAV's aerodynamic performance was generated, pressure contours will be used to highlight the aerodynamic behavior of the BWB.

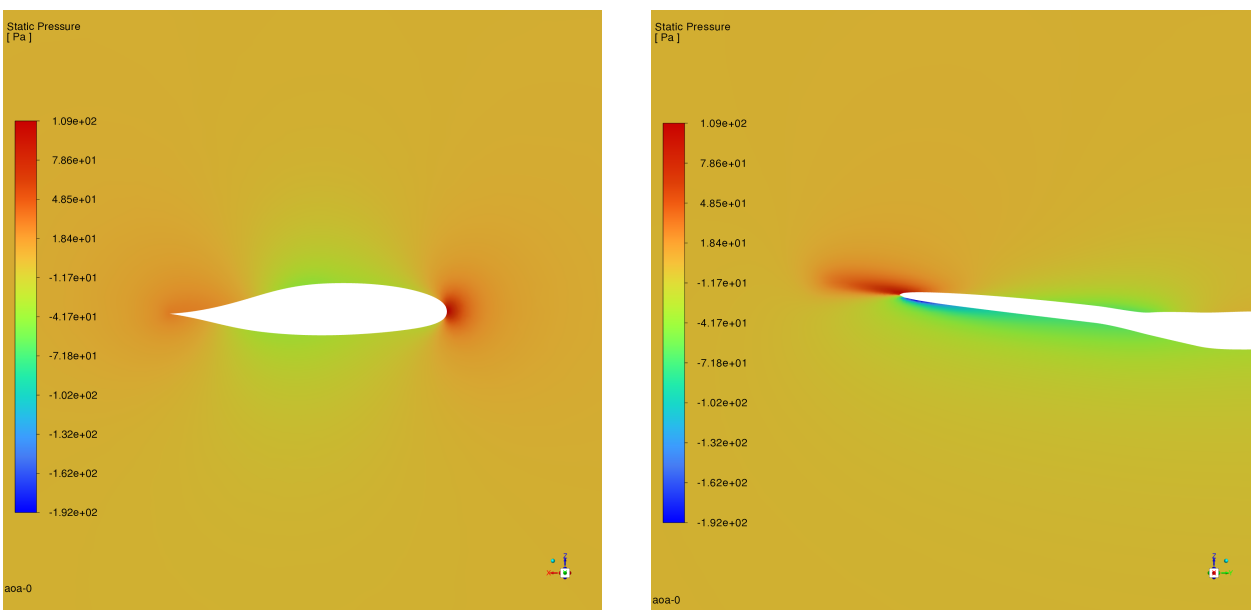

(a) Cross-Section Pressure Contour @ $\alpha = 0$ (b) Leading Edge Pressure Contour @ $\alpha = 0$

Figure 4.6: Pressure Contours @ $\alpha = 0$

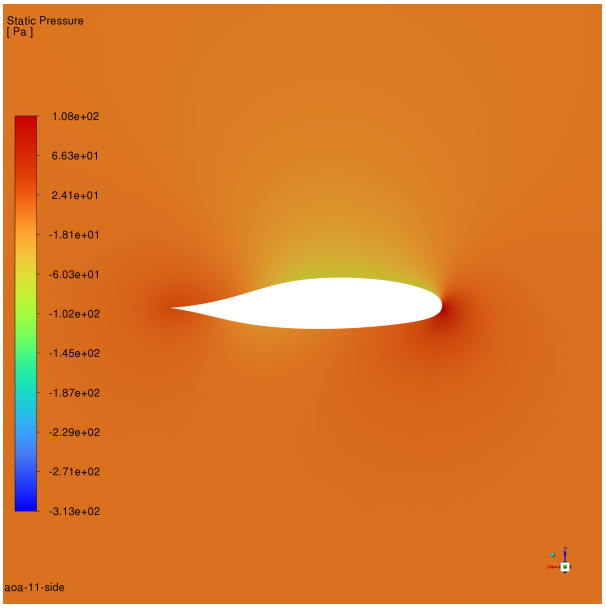

(a) Cross-Section Pressure Contour @ $\alpha = 11$

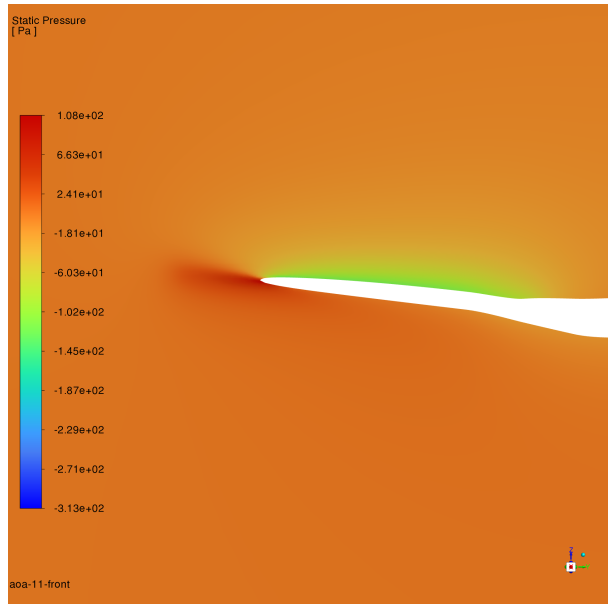

(b) Leading Edge Pressure Contour @ $\alpha = 11$

Figure 4.7: Pressure Contours @ $\alpha = 11$

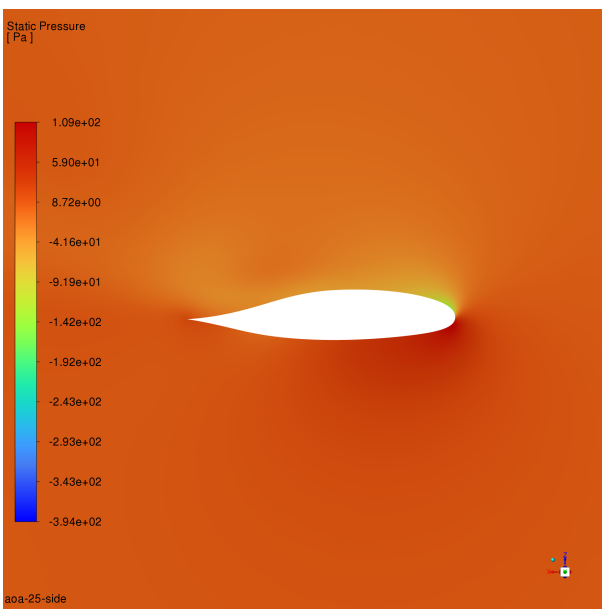

(a) Cross-Section Pressure Contour @ $\alpha = 25$

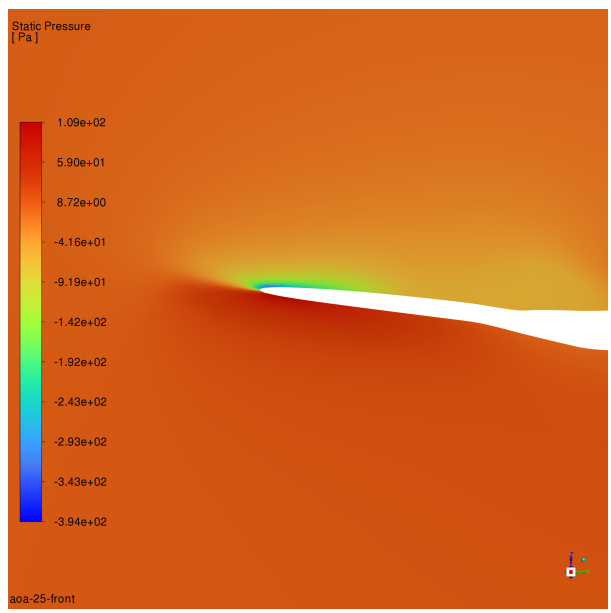

(b) Leading Edge Pressure Contour @ $\alpha = 25$

Figure 4.8: Pressure Contours @ $\alpha = 25$

Analysis of Aerodynamic Loading via Pressure Contours

The pressure contour plots generated from the Ansys Fluent simulations (Figures 6, 7, and 8) provide critical visual insight into the aerodynamic performance of the BWB UAV

across its operational envelope. y examining the static pressure distribution over the airfoil cross-section at key angles of attack (α), we can directly observe the mechanisms of lift generation and the onset of adverse aerodynamic phenomena such as flow separation and stall.

- **Neutral Lift and Tip Effects at $\alpha = 0$:** At a 0-degree angle of attack (Figure 6), the cross-section pressure contour shows a relatively symmetrical pressure distribution on the upper and lower surfaces, indicative of neutral or zero-lift conditions at the wing root. However, the leading-edge view reveals significant pressure gradients at the wingtips. The higher pressure on the upper surface and lower pressure on the lower surface at the tips suggest a negative lift in this region. This is a direct consequence of the negative twist designed into the wing, a critical feature for ensuring stability and control in a tailless BWB configuration.

- **Efficient Lift Generation at Cruise Angle of Attack $\alpha = 11$:** As the angle of attack increases to 11 degrees (Figure 7), a classic lift-generating pressure distribution becomes evident. The cross-section view shows a distinct high-pressure area on the lower surface and a significant low-pressure (suction) region on the upper surface. This pressure differential is the fundamental source of lift. The contours appear smooth and attached to the airfoil surface, indicating that the flow remains fully attached at this near-cruise angle of attack, leading to efficient flight.

- **Stall Progression and Control at High Angle of Attack $\alpha = 25$:** The contours at a 25-degree angle of attack (Figure 8) are particularly revealing about the aircraft's stall characteristics and safety. The cross-section view, representing the wing root, shows signs of flow separation; the low-pressure suction peak on the upper surface has diminished and moved forward, indicating that the root section is beginning to stall.

Crucially, however, the leading-edge contour shows that the wingtips are still effectively generating lift. The negative wing twist ensures that the local angle of attack at the tips is lower than at the root. As a result, even as the main body of the aircraft begins to stall, the tips remain attached, and the control surfaces located there remain effective. This design feature is highly encouraging, as it guarantees controllability even at high angles of attack and low speeds, a key requirement for BWB efficiency and operational safety.

4.2.3 Experimental Validation

While computational tools provide indispensable insights, they remain approximations of reality. Therefore, to anchor the theoretical and computational findings, a crucial phase of experimental validation was undertaken. This process serves as the ultimate arbiter, confirming the accuracy of the simulations and providing a high-confidence dataset of the aircraft's true aerodynamic characteristics. The validation was performed by testing a physical, scaled model of the BWB UAV in a low-speed wind tunnel.

To transition from a digital file to a testable artifact, a scaled model of the BWB airframe was manufactured using 3D printing with Polylactic Acid (PLA). This method was selected for its ability to rapidly and accurately reproduce the complex, blended curvatures of the UAV design.

A critical aspect of this phase was ensuring the experimental results would be relevant to the full-scale aircraft's real-world flight conditions. This was achieved by applying the principles of dynamic similarity, guided by the Buckingham Pi theorem. The optimization results from chapter 3 were used to determine the appropriate model scale, ensuring that key dimensionless parameters governing the flow (primarily the Reynolds number) would match the aircraft's operational flight regime as closely as possible within the wind tunnel's capabilities.

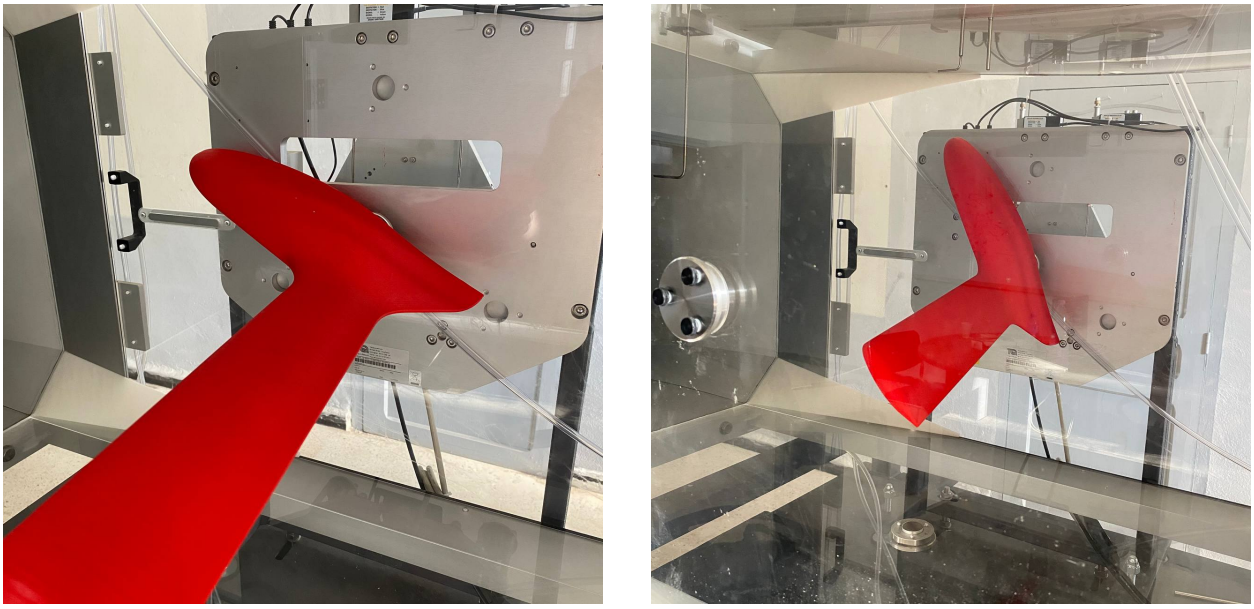

Figure 4.9: 3D Printed Scaled Model

Experimental Setup

The experimental validation phase relied on a carefully configured setup to physically measure the aerodynamic performance of the Blended Wing Body (BWB) design. The core of this setup consisted of the wind tunnel, the test model itself, and the instrumentation used for data acquisition.

The primary piece of equipment was the **TECHQUIPMENT AF1600**, a subsonic wind tunnel designed for aerodynamic testing. A diagram of the tunnel showcases its key components, which work in sequence to create the necessary test conditions.

- **Airflow Generation and Conditioning:** An Axial Fan Unit, powered by a fan motor drive, generates the airflow through the tunnel circuit then the air passes through a Settling Chamber and an Inlet Cone, which are crucial for ensuring the flow is uniform and smooth before it reaches the test area.
- **The Working Section:** This is the central test area where the BWB model was placed, it is a rectangular space with dimensions of 600mm x 600mm x 600mm The tunnel is capable of producing a maximum air velocity of 40m/s within this section.
- **Post-Test Air Management:** After passing over the model, the air moves through a diffuser to slow down efficiently, a silencer is located at the end of the circuit to reduce the aerodynamic noise generated by the fan system.

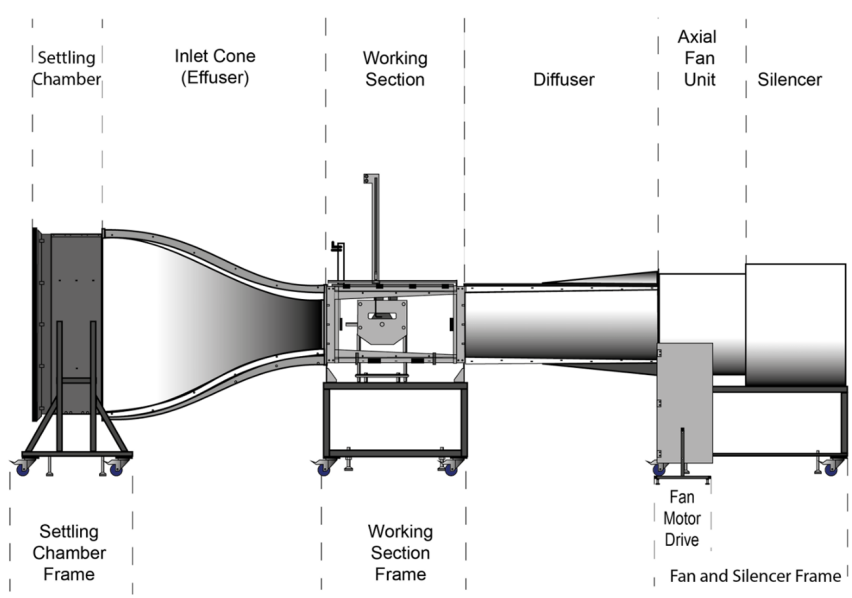

The model subjected to testing was a scaled replica of the BWB UAV, fabricated using 3D printing with Polylactic Acid (PLA) as the material. The scale of the model was not arbitrary; it was precisely calculated using an optimization algorithm to satisfy the criteria of the Pi theorem, thereby allowing the test to accurately simulate real flight conditions.

To capture the model's performance, the setup was instrumented to gather force and moment data. This system measured the aerodynamic forces and moments acting on the model across a range of different angles of attack. The objective of this data collection was to determine the true aerodynamic coefficients, specifically the Lift Coefficient (CL), Drag Coefficient (CD), and Moment Coefficient (Cm), providing the empirical data needed for validation.

Following the successful data acquisition campaign in the TECHQUIPMENT AF1600 wind tunnel, a comprehensive dataset of the BWB UAV's fundamental aerodynamic characteristics was obtained. This empirical data provides the definitive benchmark against which the predictive accuracy of the computational models can be assessed. The following section presents a comparative analysis, plotting the experimental results alongside the predictions from the low-fidelity Vortex Lattice Method (VLM) and the high-fidelity Spalart-Allmaras RANS simulations. This comparison is essential for validating the computational workflow and confirming the aircraft's performance and stability characteristics.

Comparison of Experimental and Numerical Results

The culmination of the aerodynamic design loop is the direct comparison between the physical measurements obtained from the wind tunnel experiment and the predictions generated by the computational models.

This section provides a detailed evaluation of the aircraft's aerodynamic performance by juxtaposing the experimental data against the results from the low-fidelity Vortex Lattice Method (VLM) and the high-fidelity RANS CFD simulations.

The analysis encompasses multiple CFD configurations: 'E1', which corresponds to the geometry tested in the wind tunnel; 'E2', representing a subsequent design iteration from the optimization process; and 'Fd', the final proposed design which incorporates winglets. This multi-faceted comparison is critical not only for validating the computational workflow but also for quantifying the aerodynamic impact of successive design refinements.

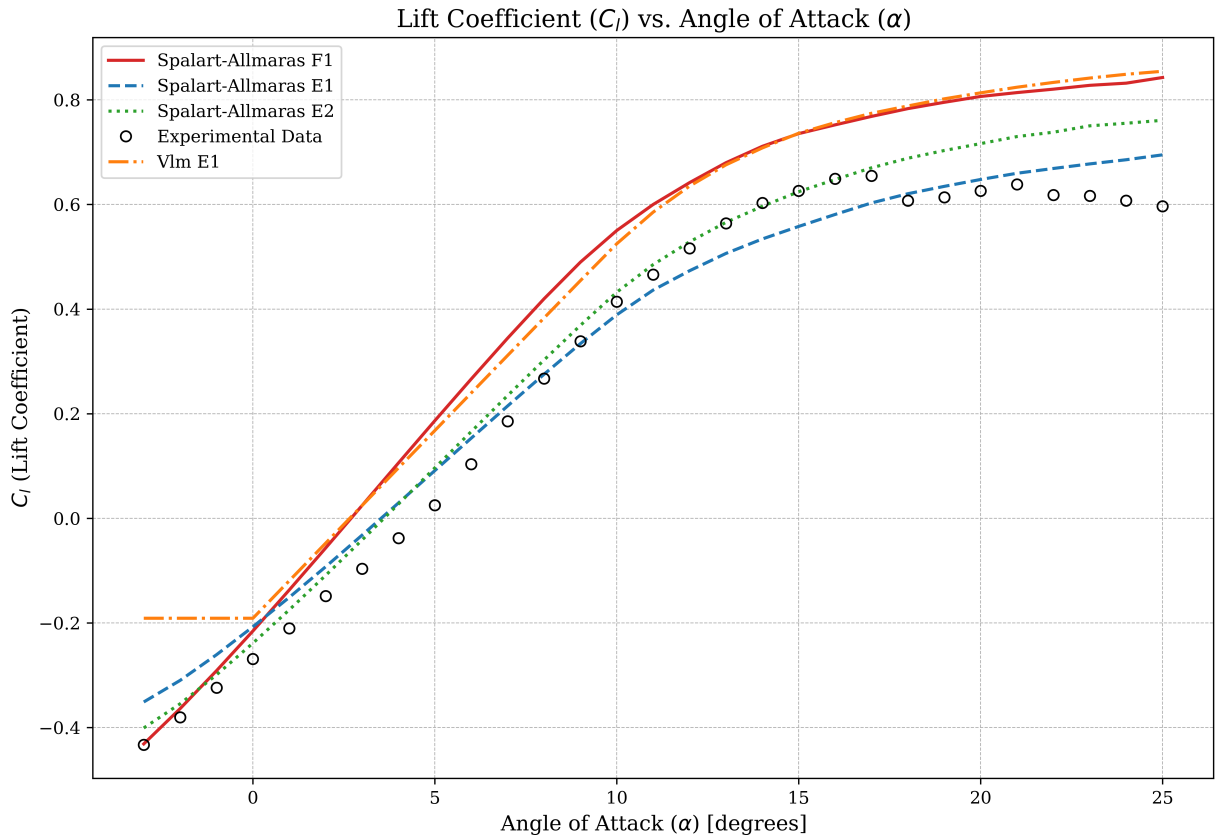

The relationship between the lift coefficient (CL) and the angle of attack (α) is arguably the most critical indicator of an aircraft's lifting capability and operational ceiling. The comparative plot of CL vs. α reveals several key insights In the linear region of flight, from approximately -4° to 10° angle of attack, there is a commendable qualitative agreement across all datasets. The lift curve slope, which dictates the aircraft's response to control inputs, is closely matched by the CFD simulations and the experimental data.

The increase in lift in the final design can be attributed to the addition of winglets which in turn increase the effective AR, which is known that it increases Clmax in blended wing body aircraft, and while the VLM captures the general trend, exhibits a slightly steeper slope, a common characteristic of potential flow methods which do not account for viscous boundary layer growth.

The primary divergence between the models occurs at higher angles of attack as the aircraft approaches stall. The experimental data, representing the physical ground truth,

shows a gradual flattening of the lift curve beginning around α=15°, indicating the onset of flow separation and a maximum lift coefficient (CLmax) of approximately 0.7. In contrast, all computational models exhibit a tendency to over-predict the maximum lift coefficient. This discrepancy is expected; RANS simulations, even with advanced turbulence models like Spalart-Allmaras, often struggle to precisely capture the complex, unsteady, three-dimensional flow separation that characterizes the stall of a complex geometry like a BWB.

The VLM, being an inviscid method, is fundamentally incapable of modeling stall and continues to predict an increase in lift far beyond the physical stall angle. Nevertheless, the CFD results for the E1 configuration track the experimental data with reasonable fidelity up to the stall angle, providing confidence in its predictive capability within the normal flight envelope.

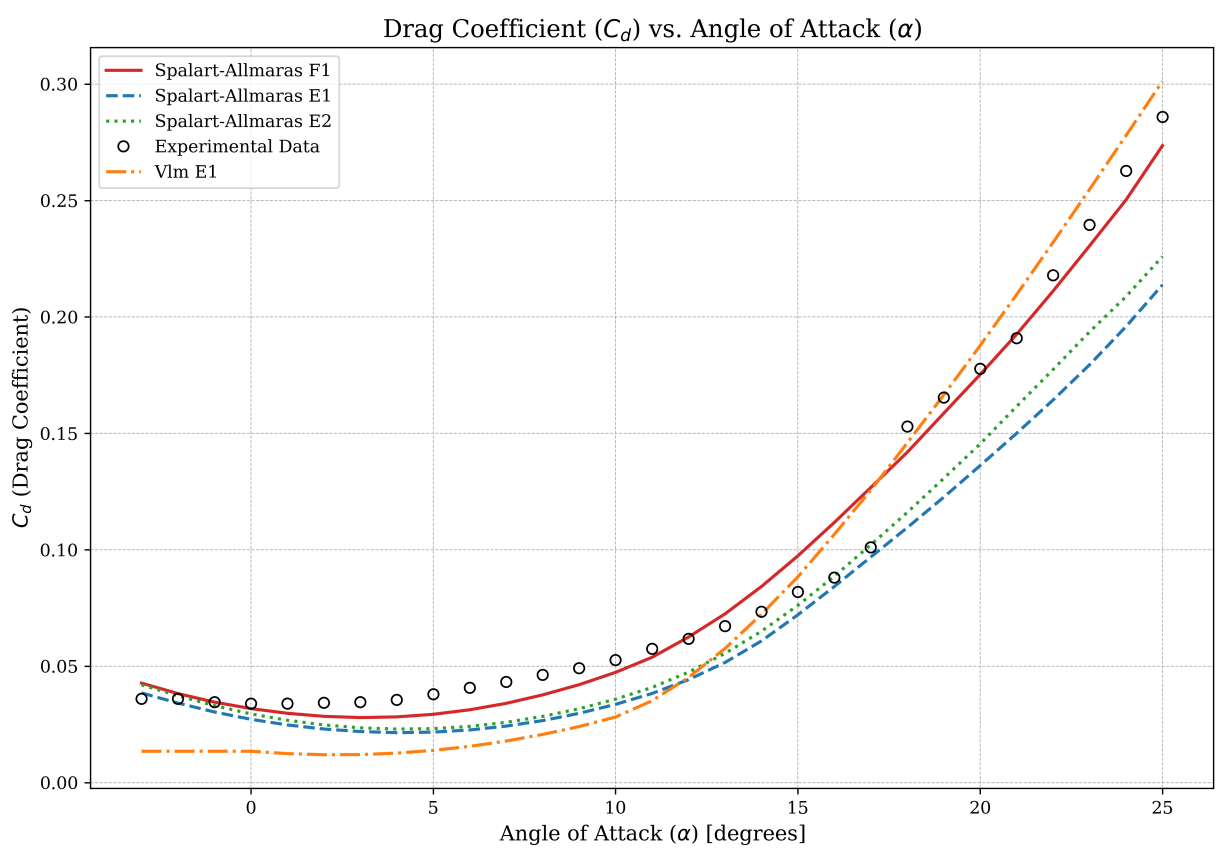

The drag coefficient (Cd) versus angle of attack plot is essential for evaluating the aircraft's efficiency and power requirements. The analysis highlights the strengths and weaknesses of

the different fidelity models.

A defining feature is the "drag bucket," the region of minimum drag, which is accurately captured by both the experimental data and the CFD simulations. The discrepancy of the Cd for all configurations can be attributed to near wall effects and wind tunnel wind tunnel interference, since the tip of the wing was relatively close to wind tunnel wall. which makes it subject to 'wall effects' that are known to increase measured drag. The CFD simulation, conversely, models an ideal 'free-flight' condition without these physical boundaries.

With that taken into consideration the close correlation between CFD and experimental results validates the meshing strategy, physics setup, and the choice of the Spalart-Allmaras turbulence model for predicting viscous and pressure drag components with high accuracy.

Conversely, the VLM results starkly illustrate the limitations of an inviscid model for drag prediction. By neglecting viscous friction, the VLM significantly under-predicts the total drag, yielding a drag bucket that is both narrower and substantially lower than reality. This confirms that for accurate performance analysis, especially for range and endurance calculations, high-fidelity CFD is indispensable.

The Lift-to-Drag (L/D) ratio is the ultimate measure of an aircraft's aerodynamic efficiency. The comparison plot for L/D vs. α synthesizes the lift and drag findings into a single, performance-defining curve.

The experimental data reveals that the physical model achieves a maximum L/D ratio of approximately 8.5 at an angle of attack of around 12°. The CFD simulations for the E1 and E2 configurations align well with this finding, predicting a peak efficiency of around 11-12 in a similar angle of attack range. The difference between the CFD and experimental peak values can be attributed to minor manufacturing imperfections in the 3D-printed model and due to near wall effects increasing drag in the wind tunnel, which are not present in the idealized CFD environment.

The VLM, due to its severe under-prediction of drag, yields a wildly optimistic L/D ratio peaking near 20. While incorrect in magnitude, it is noteworthy that the VLM does predict the peak efficiency to occur at a similar angle of attack to the other methods, suggesting its utility for identifying the optimal cruise condition, if not the performance at that condition. The 'Fd' configuration, with winglets, shows a promising improvement in L/D, particularly at higher angles of attack, confirming the winglets' effectiveness in reducing induced drag.

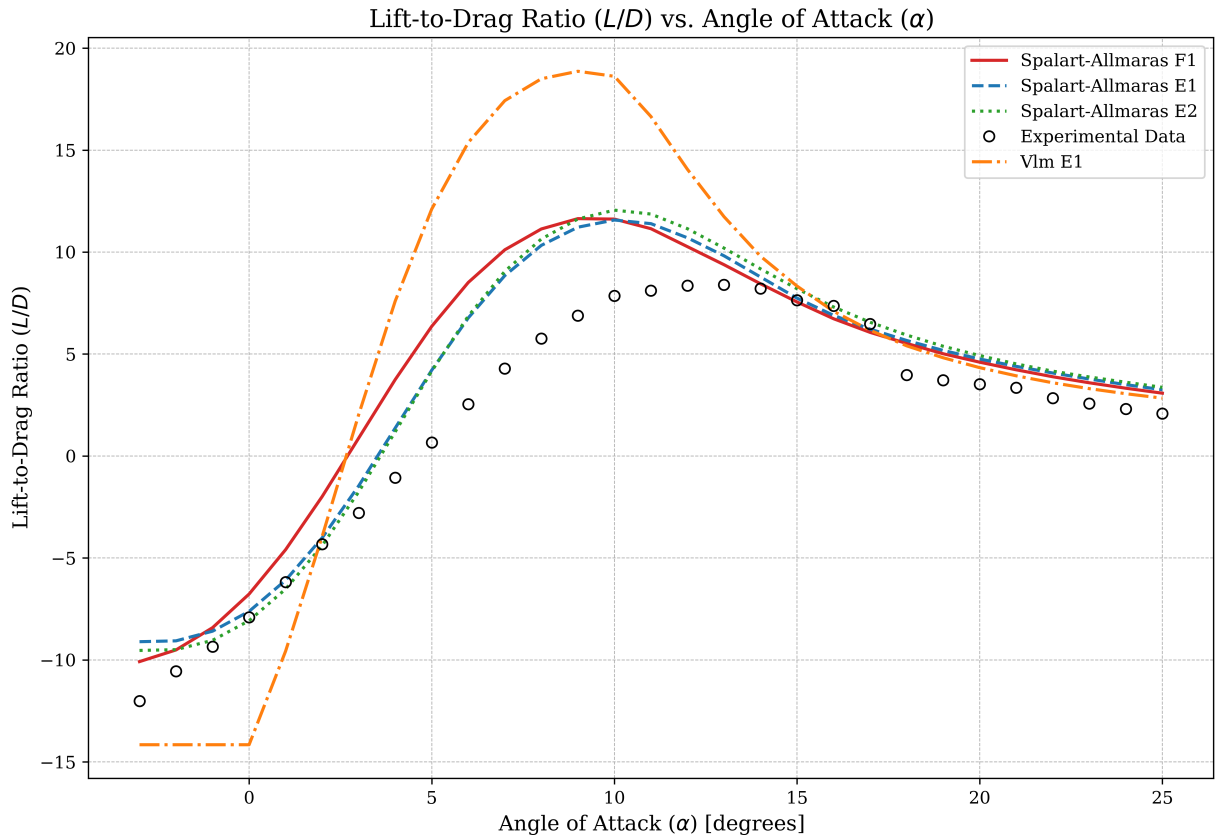

For a tailless aircraft, confirming longitudinal static stability is the most critical validation task. This is assessed by examining the pitching moment coefficient (C_{m_y}) as a function of angle of attack. For an aircraft to be statically stable, it must exhibit a negative pitching moment slope ($C_{m_y} < 0$), ensuring it has a natural tendency to return to its trim angle after a disturbance.

The plot of C_{m_y} vs. α provides the most encouraging result of the validation campaign. All methods—experimental, VLM, and all CFD variations—unambiguously show a negative slope across the operational flight envelope (from 0° to beyond the stall angle). This unanimous agreement provides high confidence that the design is inherently stable.

While there are quantitative differences in the exact value of C_{m_y} between the datasets—a common outcome as moment predictions are extremely sensitive to pressure distribution—the qualitative trend is consistent. The trim point, where the pitching moment curve crosses zero (C_{m_y}=0), is observed in the experimental data to occur near α=14°. The CFD and VLM models predict slightly different trim points, but all fall within a reasonable range, confirming

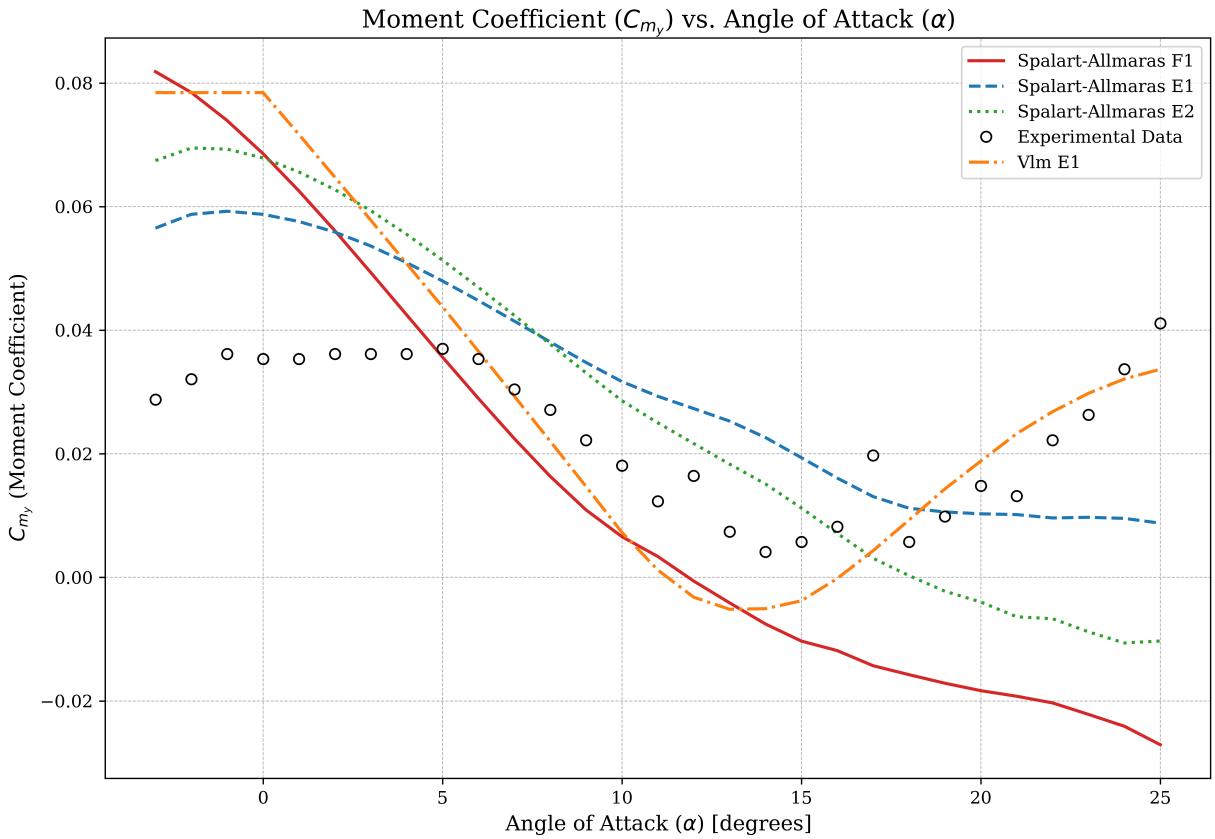

that the aircraft can be trimmed for stable flight near its most efficient angle of attack. The plot of CL vs. C_{m_y} further reinforces this conclusion, showing a stable relationship between lift generation and the aircraft's pitching moment.

In conclusion, the comprehensive comparison between the numerical simulations and the experimental wind tunnel data provides a robust validation of the aerodynamic design and the computational tools employed. The high-fidelity CFD has been shown to be a reliable predictor of drag, efficiency, and, most importantly, stability, while the limitations of lower-fidelity methods have been clearly quantified. This successful validation anchors the computational results in physical reality, providing the necessary confidence to proceed with the final design refinements and structural analysis.

4.3 Executive Summary

This chapter details a rigorous and iterative workflow to translate a theoretically optimized Blended Wing Body (BWB) UAV design into a physically validated, aerodynamically sta-

ble aircraft. The core methodology rejects a linear design sequence in favor of a modern validation loop that integrates low and high-fidelity computational analysis with physical experimentation. The process begins with parametric geometry creation and low-fidelity aerodynamic assessment, progresses to an in-depth high-fidelity Computational Fluid Dynamics (CFD) analysis, and culminates in a decisive experimental validation campaign using a physical model in a wind tunnel. The chapter's primary achievement is the robust validation of the aircraft's aerodynamic performance and, most critically, its inherent longitudinal static stability, which provides the necessary confidence to proceed with the final structural design and prototyping.

4.4 Initial Design and Low-Fidelity Analysis

The initial phase focused on establishing a baseline geometry and performing a preliminary stability analysis.

4.4.1 Geometry Generation

The 3D geometry of the BWB airframe was created using OpenVSP, an open-source parametric aircraft modeling tool developed by NASA. This software allows for rapid design iterations by defining the aircraft's shape through key engineering parameters like wing span, chords, and sweep angle.

4.4.2 Preliminary Stability Assessment

To quickly assess stability, the integrated VSPAERO tool was used, which employs a computationally inexpensive Vortex Lattice Method (VLM). The primary objective was to locate the aircraft's neutral point—the aerodynamic center for the entire vehicle. For the aircraft to be inherently stable, its Center of Gravity (CG) must be positioned forward of this neutral point, creating a positive static margin. By analyzing the pitching moment coefficient (C_m) across a range of attack angles, the neutral point was precisely located, establishing a target CG range to guarantee a statically stable flight configuration.

4.5 High-Fidelity CFD Analysis and Meshing

With a provisionally stable geometry established, the process moved to a high-fidelity aerodynamic analysis using Ansys Fluent, automated by a custom Python API script.

4.5.1 Meshing Workflow

The foundation of the analysis was the creation of a high-quality computational mesh using the Ansys Fluent "Watertight Geometry" workflow, designed for ideal, "clean" CAD models. This task-based process included:

- Importing the geometry and specifying its physical nature (e.g., for an external flow simulation).
- Applying local sizing controls to create a finer mesh in regions of high geometric complexity or where high-resolution flow physics were expected.
- Generating a high-quality surface mesh as the foundation for the volume mesh.
- Adding boundary layers (inflation layers) with prismatic cells normal to the wall to accurately capture the physics of wall-bounded turbulent flows.
- Filling the domain with a Mosaic (poly-hexacore) volume mesh, which optimally balances accuracy and computational cost.

4.5.2 Mesh Independence and Solver Setup

A mesh sensitivity study was conducted to find the optimal grid, resulting in a finalized mesh of **517,036 cells**. The **Spalart-Allmaras** one-equation turbulence model was selected for the simulations. This model is considered an industry "workhorse" for its exceptional robustness, computational economy, and proven accuracy for external aerodynamic flows, from subsonic to hypersonic regimes.

4.6 Aerodynamic Performance and Flow Analysis

The CFD simulations, run at the UAV's cruise conditions across angles of attack from $-3°$ to $25°$, yielded detailed insights into the aircraft's flight characteristics.

- **At Zero Lift ($\alpha = 0°$):** Pressure contours showed a symmetrical pressure distribution at the wing root, but also revealed significant negative lift at the wingtips. This is a direct result of the negative twist designed into the wing, a critical feature for ensuring stability in a tailless BWB configuration.
- **At Cruise ($\alpha = 11°$):** A classic lift-generating pressure distribution was observed, with a high-pressure zone on the lower surface and a large low-pressure suction region

on the upper surface. Smooth, attached flow contours indicated efficient flight at this near-cruise angle of attack.

- **At High Angle of Attack ($\alpha = 25°$):** The contours provided highly encouraging results regarding safety and stall characteristics. While the wing root showed signs of flow separation and the onset of stall, the wingtips were still effectively generating lift. The negative wing twist ensures the tips operate at a lower local angle of attack, keeping the control surfaces effective even as the main body begins to stall, which guarantees controllability at high angles of attack and low speeds.

4.7 Experimental Validation

To anchor the computational findings in reality, a crucial experimental validation phase was undertaken.

4.7.1 Model and Setup

A scaled model of the BWB airframe was manufactured via 3D printing using Polylactic Acid (PLA). The scale was precisely calculated using the Buckingham Pi theorem to ensure dynamic similarity with the full-scale aircraft's operational Reynolds number. Testing was performed in the **TECHQUIPMENT AF1600**, a subsonic wind tunnel with a $600mm \times 600mm \times 600mm$ working section.

4.7.2 Data Acquisition

The model was instrumented to measure aerodynamic forces and moments across a range of attack angles, providing the true values for the Lift (C_L), Drag (C_D), and Moment (C_m) coefficients needed for a definitive validation.

4.8 Validation Results and Final Conclusions

The direct comparison of experimental data against VLM and CFD predictions for multiple design iterations ('E1', 'E2', and the final 'Fd' design with winglets) served as the ultimate test of the design.

- **Lift and Drag:** While VLM was useful for trends, it was incapable of modeling stall and severely under-predicted drag by neglecting viscosity. The CFD results, however,

tracked the experimental data with reasonable fidelity, correctly capturing the lift curve slope and the shape of the "drag bucket". The CFD predicted a lower absolute drag value, which was attributed to the absence of wind tunnel wall effects that increase drag on the physical model.

- **Aerodynamic Efficiency (L/D):** The physical model achieved a maximum L/D ratio of approximately **8.5**. The CFD simulations predicted a higher peak efficiency of around **11-12**, with the difference attributed to minor manufacturing imperfections and wind tunnel interference. The final 'Fd' design with winglets showed a promising improvement in L/D, confirming their effectiveness.

- **Longitudinal Stability (Pitching Moment C_m):** This was the most critical and encouraging result of the entire campaign. All methods—experimental data, VLM, and all CFD variations—unambiguously showed a **negative pitching moment slope** ($C_{m_y} < 0$) across the entire operational flight envelope. This unanimous agreement provides extremely high confidence that the BWB design is **inherently statically stable**. The experimental data showed the aircraft trims (where $C_{m_y} = 0$) near an angle of attack of 14°, confirming it can be trimmed for stable flight near its most efficient condition.

In conclusion, the comprehensive comparison robustly validated the aerodynamic design and the computational workflow. It demonstrated that the high-fidelity CFD is a reliable predictor of the aircraft's performance, efficiency, and most importantly, its stability, anchoring the computational results in physical reality.

Chapter 5

Flight Dynamics Analysis

5.1 Introduction

As previously mentioned BWB configurations represent a radical departure from the conventional "tube-and-wing" aircraft design paradigm that has dominated aviation for nearly a century By seamlessly integrating the fuselage and wings into a single, continuous lifting surface, the BWB configuration promises significant performance advantages. This integrated shape drastically reduces the wetted surface area and interference drag compared to conventional designs, leading to superior aerodynamic efficiency and potential fuel savings of over 20% [3].

Despite these compelling benefits, which date back to concepts from the 1920s and were advanced significantly by McDonnell Douglas and NASA in the 1990s, the BWB's widespread adoption has been hindered by formidable technical hurdles.1 The core of this challenge lies in the physics of flight stability and control.

5.2 The Principles of Aircraft Stability

An aircraft's stability is its ability to maintain a state of equilibrium in flight or to return to that state when disturbed, without requiring pilot intervention. This property is fundamental to safety, handling qualities, and pilot workload. Stability is analyzed in two distinct but related regimes: static and dynamic.

5.2.1 Static Stability

Static stability describes an aircraft's initial tendency—its immediate, instinctive reaction—to return to its original equilibrium (or "trimmed") position after being disturbed by an external force, such as a gust of wind or a control input.17 It is the first response of the airframe to a perturbation. This tendency can be categorized into one of three states.

- **Positive Static Stability:** The aircraft generates restoring forces and moments that immediately begin to move it back toward its original attitude. If the nose pitches up, a nose-down moment is created to counteract the disturbance. This is the desired state for most aircraft, as it ensures a natural return to controlled flight.
- **Neutral Static Stability:** The aircraft, when disturbed, remains in its new attitude and shows no tendency to return to its original position or diverge further. For example, if turbulence pitches the nose up by 5 degrees, the aircraft will simply maintain that new 5-degree nose-up attitude.
- **Negative Static Stability (Instability):** The aircraft generates forces and moments that cause it to continue moving away from its original attitude, amplifying the initial disturbance. A small nose-up pitch would result in a moment that pitches the nose up even further. This is a highly undesirable and dangerous condition, often rendering the aircraft uncontrollable without rapid, continuous computer-aided correction.

5.2.2 Dynamic Stability

While static stability describes the initial response, dynamic stability describes the aircraft's behavior over time as it seeks equilibrium following that initial response.17 It characterizes the nature of the motion, which is often oscillatory, as the aircraft returns to its trimmed state. Like static stability, dynamic stability is classified into three types

- **Positive Dynamic Stability (Damped Oscillations):** The aircraft oscillates back and forth around its equilibrium position, but the amplitude of these oscillations progressively decreases with each cycle until it eventually settles back at its original attitude. This is the ideal state for predictable and comfortable flight.
- **Neutral Dynamic Stability (Undamped Oscillations):** The oscillations continue indefinitely with a constant amplitude and frequency. The aircraft never settles down, instead continuing a "roller-coaster" motion that, while not divergent, is undesirable and increases pilot workload.

- **Negative Dynamic Stability (Divergent Oscillations):** The amplitude of the oscillations increases with each cycle. Each overshoot is larger than the last, quickly leading to a complete loss of control. This is a critically unstable condition.

A special case of positive dynamic stability is known as subsidence or a "deadbeat" response, where the aircraft returns to equilibrium smoothly and quickly without any oscillation. While this might seem ideal, it is rare in practice because achieving such strong damping typically requires larger-than-desirable control surfaces, which impose significant weight and drag penalties.

5.2.3 The Critical Relationship: Static as a Prerequisite for Dynamic

The concepts of *static* and *dynamic* stability are not independent; they are hierarchical. An aircraft must possess positive static stability to have any chance of being dynamically stable. This relationship can be understood as a two-part engineering test for stability.

First, the aircraft must pass the static stability test. When disturbed, does it generate forces that attempt to restore it? If the answer is no—if it is statically unstable—it will simply diverge from its flight path. There is no oscillatory motion to be damped, only a continuous departure from equilibrium. In this case, the question of dynamic stability is moot.

If the aircraft passes the first test and is statically stable, it then proceeds to the second test: dynamic stability. How does it attempt to return to equilibrium over time? Does it do so in a controlled, damped manner (dynamically stable), or do the oscillations grow until it loses control (dynamically unstable)? An aircraft can be statically stable but dynamically unstable if, for example, it has strong restoring forces but insufficient aerodynamic damping to quell the resulting oscillations. This two-gate framework is crucial for understanding the BWB's design challenges. Engineers must first devise novel methods to achieve static stability without a tail, and only then can they address the complex task of ensuring all resulting dynamic modes are stable.

5.3 Introduction to Aerodynamic Derivatives

To move from qualitative descriptions to quantitative analysis and design, aerospace engineers employ a mathematical framework based on aerodynamic coefficients and their derivatives. These *stability derivatives* are the language used to precisely define and predict an aircraft's stability characteristics.

5.3.1 Quantifying Stability

A stability derivative is a non-dimensional number that quantifies the change in an aerodynamic force or moment coefficient resulting from a small change in a flight condition variable (such as angle of attack, sideslip angle, or pitch rate). These derivatives are derived by linearizing the complex, nonlinear equations of motion around a steady, trimmed flight condition. They allow engineers to model an aircraft's response to small disturbances and are essential for wind tunnel testing, simulation, and control system design.

5.3.2 Longitudinal Stability Derivatives (The Pitching Plane)

Longitudinal stability concerns the aircraft's motion in the pitch axis (nose up or down) and is often considered the most critical aspect of stability.

- **Pitching Moment Coefficient (C_m) versus Angle of Attack (α):** The relationship between the pitching moment and the angle of attack is the cornerstone of longitudinal static stability.
  - $C_{m\alpha}$ **(Pitch Stiffness):** This derivative, defined as the slope of the pitching moment coefficient curve with respect to the angle of attack ($\frac{\partial C_m}{\partial \alpha}$), represents the aircraft's "pitch stiffness." For an aircraft to be statically stable in pitch, $C_{m\alpha}$ must be negative. A negative value signifies that an increase in angle of attack (e.g., from a vertical gust) generates a negative, or nose-down, pitching moment, which acts to restore the aircraft to its original trim attitude.
  - C_{m0} **(Pitching Moment at Zero Lift):** For a stable aircraft to be trimmable (i.e., to achieve zero pitching moment) at a positive lift coefficient (required for level flight), the pitching moment coefficient at zero lift, C_{m0}, must be positive. This nose-up moment at zero lift is typically provided by a cambered airfoil or, in the case of a conventional aircraft, the tailplane setting.
- **Lift Coefficient (C_L) versus Angle of Attack (α):**

  - $C_{L\alpha}$ **(Lift Curve Slope):** This derivative, $\frac{\partial C_L}{\partial \alpha}$, quantifies how effectively the wing generates lift as the angle of attack changes. It is a fundamental parameter in the equations that determine the overall stability of the aircraft.

- **The Static Margin:** This is the practical, physical measure of an aircraft's longitudinal static stability. It is defined by the relative positions of two key points:
  - **Center of Gravity (CG):** The point where the aircraft's total weight is considered to act. Its location can change with fuel burn and payload distribution.
  - **Neutral Point (NP):** An aerodynamic property of the aircraft, representing the CG location at which the aircraft would have neutral static stability ($C_{m\alpha} = 0$).
  - For positive longitudinal static stability, the CG must be located forward of the Neutral Point. The distance between the CG and the NP, expressed as a percentage of the wing's mean aerodynamic chord, is the static margin. A larger static margin implies greater stability but can also make the aircraft less maneuverable and increase trim drag.

5.3.3 Lateral-Directional Stability Derivatives (The Coupled Roll-Yaw Motion)

Lateral (roll) and directional (yaw) stability are intrinsically coupled; a disturbance in one axis almost always induces a motion in the other.

- **Yawing Moment Coefficient (C_n) versus Sideslip Angle (β):**
  - $C_{n\beta}$ **(Weathercock Stability):** This derivative, $\frac{\partial C_n}{\partial \beta}$, measures the aircraft's tendency to align itself with the relative wind, like a weathervane. For positive directional stability, $C_{n\beta}$ must be positive. This means a positive sideslip (relative wind coming from the right) must generate a positive (nose-right) yawing moment to correct the misalignment.

- **Rolling Moment Coefficient (C_l) versus Sideslip Angle (β):**
  - $C_{l\beta}$ **(Dihedral Effect):** This derivative, $\frac{\partial C_l}{\partial \beta}$, quantifies the rolling moment generated by a sideslip. For positive lateral stability (the tendency to level the wings), $C_{l\beta}$ must be negative. A positive sideslip (wind from the right) causes the right wing to drop. A negative $C_{l\beta}$ ensures this generates a negative (left-wing-down) rolling moment, which acts to restore the wings to a level attitude. This effect is primarily achieved through wing dihedral or sweep.

5.3.4 Damping Derivatives and Dynamic Stability

While the derivatives above govern static stability, a separate set of derivatives related to rotation rates is crucial for dynamic stability. They represent the aerodynamic damping that resists angular motion.

- **Cmq (Pitch Damping):** The change in pitching moment due to pitch rate (q). A negative value is required to oppose and damp out pitching oscillations.
- **Clp (Roll Damping):** The change in rolling moment due to roll rate (p). A strongly negative value is required to resist and rapidly damp rolling motions.
- **Cnr (Yaw Damping):** The change in yawing moment due to yaw rate (r). A negative value is required to damp out yawing oscillations, a key factor in controlling Dutch roll.

5.4 Stability Analysis Methodology

To translate the theoretical principles of stability into a quantitative assessment of the BWB UAV design, a rigorous three-stage computational methodology was employed. This process was designed to ensure an accurate and reproducible analysis, moving from mass properties to aerodynamic characterization and finally to dynamic simulation.

First, to obtain an accurate mass distribution and the true moments of inertia, the light weighted airframe geometry was analyzed using nTop. This advanced implicit modeling software is uniquely suited for calculating the physical properties of complex, lattice-based structures typical of additive manufacturing, providing a more precise estimate than traditional CAD programs would allow.

Next, the validated 3D model of the UAV underwent a comprehensive aerodynamic stability analysis using OpenVSP's integrated Vortex Lattice Method (VLM) tool, VSPAERO. This combination was selected for its rapid geometry modeling capabilities and its efficiency as a well-validated method for extracting subsonic aerodynamic derivatives. The key longitudinal and lateral-directional stability and control derivatives—such as C_{m_α}, C_{n_β}, and C_{l_p} were calculated by simulating forces and moments across a range of flight conditions. The analysis was centered around a trimmed, straight-and-level flight condition representing the UAV's intended operational state. These coefficients, which quantify the inherent static stability of the airframe, served as the primary input for the subsequent dynamic analysis.

Finally, the aerodynamic derivatives extracted from VSPAERO were implemented in a modified Python program taken from a GitHub repository [17] to analyze the aircraft's dynamic stability. This program, adapted from a validated aerospace engineering repository , mathematically models the UAV's linearized equations of motion in a state-space representation. This approach uses a standard state vector comprising perturbations in velocity, angle of attack, pitch rate, and pitch angle for the longitudinal dynamics, and sideslip, roll rate, yaw rate, and roll angle for the lateral-directional dynamics. By populating the system matrices with the calculated derivatives, the program simulates the aircraft's characteristic modes of motion: the short-period and phugoid modes in the longitudinal plane, and the Dutch roll, spiral, and roll subsidence modes in the lateral-directional plane. The primary output is a definitive, time-based simulation of the aircraft's response to disturbances, allowing for a conclusive assessment of its dynamic stability.

5.5 Stability Simulation Results

The simulation results demonstrate that the UAV is statically stable and dynamically stable in its most critical modes of motion. While the analysis reveals a mild spiral instability, this characteristic is common, acceptable, and easily managed in aircraft design. The overall findings confirm that the UAV possesses safe, predictable, and controllable flight characteristics, thereby successfully validating the stability and control design of the BWB airframe.

The conclusive finding that the UAV is dynamically stable is supported by a detailed analysis of its individual modes of motion. The following series of figures presents this evidence, beginning with an Eigenvalue S-Plane plot which offers a complete summary of the system's stability. Each subsequent figure then provides a time-domain simulation, illustrating the specific character—be it oscillatory, subsident, or mildly divergent—of the aircraft's short-period, phugoid, roll, Dutch roll, and spiral modes. Together, these visualizations provide a quantitative and intuitive understanding of the aircraft's response to disturbances, confirming its safe and controllable flight dynamics.

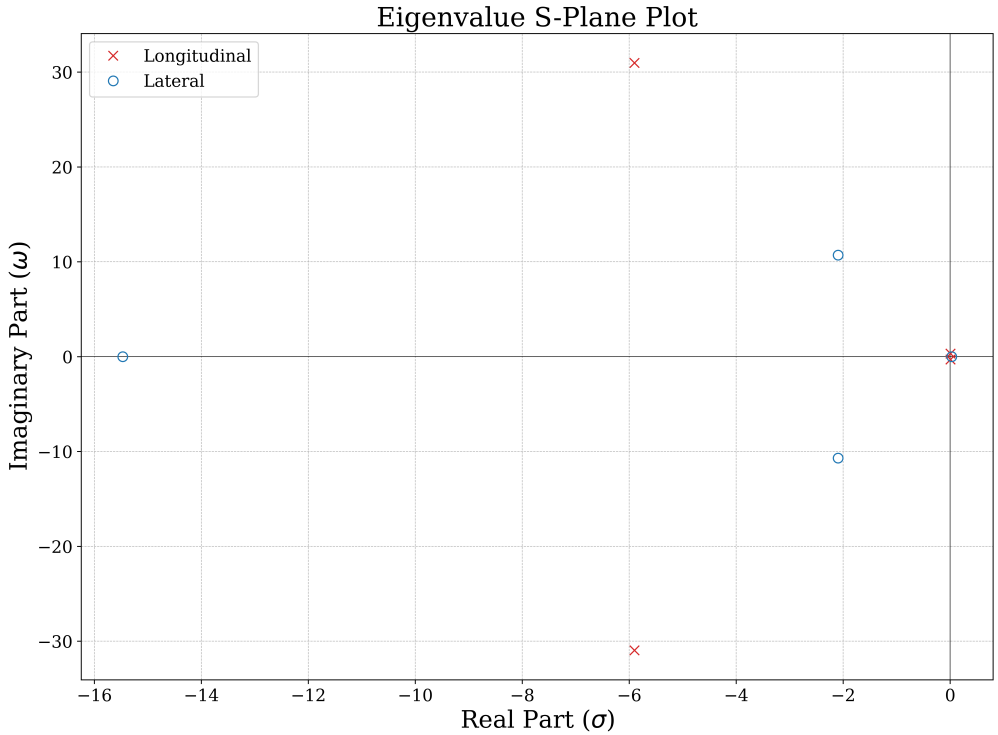
Eigenvalue S-Plane Plot
Longitudinal
Lateral
Imaginary Part (ω)
Real Part (σ)
30
20
10
0
−10
−20
−30
−16
−14
−12
−10
−8
−6
−4
−2
0

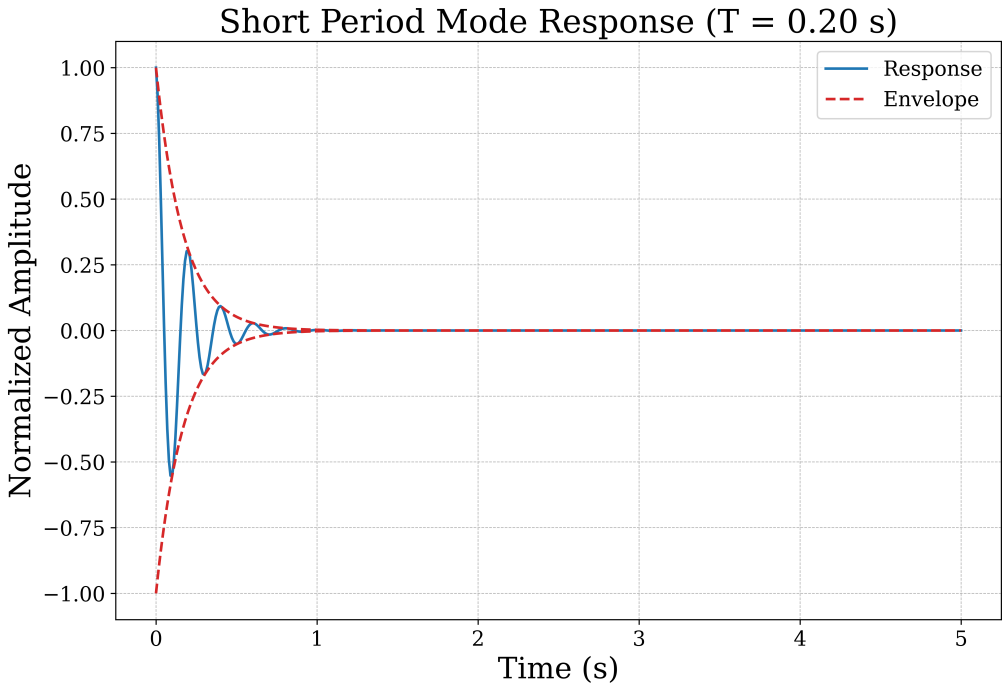
Short Period Mode Response (T = 0.20 s)
Response
Envelope
Normalized Amplitude
Time (s)
1.00
0.75
0.50
0.25
0.00
−0.25
−0.50
−0.75
−1.00
0
1
2
3
4
5

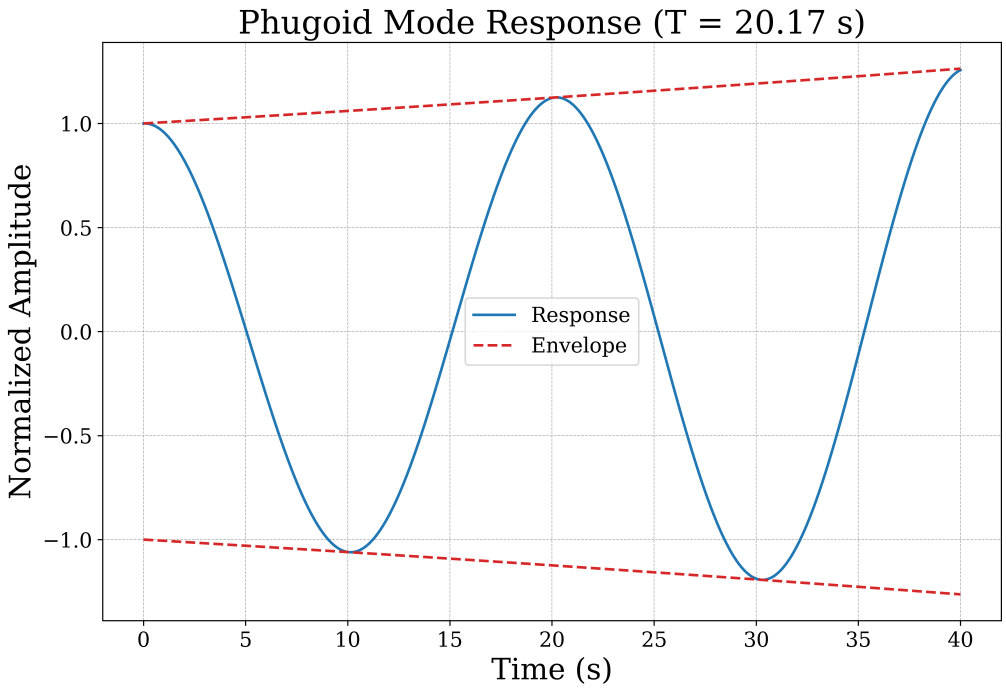
Phugoid Mode Response (T = 20.17 s)
Normalized Amplitude
Time (s)
Response
Envelope
1.0
0.5
0.0
−0.5
−1.0
0
5
10
15
20
25
30
35
40

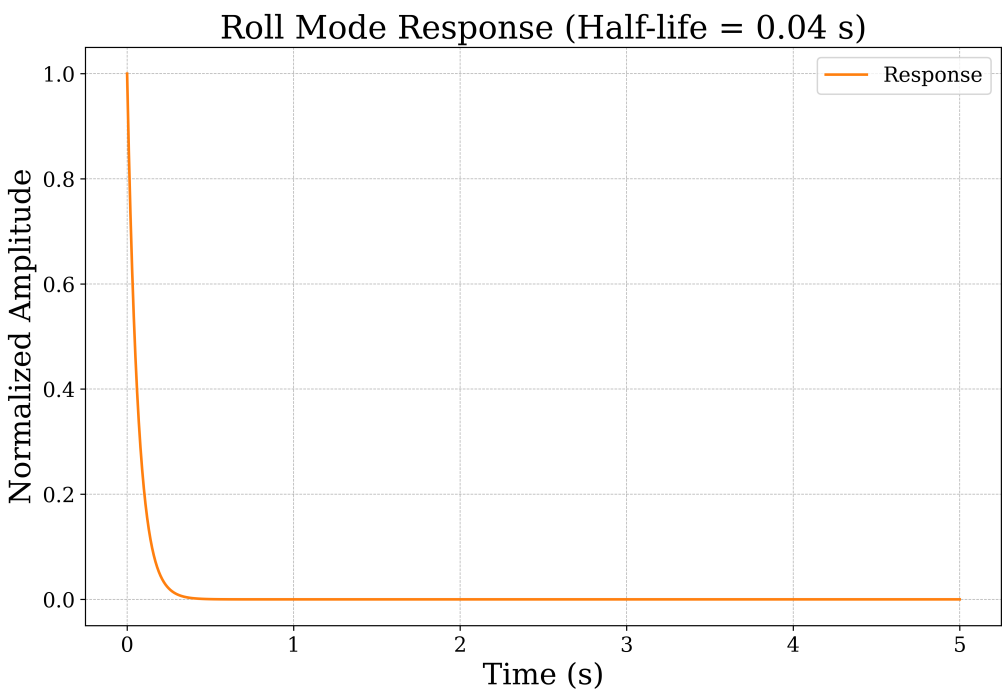
Roll Mode Response (Half-life = 0.04 s)
Normalized Amplitude
Time (s)
Response
1.0
0.8
0.6
0.4
0.2
0.0
0
1
2
3
4
5

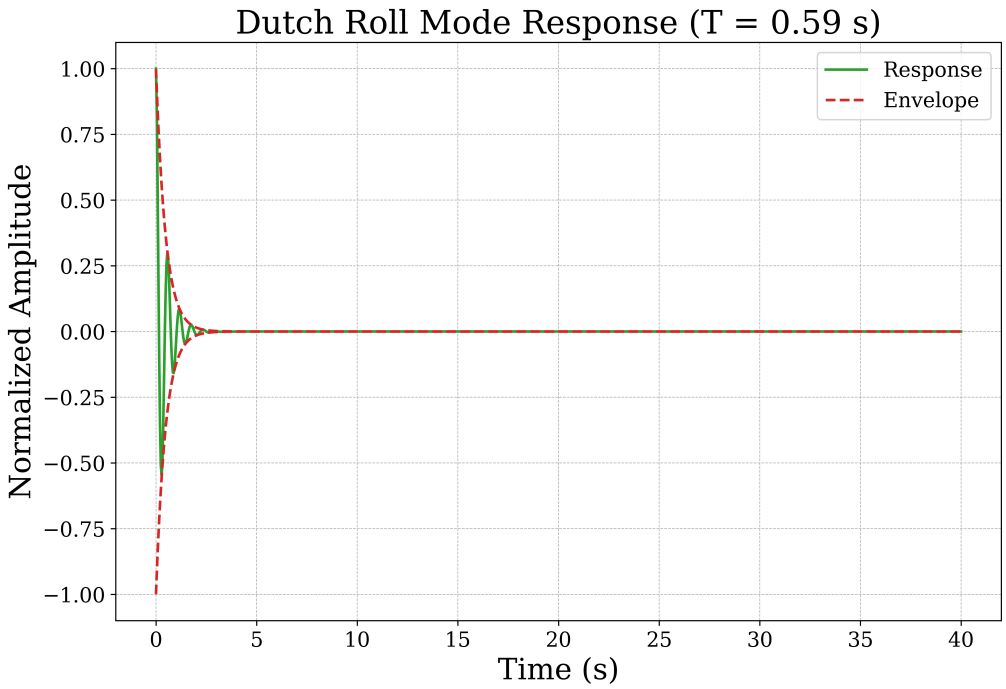
Dutch Roll Mode Response (T = 0.59 s)
Response
Envelope
Normalized Amplitude
1.00
0.75
0.50
0.25
0.00
−0.25
−0.50
−0.75
−1.00
0
5
10
15
20
25
30
35
40
Time (s)

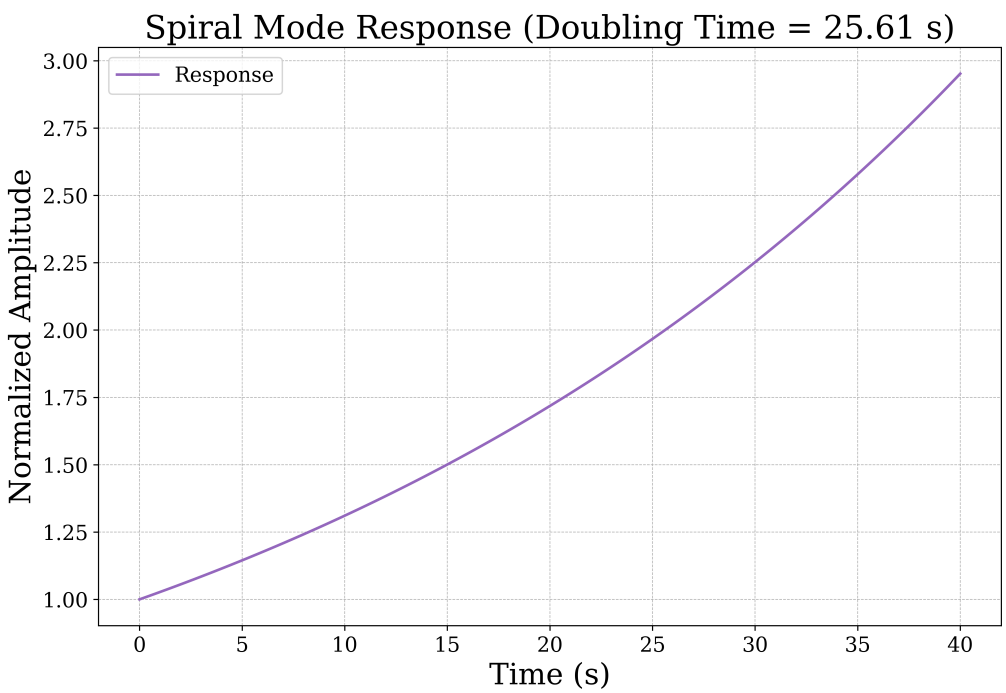
Spiral Mode Response (Doubling Time = 25.61 s)
Response
Normalized Amplitude
3.00
2.75
2.50
2.25
2.00
1.75
1.50
1.25
1.00
0
5
10
15
20
25
30
35
40
Time (s)

- **Short Period Mode Response:** The Short Period mode is highly stable. It has a very short period of just 0.20 seconds, and the oscillation is quickly quelled, as shown by the rapidly contracting envelope. This strong damping is characteristic of a safe and responsive aircraft, ensuring it settles immediately after a gust or control input without excessive pitching motion.

- **Phugoid Mode Response:** The Phugoid mode is shown to be dynamically stable. It is characterized by a very long period oscillation (T = 20.17 s) that is slowly but positively damped. While the damping is light, the stability ensures the aircraft will eventually return to its trim condition. This behavior is desirable and typical for most aircraft.

- **Roll Mode Response:** The Roll mode is very stable and heavily damped. The response is not an oscillation but a rapid "deadbeat" subsidence back to zero. The half-life is extremely short at just 0.04 seconds, signifying very strong roll damping (governed by the C_{l_p} derivative). This is crucial for good handling, as it ensures any rolling motion ceases almost instantly when control input is neutralized.

- **Dutch Roll Mode Response:** The Dutch Roll mode is dynamically stable. The simulation shows a damped oscillatory response with a period of 0.59 seconds. The amplitude of the coupled motion clearly decreases over subsequent cycles, preventing the nauseating roll-yaw motion from persisting. Sufficient Dutch roll damping is a key factor in ensuring good flying qualities and reducing pilot workload.

- **Spiral Mode Response:** The analysis reveals a mild spiral instability, characterized by a long doubling time of 25.61 seconds. This means the aircraft's bank angle, if left entirely uncorrected, would double in about 26 seconds. A slow spiral divergence like this is a common and perfectly acceptable characteristic in most aircraft designs. The motion develops so gradually that it is easily and often subconsciously corrected by the pilot or a simple autopilot, and it does not compromise the aircraft's overall safety.

5.6 Summary

This chapter undertook a quantitative assessment of the flight stability characteristics of the BWB UAV design. Following a theoretical review of stability principles, a computational methodology was employed using OpenVSP's VSPAERO tool and a Python-based program to simulate the aircraft's characteristic modes of motion based on its calculated aerodynamic derivatives.

The simulation results confirmed the airframe possesses positive static stability. The analysis further revealed that the critical flight modes are dynamically stable, with the exception of a mild spiral instability. This slow divergence is a common and acceptable characteristic in aircraft design that does not compromise safety and is easily managed. Collectively, these results provide a definitive validation of the BWB airframe's design, confirming it possesses safe, predictable, and controllable flight dynamics.

Conclusions and Future Work

Chapter 6

Prototype Fabrication

6.1 Introduction

For decades, the production of aerial vehicles has relied on a portfolio of established manufacturing technologies, each with a well-understood envelope of capabilities and limitations. While these traditional methods are capable of producing high-quality components, they present significant economic and logistical barriers to the agility required by the modern UAV market.

Subtractive manufacturing, primarily Computer Numerical Control (CNC) machining, offers exceptional precision and is compatible with high-strength metals and composites. However, it is an inherently wasteful process, often removing 30% to 70% of the initial material block, which is particularly costly when using aerospace-grade alloys. Furthermore, its cost escalates dramatically with part complexity, and long lead times for programming and setup make it ill-suited for rapid iteration.

Formative manufacturing, exemplified by plastic injection molding, is the cornerstone of mass production. It can produce millions of identical parts with extremely low per-unit costs and high repeatability. Its primary drawback, however, is the astronomical upfront cost of tooling. The creation of a steel or aluminum mold can cost tens of thousands of dollars and take many weeks, making this method economically unviable for the low-volume, customized production runs that characterize much of the specialized UAV market. Design changes are prohibitively expensive, effectively locking in a design and stifling innovation.

Advanced composite layup techniques, such as those using carbon fiber or Kevlar, produce parts with unparalleled strength-to-weight ratios, making them the gold standard for high-

performance aerospace structures. Yet, these methods are notoriously labor-intensive, time-consuming, and expensive, often requiring specialized equipment like autoclaves and a highly skilled workforce. The high entry cost and complex processes limit their accessibility and scalability for many UAV applications.

It is within this context of traditional manufacturing constraints that Additive Manufacturing (AM), and specifically Fused Filament Fabrication (FFF), emerges as a disruptive and enabling technology. FFF, a material extrusion process, fundamentally alters the established manufacturing equation of cost, volume, and complexity. By constructing parts layer-by-layer directly from a digital Computer-Aided Design (CAD) file, FFF eliminates the need for molds, tooling, or complex setup procedures.

This capability represents a paradigm shift for UAV production. It empowers designers and engineers with unprecedented geometric freedom, allowing for the creation of intricate, lightweight structures that were previously unmanufacturable.

It drastically shortens development cycles from weeks to days, enabling rapid prototyping and iterative design optimization at a fraction of the traditional cost. The economic model of FFF, characterized by low fixed costs, makes on-demand and low-volume production not only possible but financially prudent. The diversification of the UAV market is the primary catalyst driving the adoption of AM, and as UAVs evolve from general-purpose platforms to highly specialized tools, the need for rapid, low-cost customization invalidates the economic models of traditional mass-production techniques. A manufacturer cannot justify a $50,000 injection mold for a production run of only a few hundred specialized agricultural drones. This creates an economic and technological vacuum for a manufacturing process that is cost-effective at low-to-medium volumes and allows for seamless design changes. FFF, with its zero-tooling cost structure, directly fills this vacuum, making it a strategically superior manufacturing choice for a large and growing segment of the UAV industry.

6.2 A Comparative Overview of Traditional Methods

The choice between these traditional manufacturing methods is a complex engineering decision dictated by a matrix of competing factors: required performance, production volume, design maturity, and budget. No single method is universally superior; each occupies a specific niche within the manufacturing landscape. The following table provides a synthesized

comparison of these foundational technologies, highlighting the trade-offs that define the production environment into which additive manufacturing now enters

Table 6.1: Comparative Analysis of Traditional UAV Manufacturing Methods

Feature	CNC Machining	Injection Molding	Composite Layup (Prepreg)
Core Principle	Subtractive (Material Removal)	Formative (Material Shaping)	Additive/Laminating (Layer Building)
Key Advantages	High precision, excellent material properties, good for complex shapes	Extremely low cost-per-part at high volumes, high speed, high repeatability	Unmatched strength-to-weight ratio, design flexibility for aerodynamic shapes
Key Disadvantages	High material waste, high cost for low volumes, long setup times	Prohibitive upfront tooling cost, inflexible to design changes, only for high volumes	Extremely labor-intensive, very high material and equipment costs, long cycle times
Primary Cost Drivers	Skilled labor, machine time, raw material (especially with high waste)	Mold/Tooling Cost (NRE)	Skilled labor, raw material cost (prepreg), autoclave time
Typical Lead Time	Days to Weeks (for programming and setup)	Weeks to Months (for mold creation)	Weeks to Months (for mold creation and layup)
Material Compatibility	Metals (Aluminum, Titanium), Plastics, Composites	Thermoplastics	Fiber Reinforcements (Carbon, Glass, Kevlar) with Thermoset Resins (Epoxy)
Ideal Production Volume	Low to Medium (1 - 1,000s)	High to Mass (10,000+)	Low (1 - 100s)
Typical UAV Application	Motor mounts, landing gear, high-stress structural nodes, prototypes	Propellers, electronic housings, lens covers, non-structural components	Wings, fuselage, airframe structures, high-performance components

This comparative landscape reveals a clear gap: there is no traditional method that cost-effectively produces complex, customized parts at low-to-medium volumes. It is this specific

void that Fused Filament Fabrication is uniquely positioned to fill.

6.3 Principles of Material Extrusion (FFF)

Fused Filament Fabrication, a term used interchangeably with the trademarked Fused Deposition Modeling (FDM), is a material extrusion-based additive manufacturing process. The technology functions by feeding a solid thermoplastic filament from a spool into a heated extruder, often called a print head. The extruder melts the filament to a semi-liquid state and deposits it through a small nozzle onto a build platform. The print head moves in the X-Y plane, tracing the cross-sectional shape of a digital model for a single layer. Once a layer is complete, the build platform moves down (or the print head moves up) along the Z-axis by a precise increment, and the process repeats. The extruded material fuses with the layer below it and solidifies, building the three-dimensional object layer by layer directly from the CAD data.

This process is controlled by software known as a "slicer," which takes a 3D model and "slices" it into hundreds or thousands of horizontal layers, generating the specific toolpaths the printer will follow. The slicer also allows the user to define critical printing parameters, such as layer height, infill density and pattern, and print speed, which have a direct impact on the final part's properties.

The layer-by-layer nature of FFF unlocks several profound advantages for the design and manufacturing of UAVs, directly addressing the primary limitations of traditional methods.

- **Geometric Freedom and Part Consolidation**
- **Accelerated Iteration: From Prototyping to Production**
- **On-Demand and Distributed Manufacturing Potential**

Despite its transformative potential, FFF is not without its challenges. Achieving aerospace-grade quality and reliability requires a deep understanding of the process's limitations and the implementation of strategies to mitigate them.

- **Anisotropy and Inter-Layer Adhesion**
- **Dimensional Accuracy and Surface Finish**
- **Process Optimization for Aerospace-Grade Components**

6.4 Material Selection for High-Performance FFF

The viability of Fused Filament Fabrication for producing functional, end-use UAV components is fundamentally dependent on the choice of material. While the geometric freedom of FFF is a powerful tool, the final part is only as good as the thermoplastic from which it is made. The material must not only possess the requisite mechanical properties—strength, stiffness, and toughness—but also exhibit robust resistance to the harsh environmental conditions inherent to UAV operation. An analysis of the available thermoplastic spectrum reveals that Acrylonitrile Styrene Acrylate (ASA) emerges as a superior choice, offering a uniquely balanced profile of mechanical performance and environmental durability.

The library of materials available for FFF is vast and can be broadly categorized based on performance and application. At one end are hobbyist-grade materials like Polylactic Acid (PLA), prized for its ease of printing but limited by low thermal and impact resistance. In the middle are general-purpose workhorse materials such as Acrylonitrile Butadiene Styrene (ABS) and Polyethylene Terephthalate Glycol (PETG), which offer a better balance of properties. At the high-performance end are engineering-grade materials like Nylon (Polyamide) and its fiber-reinforced composites, which provide excellent toughness and strength but can be more challenging to print.

The selection of a material for a structural UAV component requires a quantitative comparison of its key properties. The following table presents the critical mechanical and thermal data for the most common FFF filaments, providing a foundation for a rigorous selection process.

Table 6.2: Comparison of Mechanical and Thermal Properties of Common FFF Filaments

Property	**PLA**	**ABS**	**PETG**	**ASA**	**Nylon (PA)**
Tensile Strength (MPa)	53 - 59	34 - 50	38 - 60	42 - 55	50 - 90
Bending/Elastic Modulus (MPa)	∼2300	∼2000	∼2000	1200 - 2210	∼1400
Izod Impact Strength (kJ/m^2)	Low	High	High	19 - 20	Very High
Heat Deflection Temp. (°C @ 0.45 MPa)	∼60	81 - 100	∼75 - 85	86 - 100	∼70 - 90
Typical Print Temp. (°C)	190 - 220	220 - 250	230 - 250	240 - 260	255±15

Note: Values represent typical ranges and can vary significantly based on manufacturer, additives, and testing standards.

A purely mechanical analysis is insufficient for selecting a UAV airframe material. The operational environment of a drone is outdoors, where it is subjected to a relentless barrage of environmental stressors. A material that performs well in the lab can fail rapidly in the field if it lacks the necessary environmental resilience.

The most significant environmental threat to most polymers is prolonged exposure to sunlight. The ultraviolet radiation in sunlight is energetic enough to break the chemical bonds within polymer chains, a process known as photodegradation. This leads to a cascade of undesirable effects: the material becomes brittle, loses its impact strength, and undergoes significant color fading or yellowing. For a UAV airframe, this degradation is not merely cosmetic; it is a critical safety issue that can lead to catastrophic structural failure in flight.

Table 6.3: Environmental Resistance Profile of Key Thermoplastics

Material	UV Resistance	Water/Moisture Resistance	Chemical Resistance	Key Advantage	Key Disadvantage
ABS	Poor	Moderate	Good	Low Cost, Good Strength	Degrades quickly in sunlight
PETG	Moderate	Good	Good	Easy to print, Food-safe grades	Degrades with prolonged UV exposure
ASA	Excellent	High	Good	Superior weatherability	More difficult to print, higher cost

When the mechanical requirements from Table 6.2 are synthesized with the critical environmental demands from Table 6.3, Acrylonitrile Styrene Acrylate (ASA) unequivocally emerges as the most suitable material for printing functional, durable, and long-lasting UAV components.

6.4.1 Case Studies and Applications: ASA in Demanding Environments

The theoretical superiority of ASA is validated by its practical application in real-world, demanding environments. Its use is explicitly recommended by material experts for drone parts due to its combination of mechanical robustness and environmental resilience. A compelling case study is the use of Prusament ASA by Seamor Marine to create components for their underwater remotely operated vehicles (ROVs). [18]

These components, including internal electronics mounts and prototype propellers, must withstand immense pressures at depths of up to 600 meters (equivalent to 6,000 kPa) and operate reliably in a corrosive saltwater environment. Seamor Marine chose ASA for its strength, durability, and consistent properties. Another example involves the construction of a fixed-wing UAV using an ASA-Carbon Fiber (ASA-CF) composite filament, a material chosen specifically for its excellent resistance to water, wind, heat, and UV radiation. [19]

These applications underscore the confidence that engineers place in ASA for creating functional parts that must perform flawlessly in the most challenging conditions, making it an ideal and proven material for the next generation of 3D-printed UAVs.

6.5 Final Prototype Fabrication

Having established Acrylonitrile Styrene Acrylate (ASA) as the optimal material due to its superior mechanical properties and environmental resistance, the next crucial phase was the translation of the digital CAD model into a physical prototype through Fused Filament Fabrication (FFF). This section details the specific printing process, addressing the inherent challenges of FFF to ensure the final components met the required standards for a functional UAV. The successful fabrication of aerospace-grade components is not merely a function of material choice; it demands a deep understanding and meticulous control of the printing process itself.

6.5.1 Slicer Configuration and Print Preparation

The digital fabrication process began with the 'slicer' software, which translates the 3D CAD models into layer-by-layer toolpaths for the printer. The configuration of printing parameters within the slicer was critical to achieving the desired mechanical performance and dimensional accuracy of the final UAV components, the slicer used in our case was OrcaSlicer, manually configured to run with the Raise3d Pro2 Plus, Key parameters that were meticulously calibrated include:

- **First Layer Height:** A 0.35mm layer height was chosen to achieve appropriate bed adhesion This parameter is fundamental to success of the 3d printed part, as ASA is notoriously difficult to get good first layer adhesion with, a thick first layer is a necessity

- **First Layer Line Width:** Similar to first layer height, this parameter is fundamental to getting a good first layer, ASA requires printing a thick and Hot and slow first layer

- **Infill Density and Pattern:** An infill density and pattern were selected to provide internal structural support and enhance the strength-to-weight ratio, crucial for aerospace parts. This allowed for a lightweight internal structure without compromising the component's integrity, addressing a key advantage of FFF in creating lightweight designs.

- **Layer Print Speed:** Print speed was carefully managed, as it directly impacts layer adhesion and the overall quality of the print. An optimal speed ensures that the extruded material has sufficient time to properly fuse with the preceding layer, enhancing part strength.

- **Print Temperature:** The extruder temperature was set to 260° for ASA to ensure proper melting and fusion between layers, which is vital for part strength. The extruder melts the solid thermoplastic filament to a semi-liquid state for deposition, and the correct temperature is paramount for this process.

- **Part Cooling:** Part cooling was entirely turned off during the printing process since ASA is very sensitive to large temperature gradients and could cause weak inter layer adhesion

6.6 Fabrication Results and Post-Processing

The calibration of the slicer parameters resulted in the successful fabrication of all necessary UAV components from ASA. The following figure shows an overview of the final printed parts, which exhibit excellent dimensional accuracy and strong layer adhesion, and warping was kept to a minimum, validating the chosen print settings.

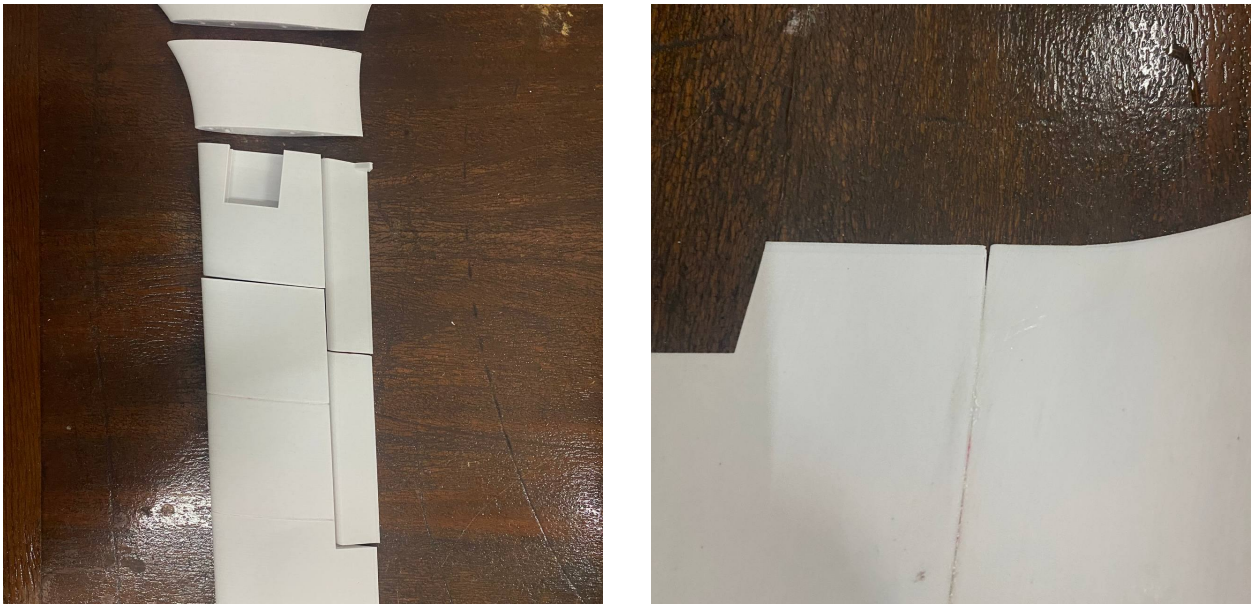

Figure 6.1: 3D Printed Scaled prototype

6.7 Summary

This chapter detailed the manufacturing methodology for the UAV prototype, beginning with a comparative assessment of traditional fabrication technologies. An analysis of CNC machining, injection molding, and composite layups revealed significant economic and logistical barriers for specialized, low-volume production. This established a clear need for an alternative process, identifying Fused Filament Fabrication (FFF) as a strategically superior choice. Following this, a data-driven material selection process was conducted, comparing common thermoplastics and concluding that Acrylonitrile Styrene Acrylate (ASA) offers the optimal balance of mechanical properties and environmental resilience required for durable UAV components.

The chapter then documented the successful translation of the digital CAD model into a physical prototype using the selected FFF process and ASA material. The fabrication was achieved through the meticulous configuration of slicer parameters, including layer height, print temperature, and cooling, to overcome the inherent challenges of printing with ASA and ensure part integrity. The resulting components exhibited excellent dimensional accuracy and strong layer adhesion with minimal warping. Collectively, these results provide a definitive validation of the manufacturing approach, confirming that FFF combined with ASA is a viable and effective method for producing functional, aerospace-grade UAV parts.

Chapter 7

Conclusions and Future Work

7.1 Conclusion

This thesis has successfully addressed the design and validation of a novel Medium-Altitude, Long-Endurance (MALE) Unmanned Aerial Vehicle (UAV) intended to serve as a versatile, high-performance aerial test platform for the Algerian Space Agency (ASAL). The research was initiated to bridge a well-defined technological gap: the absence of a UAV system capable of simultaneously meeting a demanding set of performance requirements, including an endurance of over 14 hours, a 5 kg payload capacity, operation at or above 3 km altitude, and a wingspan under 4 meters. The work presented herein has demonstrated that by synergistically integrating a Blended-Wing-Body (BWB) airframe, advanced computational design methodologies, and modern manufacturing techniques, it is possible to develop a platform that meets these challenging specifications.

The core of this research was the development and application of a custom, integrated computational design framework. This Python-based tool, leveraging a Non-dominated Sorting Genetic Algorithm II (NSGA-II), proved indispensable for navigating the complex, multidisciplinary design space. A key outcome of this framework was a data-driven, two-stage optimization process that yielded a final, realistic design with a predicted endurance of 7.40 hours, a total weight of 12.84 kg, and a wingspan of 4 meters. This process underscored the critical importance of incorporating high-fidelity, experimentally-derived data to refine theoretical models and converge on a physically achievable solution.

A rigorous validation campaign formed the cornerstone of this thesis, anchoring the computational design in physical reality. Through a meticulous workflow integrating low-fidelity Vortex Lattice Method (VLM) analysis, high-fidelity Computational Fluid Dynamics (CFD),

and experimental wind tunnel testing, the aerodynamic characteristics of the BWB airframe were thoroughly investigated. The results provided a definitive validation of the aircraft's performance and, most critically, its inherent flight stability. The unanimous agreement between experimental data and computational models on the negative pitching moment slope provided high confidence in the design's longitudinal static stability. Furthermore, a detailed flight dynamics analysis confirmed that all critical modes of motion are dynamically stable, with the exception of a mild, slow, and easily manageable spiral instability, a common and acceptable trait in aircraft design.

Finally, this thesis addressed the practical challenge of fabrication. By conducting a comparative analysis of manufacturing methods, Fused Filament Fabrication (FFF) was identified as the strategically superior choice for low-volume, high-complexity prototyping. A subsequent data-driven material selection process identified Acrylonitrile Styrene Acrylate (ASA) as the optimal material, balancing mechanical strength with crucial environmental resistance. The successful fabrication of prototype components validated this manufacturing approach, demonstrating a viable pathway from digital design to physical artifact.

In summary, this thesis has delivered on its primary objectives. It has produced a complete, validated design for an aerodynamically efficient and stable BWB airframe. It has established a repeatable computational workflow that effectively balances aerodynamics, structures, and manufacturability. And it has laid the groundwork for the physical realization of a next-generation UAV, providing a crucial tool to advance Algeria's national scientific and technological objectives in aerospace.

7.2 Limitations of the Current Research

While this thesis successfully achieved its core objectives, it is important to acknowledge the boundaries of its scope. The following aspects, by design, were not addressed in this work and represent areas for further investigation:

- **Solar Power System Integration:** The design focused on creating an airframe with the *capability* to support solar-extended endurance. The detailed design, analysis, integration, and testing of the complete solar power system—including the selection and placement of photovoltaic (PV) cells, Maximum Power Point Tracking (MPPT) controllers, and the Battery Management System (BMS)—remains a future task.

- **Flight Control and Avionics:** This research validated the inherent aerodynamic stability of the airframe but did not extend to the design, implementation, or testing of the flight control system, autopilot, sensors, or communication systems required for autonomous operation.

- **Detailed Structural Analysis of Lattice Structures:** The thesis proposed the use of novel lattice structures for lightweighting and used advanced software to determine their mass properties for stability analysis. However, a comprehensive Finite Element Analysis (FEA) to validate the structural integrity of these complex lattices under all flight loads was beyond the scope of this work.

- **Propulsion System Optimization:** While the powertrain was modeled and selected through the MDO framework, a detailed experimental validation of the motor, ESC, and propeller combination was not performed.

7.3 Future Work

The successful validation of the BWB airframe design opens up several exciting and critical avenues for future research and development. The following steps are proposed to build upon the foundation established by this thesis and move the project toward a fully operational system.

1. **Full-Scale Prototype Fabrication and Flight Testing:** The immediate next step is to fabricate the full-scale, 4-meter wingspan UAV based on the final design and manufacturing methods detailed in this thesis. This will be followed by a comprehensive flight test campaign to validate the real-world performance against the predictions from CFD and wind tunnel testing. This will provide the ultimate validation of the aircraft's performance, stability, and handling qualities.

2. **Integration and Optimization of the Solar Power System:** A dedicated research effort is required to integrate the solar-electric propulsion system. This work should include:

    - **PV Cell Integration:** Researching and testing methods for seamlessly integrating flexible, high-efficiency solar cells onto the curved upper surface of the BWB to minimize aerodynamic drag.

    - **Energy Management System (EMS) Development:** Designing and implementing a sophisticated EMS to optimize the harvesting, storage, and expenditure

of energy over a 24-hour cycle, adapting to changing environmental conditions to maximize endurance.

3. **Advanced Structural Design with Multifunctional Lattices:** Building on the proposed use of lattice structures, future work should focus on:
   - **Hybrid Additive-Composite Structures:** Investigating hybrid manufacturing techniques that combine the 3D-printed lattice core with lightweight carbon fiber composite skins. This approach could yield a true structural optimum, leveraging the compressive strength of the lattice and the tensile strength of the composite skin.
   - **Multifunctional Lattice Exploration:** Moving beyond purely structural applications, this research should explore the design of lattices that are optimized for multifunctionality, such as acting as integrated heat sinks for battery and electronics thermal management, or providing tailored vibration damping to protect sensitive payloads.
4. **Development of a Tailored Flight Control System:** A robust flight control system and autopilot must be developed specifically for the unique flight dynamics of the BWB airframe. This will involve:
   - **System Identification:** Performing flight tests to refine the aerodynamic model and create a high-fidelity digital twin of the aircraft.
   - **Control Law Design:** Developing and testing advanced control laws in simulation and in flight to ensure robust, reliable, and efficient autonomous operation across the entire flight envelope.

By pursuing these avenues, the foundational work of this thesis can be advanced toward the ultimate goal: the deployment of a long-endurance, solar-powered MALE UAV that provides a persistent and cost-effective platform for scientific research, technological validation, and national development.

References

[1] K. P. Valavanis, Ed., *Advances in Unmanned Aerial Vehicles: State of the Art and the Road to Autonomy* (Intelligent Systems, Control and Automation: Science and Engineering). Dordrecht, The Netherlands: Springer, 2007, vol. 33, ISBN: 9781402061142.

[2] J. Gundlach, *Designing Unmanned Aircraft Systems: A Comprehensive Approach* (AIAA Education Series), J. A. Schetz, Ed. Reston, Virginia: American Institute of Aeronautics and Astronautics, Inc., 2012, Retrieved from www.knovel.com.

[3] R. H. Liebeck, "Design of the blended wing body subsonic transport," *Journal of aircraft*, vol. 41, no. 1, pp. 10–25, 2004.

[4] C. Pan, Y. Han, and J. Lu, "Design and optimization of lattice structures: A review," *Applied Sciences*, vol. 10, no. 18, 2020, ISSN: 2076-3417. DOI: 10.3390/app10186374. [Online]. Available: https://www.mdpi.com/2076-3417/10/18/6374.

[5] Mohd Saad, Nornashiha, Wisnoe, Wirachman, Mohd Nasir, Rizal Effendy, Mohd Ali, Zurriati, and Askari, Ehan Sabah Shukri, "Aerodynamic analysis of blended wing body - unmanned aerial vehicle (bwb-uav) equipped with horizontal stabilizers," *MATEC Web Conf.*, vol. 256, p. 02 004, 2019. DOI: 10.1051/matecconf/201925602004. [Online]. Available: https://doi.org/10.1051/matecconf/201925602004.

[6] Dimopoulos, Thomas, Panagiotou, Pericles, and Yakinthos, Kyros, "Stability study and flight simulation of a blended-wing-body uav," *MATEC Web Conf.*, vol. 304, p. 02 013, 2019. DOI: 10.1051/matecconf/201930402013. [Online]. Available: https://doi.org/10.1051/matecconf/201930402013.

[7] K. Lehmkuehler, K. Wong, and D. Verstraete, "Design and test of a uav blended wing body configuration," in *Proceedings of the 28th Congress of the International Council of the Aeronautical Sciences*, 2012, pp. 23–28.

[8] V. Mukhopadhyay, "Blended wing body (bwb) fuselage structural design for weight reduction," in *46th AIAA/ASME/ASCE/AHS/ASC structures, structural dynamics and materials conference*, 2005, p. 2349.

[9] J. R. C. da Silva and G. M. Pacheco, "An extended methodology for sizing solar unmanned aerial vehicles: Theory and development of a python framework for design assist," *Sensors*, vol. 21, no. 22, p. 7541, 2021.

[10] V. Cipolla, A. Dine, A. Viti, and V. Binante, "Mdao and aeroelastic analyses of small solar-powered uavs with box-wing and tandem-wing architectures," *Aerospace*, vol. 10, no. 2, 2023, ISSN: 2226-4310. DOI: 10.3390/aerospace10020105. [Online]. Available: https://www.mdpi.com/2226-4310/10/2/105.

[11] K. Sornek, J. Augustyn-Nadzieja, I. Rosikoń, R. Łopusiewicz, and M. Łopusiewicz, "Status and development prospects of solar-powered unmanned aerial vehicles—a literature review," *Energies*, vol. 18, no. 8, 2025, ISSN: 1996-1073. DOI: 10.3390/en18081924. [Online]. Available: https://www.mdpi.com/1996-1073/18/8/1924.

[12] M. MA-Accounting. "World's most efficient flexible solar cell hits 26.4%, As drone industry braces For A massive, next-gen power leap," Sustainability Times, Accessed: Jul. 3, 2025. [Online]. Available: https://www.sustainability-times.com/energy/worlds-most-efficient-flexible-solar-cell-hits-26-4-as-drone-industry-braces-for-a-massive-next-gen-power-leap/.

[13] Y. Chu, C. Ho, Y. Lee, and B. Li, "Development of a solar-powered unmanned aerial vehicle for extended flight endurance," *Drones*, vol. 5, no. 2, 2021, ISSN: 2504-446X. DOI: 10.3390/drones5020044. [Online]. Available: https://www.mdpi.com/2504-446X/5/2/44.

[14] Z. Zhang, R. Zhang, J. Zhu, T. Gao, F. Chen, and W. Zhang, "Integrated batteries layout and structural topology optimization for a solar-powered drone," *Chinese Journal of Aeronautics*, vol. 34, Jan. 2021. DOI: 10.1016/j.cja.2020.10.020.

[15] S. Gudmundsson, *General Aviation Aircraft Design: Applied Methods and Procedures*. Oxford, UK: Butterworth-Heinemann, 2014, ISBN: 9780123973085.

[16] L. Traub, "Range and endurance estimates for battery-powered aircraft," *Journal of Aircraft*, vol. 48, pp. 703–707, Mar. 2011. DOI: 10.2514/1.C031027.

[17] C. Montalvo, *aerospace: Python script for aircraft stability analysis*, version b748b67, 2024. [Online]. Available: https://github.com/cmontalvo251/aerospace.

[18] P. P. Team, *Case study: Components for underwater research drones made of prusament asa*, https://prusament.com/case-study-komponenty-pro-podmorske-vyzkumne-drony-z-prusament-asa/, Accessed: 2024-08-15, Jan. 2022.

[19] P. George, *I 3d printed a fixed wing drone with an engineering-grade filament // ep15*, http://www.youtube.com/watch?v=Dlj6ti7-9io, Accessed: 2024-08-15, Jun. 2025.